

The effects of waves and turbulence on sediment suspension and mixing within seagrass ecosystems

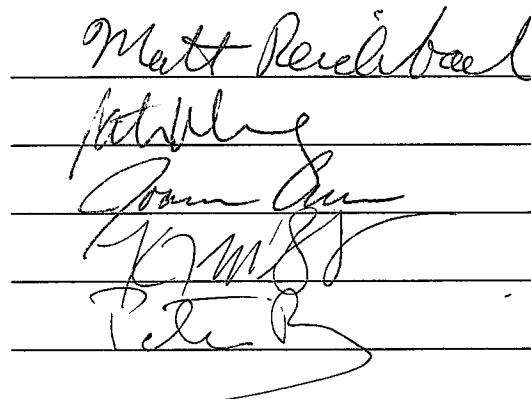
Jennifer Christine Hansen  
Bakersfield, CA

B.S. Aquatic Biology, University of California Santa Barbara, 2007

A Dissertation presented to the Graduate Faculty  
of the University of Virginia in Candidacy for the Degree of  
Doctor of Philosophy

Department of Environmental Sciences

University of Virginia  
May, 2013

  
The image shows five handwritten signatures, each written on a horizontal line. From top to bottom, the signatures are: 1. 'Matt Perchival' in cursive. 2. A signature that appears to be 'John' or 'Johnnie' in cursive. 3. A signature that appears to be 'John' or 'Johnnie' in cursive. 4. A signature that appears to be 'K.M.S.' in cursive. 5. A signature that appears to be 'Peter B.' in cursive.

## ABSTRACT

Seagrass meadows create significant benthic structure, which attenuates wave energy and near-bottom currents, altering mixing across the seagrass canopy and reducing bottom shear stresses. This enhances the deposition of suspended sediment and increases light availability to the benthos. To quantify how meadow structure influences the physical environment, spatial and temporal density gradients within *Zostera marina* and *Thalassia testudinum* meadows in South Bay, Virginia, and Florida Bay, Florida, were monitored. Results show that seagrass beds create a hydrodynamic shear layer with an inflection point of instability at the top of the canopy, which imparts substantial turbulent mixing. Seagrass beds were found to reduce near-bottom mean velocities by 25 to 85% depending on both canopy development and location within the meadow, while wave heights were reduced 10 to 70% compared to adjacent unvegetated regions. Attenuation of both velocities and waves increased with increasing seagrass canopy cover. Wave orbital velocities within the seagrass canopy were reduced by 20% compared to flow above the canopy, primarily acting as a low-pass filter by removing high-frequency wave motion. During maximum canopy development in the summer, bed shear stresses were above the critical threshold for initiating sediment suspension only 20 to 55% of the sampling time, compared to 80 to 85% in the winter and spring when seagrass canopy cover was lower. This compares to bed shear stresses that were greater than the critical threshold at the bare site > 90% of the sampling time. Overall, seagrass was found to stabilize sediment during most of the year (late spring to fall), creating a positive feedback for growth.

The *Thalassia* meadow in Florida had lower energy compared to the *Z. marina* meadow in Virginia, and oscillatory flows due to waves led to enhanced turbulence and mixing within the meadow as compared to unidirectional flows. *In situ* particle image velocimetry (PIV) was used to quantify turbulent momentum transport across the meadow. Turbulence was observed within the canopy at depths 2 to 3 times the penetration length-scale for shear layer vortices, suggesting stem-wake generated turbulence was formed within the canopy. This led to 3 times greater average Reynolds stress within the sparse canopy compared to ambient conditions above the canopy, while the dense meadow reduced Reynolds stress 16% across the canopy-water interface. Though turbulence penetration into the dense canopy was restricted, momentum transport was more efficient due to increased velocity shear at the top of the canopy, effectively increasing the canopy's ability to exchange fluids (and likely nutrients and gases), with the overlying water column.

**TABLE OF CONTENTS**

ACKNOWLEDGEMENTS	viii
CHAPTER 1: Introduction	1
Theoretical foundation	1
Research questions	6
Dissertation outline	7
CHAPTER 2: Wave and tidally driven flows in eelgrass beds and their effect on sediment suspension	9
Abstract	9
Introduction	10
Methods	14
Site Description	14
Instrumentation	16
Wave-turbulence decomposition	17
Wave orbital velocities	20
Results	21
Turbulent kinetic energy and Reynolds stress	24
Quadrant analysis of turbulence	26
Velocity spectra and wave orbitals	28
Bottom shear stresses and suspended sediment	33
Discussion	36
Wave attenuation due to interaction with the seagrass canopy	38
Bottom shear stress and sediment dynamics	39
Acknowledgements	42
CHAPTER 3: Seasonal growth and senescence of a <i>Zostera marina</i> seagrass meadow alters wave-dominated flow and sediment suspension within a coastal bay	43
Abstract	43
Introduction	44
Methods	48
Study area	48
Instrumentation	50
Wave-turbulence decomposition	51
Bottom shear stress	53
Results	54
Waves and orbital motion	58
Turbulence and momentum transport	63
Bottom shear stress and suspended sediment dynamics	66
Discussion	69

Wave interaction with the seagrass canopy	72
Sediment suspension	73
Acknowledgements	75
CHAPTER 4: Fine-scale mixing and momentum transport within a <i>Thalassia testudinum</i> seagrass meadow	76
Abstract	76
Introduction	77
Methods	80
Study area	80
Seagrass morphometrics	82
Instrumentation	83
Particle image velocimetry	84
Wave-turbulence decomposition	86
Quadrant analysis	87
Results	88
Site Characterization	88
Velocity structure	91
Velocity spectra and orbital motion	93
Turbulent kinetic energy	95
Reynolds stress and momentum transport	99
Fluid exchange and mass transport	103
Discussion	104
Acknowledgements	112
CHAPTER 5: Conclusion	113
Research summary	113
Site Comparison	116
Physical characteristics and study species	116
Seagrass influence on velocity structure	118
Seagrass influence on wave development	122
Seagrass influence on turbulence and mass transport	125
Sediment suspension and light limitation	131
Summary and future directions	135
REFERENCES	138
TABLES	
<b>2.1:</b> <i>Zostera marina</i> morphometrics across a density gradient during summer 2010	15
<b>3.1:</b> <i>Z. marina</i> morphometrics seasonally from summer 2010 through summer 2011	49

<b>3.2:</b> Seasonal averages of suspended sediment concentrations, depth, and tidal amplitudes at an unvegetated and a seagrass site	57
<b>4.1:</b> <i>Thalassia testudinum</i> morphometrics across a density gradient in Florida Bay	82
<b>4.2:</b> Turbulent kinetic energy production and dissipation, and shear stress values in current- and wave-dominated flow conditions	99
<b>5.1:</b> Morphometrics for <i>Z. marina</i> and <i>T. testudinum</i> meadows	118

## FIGURES

<b>2.1:</b> Density gradient study sites located off the eastern shore of the Delmarva Peninsula, Virginia, USA	14
<b>2.2:</b> Power spectral density of horizontal velocity	19
<b>2.3:</b> Wind magnitude and direction, water temperature, water depth, flow velocity, significant wave height, and suspended sediment concentrations	22
<b>2.4:</b> Average tidal amplitudes, significant wave heights, and flow velocity at two locations in the water column	23
<b>2.5:</b> Significant wave heights as a function of wind speed	23
<b>2.6:</b> Reynolds stress and turbulent kinetic energy under tidally- and wave-dominated flow conditions	25
<b>2.7:</b> Quadrant analysis of probability density function of Reynolds stress components at two locations in the water column for an unvegetated and a high density seagrass site	27
<b>2.8:</b> Power spectral density of horizontal flow velocity at an unvegetated and a mid-density seagrass site during tidally- and wave-dominated flow conditions	29
<b>2.9:</b> Power spectral density time series of the horizontal and vertical velocities at two locations in the water column over an unvegetated seafloor	30
<b>2.10:</b> Power spectral density time series of the horizontal and vertical velocities across a mid-density seagrass canopy	31
<b>2.11:</b> Wave orbital velocities across a seagrass density gradient measured spectrally and predicted via linear wave theory	32
<b>2.12:</b> Bottom shear stress across a seagrass density gradient	35
<b>3.1:</b> Map of long term seasonal study field sites	47
<b>3.2:</b> Power spectral density of horizontal velocity	52
<b>3.3:</b> Wind magnitude and direction, water temperature, water depth, flow velocity, significant wave height, and suspended sediment concentrations during field studies over 1 year	55
<b>3.4:</b> Average wind speed and direction at an unvegetated and a seagrass site for each season over 1 year	56
<b>3.5:</b> Average velocity over an unvegetated site and across a seagrass meadow canopy, average percent reduction in velocity across the seagrass canopy, and frontal area of the meadow in each season	58
<b>3.6:</b> Vertical profiles of velocity at an unvegetated and a seagrass site	58

<b>3.7:</b> Seasonal averages of significant wave period and height at an unvegetated and a seagrass site	59
<b>3.8:</b> Wave period and significant wave height as a function of wind speed and depth for each season	60
<b>3.9:</b> Seasonal averages of wave orbital velocities across the seagrass canopy measured spectrally and predicted with linear wave theory	61
<b>3.10:</b> Power spectral density of horizontal velocity in June and January over the unvegetated seafloor and across a seagrass canopy	63
<b>3.11:</b> Seasonal averages of normalized Reynolds stress over an unvegetated seafloor and across the seagrass canopy	64
<b>3.12:</b> Quadrant analysis of the probability density functions of Reynolds stress components at the unvegetated and seagrass sites	65
<b>3.13:</b> Bed shear stress and average suspended sediment concentrations for an unvegetated and a seagrass site seasonally	66
<b>3.14:</b> Temporal series of two-dimensional power spectral density of horizontal velocities and suspended sediment concentrations within the seagrass canopy in March	68
<b>4.1:</b> Map of field study sites in Florida Bay, FL	81
<b>4.2:</b> Wind magnitude and direction, water temperature, water depth, and horizontal velocity	89
<b>4.3:</b> Logarithmic fit to velocity profiles	90
<b>4.4:</b> Average velocity at two locations in the water column	91
<b>4.5:</b> Maps of mean velocity vectors at the bare, sparse, and dense seagrass sites obtained with particle image velocimetry	91
<b>4.6:</b> Normalized vertical profiles of average horizontal velocity across the sparse and dense seagrass canopies in current- and wave-dominated flows	92
<b>4.7:</b> Velocity power spectral density at the bare, sparse, and dense sites at two locations in the water column under both current- and wave-dominated flow conditions	93
<b>4.8:</b> Power spectral density variations by frequency and water depth across the dense canopy in unidirectional and wave-dominated flows	94
<b>4.9:</b> TKE dissipation using two calculation methods	96
<b>4.10:</b> Vertical profiles of turbulent kinetic energy production, dissipation, and turbulent transport rates at the sparse and dense seagrass sites	98
<b>4.11:</b> Vertical profiles of normalized Reynolds stress at the sparse and dense sites under both current- and wave-dominated flow conditions	100
<b>4.12:</b> Vertical profiles of Reynolds stress magnitudes and percent distribution through quadrant analysis at the bare, sparse, and dense sites	102
<b>4.13:</b> Flushing rates at two vertical locations in the water column for the bare, sparse, and dense sites	103
<b>5.1:</b> Wind speed ranges during sampling periods at all sites	117
<b>5.2:</b> Normalized velocity and normalized percent reduction in velocity as a function of shoot density and frontal area	120
<b>5.3:</b> Normalized velocity and rms velocity profiles for sparse and dense <i>Z. marina</i> and <i>T. testudinum</i> canopies	121

<b>5.4:</b> Normalized Reynolds stress and percent reductions as a function of shoot density	126
<b>5.5:</b> Vertical profiles of normalized Reynolds stress for sparse and dense <i>Z. marina</i> and <i>T. testudinum</i> canopies	128
<b>5.6:</b> Shift in the probability density function toward turbulent ejections as a function of shoot density	129
<b>5.7:</b> Average efficiency of momentum transport from PIV obtained for sparse and dense <i>Z. marina</i> and <i>T. testudinum</i> canopies under wave-dominated conditions	130
<b>5.8:</b> Percent reduction in suspended sediment concentrations within seagrass canopies compared to unvegetated sites as a function of canopy frontal area	134

## ACKNOWLEDGEMENTS

The road to a doctorate has been a surprising and exciting journey, shaped by many people. I would like to thank my advisor and committee members, Matthew Reidenbach, Karen McGlathery, Patricia Wiberg, Peter Berg, and Joanna Curran, for their guidance, inspiration, and support. My sincerest regards to my advisor for dedicating so much time to answering questions, reviewing projects, and being such a wonderful mentor. My research wouldn't have been possible without the dedicated field assistance of Savanna B., Gavin B., Matthew L., Kathleen W., Kirby W., and Elizabeth W., and funding support from the National Science Foundation, Virginia Coast Reserve LTER group, and Everglades Foundation. I am grateful for the hard work of the entire staff of the Anheuser-Busch Coastal Research Center and Thomas Frankovich; from them I received invaluable support from boating lessons to life lessons, and wonderful friendships. Surviving graduate school would have been impossible without my fellow students and friends; thanks for keeping it fun. I'm indebted to Beth W., Kirby W., Amy G., Jenn H., and Kevin G. for your incredible friendship, sharing your scientific prowess, always being willing to celebrate a Wednesday night, all the laughs, and even the occasional tears. Special thanks to Amy for going above and beyond, offering me a second home during trips to school, and to the Noriega's for providing office space to a voluntarily displaced graduate student. I am grateful to my family, blood and adopted, for their constant emotional support and for celebrating every moment, particularly to my parents for all the sacrifices, always believing in me, and the faith you taught me. Finally, words cannot express my gratitude to my husband and best friend for countless hours of editing, and being a stand-in lab mate by my side through it all.

## CHAPTER 1:

### Introduction

#### THEORETICAL FOUNDATION

Seagrass meadows are among the most productive and biodiverse ecosystems of the world's oceans and are in widespread decline (Waycott et al. 2009). The ecosystem services provided by seagrass meadows contribute \$19,004 ha<sup>-1</sup> yr<sup>-1</sup>, placing them among the most economically valuable ecosystems (Costanza et al. 1997). They are also ecologically valuable, producing organic carbon in excess of their needs that is both exported to neighboring systems and stored in the sediment (Duarte and Cebrian 1996). Seagrass meadows serve as ecosystem engineers by altering the local hydrodynamic environment and stabilizing sediment, creating positive feedbacks for their growth (Carr et al. 2010). Further, meadows act as nursery habitat for many fish (Nagelkerken et al. 2000; Nagelkerken et al. 2001; Nagelkerken et al. 2002) and invertebrate (Ehrhardt and Legault 1999; Sheridan 1992) species. The loss of seagrass systems has led to declines in species richness, biomass, and production. Even with recovery of the seagrass community, resiliency can remain low creating greater disturbance responses to natural environmental variability (Dolbeth et al. 2007).

Seagrass meadows rely on light for photosynthesis, which is generally the limiting factor for macrophytic growth (Barko et al. 1986), and controls the depth limit for seagrass meadows (Dennisen and Alberte 1985). Photosynthetic rates in *Thalassia testudinum* were found to increase with current velocity in low flow conditions, but under higher flows there was no additional enhancement due to the carbon fixation limit of the

seagrass (Koch 1994). Further, Nishihara and Ackerman (2006) found that the biological response of *Vallisneria americana* influenced mass transfer rates, leading to smaller than expected concentration boundary layers and diffusive sublayers, enhancing net photosynthetic rates. Mass et al. (2010) determined that this enhancement of photosynthesis by seagrass occurs instantaneously in response to increases in flow by enhancing oxygen efflux from the organism leading to an increased affinity of the RuBisCO to CO<sub>2</sub>. Photosynthesis is also indirectly affected by flow conditions due to the potential light limiting effects of turbidity, which is ultimately driven by the creation of horizontal shear stress resuspending sediments. As vegetation reduces turbulence near the seafloor, sediment deposition is enhanced and tends to not remobilize (Christiansen et al. 2000), creating a positive feedback for seagrass growth. However, scouring around individual canopy elements can occur with sufficiently high current velocity or large stem diameters, through the flexible nature of seagrass blades tends to reduce scouring overall (Bouma et al. 2009). Low shoot densities within seagrass meadows can also enhance sediment suspension compared to an unvegetated seafloor through direct interaction of the canopy elements with the flow (Lawson et al. 2012). When bed shear stresses become sufficient for the suspension of sediment within the meadow, light quality decreases (Lawson et al. 2007), reducing photosynthesis and therefore seagrass production. In the Dutch Wadden Sea, the loss of seagrass meadows shifted the ecosystem to an alternate stable state with a highly turbid water column that has arrested reestablishment despite restoration efforts (van derHeide et al. 2007). This high turbidity state is a result of sediment suspension that has occurred in the absence of the stabilizing influence of the meadow on the sediment (van derHeide et al. 2007). Since the removal of seagrass leads

to the breakdown of biophysical feedbacks, investigating the interaction of these plants with their fluid environment is critical to recovery.

Sediments in seagrass systems collect detrital matter from increased sedimentation and therefore serve as a nutrient supply (Chapelle 1995; Risgaard-Petersen et al. 1998). In addition, seagrass meadows can grow in or near anoxic sediments, which build up phosphate and ammonium as a result of increased alkalinity and sulfate reduction processes (Hines and Lyons 1982). The delivery of nutrients, oxygen, and carbon dioxide, the removal of waste, and the alteration of diffusive boundary layer thickness controlling chemical and gas exchange at the sediment-water interface are driven by the degree of flow penetration through the meadow. Thus, the influence of meadows on current speeds and velocity profiles will govern sedimentation and resuspension, which is critical for predicting the distribution of natural materials and contaminants (Shi et al. 2006). Due to the reduction of velocity within seagrass canopies, pressure gradients form that drive vertical flows on the downstream side of the stems and cause exfiltration of the pore-water, advecting nutrients out of the sediment, where they are produced by microbial activity, up into the canopy (Nepf and Koch 1999). Seagrasses are able to take up nutrients both in the sediment, through the rhizome, as well as directly from the water column, with their leaves (Cornelisen and Thomas 2004; Risgaard-Petersen et al. 1998; Stapel et al. 1996). Nitrogen fluxes can be controlled by light dependent nitrogen uptake in eelgrass leaves, accounting for 60% of the plant's nitrogen requirement for growth (Risgaard-Petersen et al. 1998). Bottom shear stress and turbulent energy dissipation in *T. testudinum* meadows have been shown to influence ammonium uptake rates on the seagrass leaves (Cornelisen and Thomas 2004). In a mixed

community sparsely populated by seagrass, ammonium uptake occurred near the mass-transfer limit (Cornelisen and Thomas 2009). Nutrient flux across the sediment water interface also occurs in seasonal patterns (Boynton and Kemp 1985) and can be released through sediment resuspension (Laima et al. 1998; Wainright 1990). Gacia and Duarte (2001) discovered that 85% of annual sediment deposition in seagrass beds was due to the re-settling of locally resuspended particles. This suggests that although the particles may not be transported out of the system, resuspension may still be significant and important to turbidity, nutrient dynamics, and aeration of the sediments. Therefore, understanding how turbulence and mixing across seagrass canopies is driven by local flow conditions is critical to restoration planning.

Most of the work to date on sedimentation, resuspension, and nutrient dynamics around biological structures has not considered the effects of waves and is predominantly composed of laboratory simulations and hydrological modeling based on uncertain drag coefficients (Abdelrhman 2003; Fonseca and Fisher 1986; Ghisalberti and Nepf 2002; Ghisalberti and Nepf 2005; Nepf et al. 2007; Peterson et al. 2004; Shi et al. 2006). The dynamics of waves are vastly different from unidirectional flows, are characteristic of many marine systems, and are not well understood in seagrass beds (Bryan et al. 2007). While unidirectional flow skims over beds (Koch and Gust 1999), waves cause blades to oscillate back and forth increasing fluid exchange across the canopy. This waving of seagrass blades drives flow within the canopy (Ackerman and Okubo 1993). Grizzle et al. (1996) found that in an undulating seagrass canopy, the tips of the blades contacted a greater amount of water and experienced enhanced turbulent mixing. Overall, the degree of flow reduction by the canopy is a function of velocity, wave frequency, and meadow

morphology (distance from the edge of the canopy, shoot density, strap-bladed or cylindrical blade morphology, and depth below the surface) (Fonseca and Fisher 1986; Verduin and Backhaus 2000), the result of which causes sedimentation (Gacia and Duarte 2001). Orbital velocities reaching the seagrass meadow cause blades to oscillate, disrupting the development of a boundary layer and skimming flow over the meadow. This facilitates the exchange of nutrients and waste products within the canopy. In *T. testudinum* meadows, oscillatory flows were found to enhance uptake rates of ammonium dependent on water velocity and turbulent kinetic energy (Thomas and Cornelisen 2003). The delivery of nutrients to the seagrass blades stimulates growth and photosynthesis. Waves can also increase pore water exchange between the sediment and overlying water column (Precht and Huettel 2003), and the interaction of waves and currents can increase bottom shear (Bricker et al. 2005), resulting in greater resuspension potential (Jing and Ridd 1996), and reducing the minimum depth limit for seagrass growth (Stevens and Lacy 2012).

Seagrass systems worldwide have been threatened for some time (Waycott et al. 2009). Seagrass meadows in the Everglades have suffered from disease (Robblee et al. 1991), sulfide toxicity (Carlson et al. 1994), decreased light availability (Hall et al. 1999), and severe fluctuations in salinity (Zieman et al. 1999). In the coastal lagoons of Virginia, seagrass meadows were devastated by eelgrass wasting disease and a destructive hurricane (Orth et al. 2006; Short et al. 1987). For these reasons, research efforts for this dissertation concentrate on seagrass systems in Florida and Virginia with the goal of understanding hydrodynamic parameters contributing to sediment resuspension and ecosystem function. Integrated data on physical and biological interactions in these

systems will aid in determining the thresholds for positive and negative effects of wave motion, sedimentation, resuspension, turbulence, and fluid retention and circulation within seagrass meadows. Understanding these relationships *in situ* allows for more appropriate modeling of these ecosystems, more precise predictions of future growth, and has vast impacts on the success of conservation planning.

## RESEARCH QUESTIONS

This study investigates biophysical interactions within two different seagrass ecosystems under current and wave dominated flows. Specifically, this study focuses on the following questions:

- (1) How does seagrass shoot density and meadow morphology influence turbulence and wave development?
- (2) What are the combined effects of waves and currents, in concert with meadow morphology, on sediment suspension?
- (3) How are the driving mechanisms for mixing across a seagrass canopy influenced by shoot density and flow conditions?

In order to investigate the influences of shoot density on local hydrodynamics, physical parameters of water velocity, turbulence intensity, wave height and period, and suspended sediment concentration were measured across a spatial density gradient of *Zostera marina* in a temperate, lagoonal system in coastal Virginia. Since canopy height and location within the meadow also influence the hydrodynamics and resulting sediment suspension, the same meadow was monitored seasonally over a one-year period. By holding the location constant, alterations to the fluid environment, as compared to an

unvegetated site, were controlled by the seasonal senescent pattern of the meadow. Finally, to determine fine-scale mixing parameters, two different density *Thalassia testudinum* meadows in the clear, relatively low energy waters of Florida Bay were monitored utilizing an underwater particle image velocimetry technique.

## DISSERTATION OUTLINE

The chapters that follow detail field experiments employed to investigate these biophysical interactions. Chapters 2 and 3 address research questions 1 and 2. First, in Chapter 2, results from a spatial density gradient study are presented. Four locations, one unvegetated and three within a large *Z. marina* meadow in South Bay, Virginia, were chosen with shoot densities varying from 150 to 560 shoots  $\text{m}^{-2}$ . Each of the four sites was measured over a 5-week period from May to June 2010. Results quantify the influence of both shoot density and the location within the meadow on wave development and turbulence magnitude. Further, differences in turbulence under tidal- and wave-dominated flows are presented. Lastly, the relative responses of sediment suspension to bed shear stresses from combined current and wave flows based on both shoot density and the location within the meadow are discussed.

In Chapter 3, alterations to the seagrass meadow due to seasonal growth and senescence are presented. The highest density seagrass and unvegetated sites from Chapter 2 were monitored for 1 year, following the data presented in Chapter 2, in June 2010 (Chapter 2 data), October 2010, January 2011, March 2011, and June 2011. Results quantify how changes in meadow structure control wave development and turbulence magnitudes near the seafloor, and how oscillatory motion penetrates the meadow as a

function of seagrass shoot density. Also, how canopy development (through seasonal senescence and re-growth) controls the degree of sediment suspension, shifting the environment from depositional to erosional through the seasons, is discussed.

Chapter 4 addresses the third research question of fine-scale mixing within a seagrass meadow through the use of a novel *in situ* particle image velocimetry (PIV) system. PIV allows for detailed visualization of flow and turbulence structure over a 70-cm<sup>2</sup> area across the seagrass canopy. Due to the two dimensional spatial resolution, mixing at the canopy can be investigated through analysis of the turbulent kinetic energy (TKE) budget and the efficiency of momentum transport. A spatial density gradient across *T. testudinum* meadows in Florida Bay was established and mixing parameters were analyzed for unidirectional and oscillatory flows.

Finally, Chapter 5 summarizes conclusions of the influence of seagrass structure on flow attenuation, turbulence structure, wave development, and sediment suspension. Also, comparisons between these similar meadows, in very different environments, are addressed.

**CHAPTER 2:****Wave and tidally driven flows in eelgrass beds and their effect on sediment suspension\***

\*This chapter has been published, with citation: Hansen, JCR, and MA Reidenbach (2012) Wave and tidally driven flows in eelgrass beds and their effect on sediment suspension. *Marine Ecology Progress Series* 448: 271-287.

**ABSTRACT**

Seagrass beds alter their hydrodynamic environment by inducing drag on the flow, thereby attenuating wave energy and near-bottom currents. This alters the turbulent structure and shear stresses within and around the seagrass bed that are responsible for the suspension and deposition of sediment. To quantify these interactions, velocity, pressure, and sediment measurements were obtained across a density gradient of an eelgrass *Zostera marina* bed within a shallow coastal bay (1 to 2 m depth). Eelgrass beds were found to reduce near-bottom mean velocities by 70 to 90%, while wave heights were reduced 45 to 70% compared to an adjacent unvegetated region. Wave orbital velocities within the eelgrass bed were reduced by 20% compared to flow above the bed, primarily acting as a low-pass filter by removing high-frequency wave motion. However, relatively little reduction in wave energy occurred at lower wave frequencies, suggesting that longer period waves were able to effectively penetrate the seagrass meadow.

Average bottom shear stresses ( $\tau_b$ ) at the unvegetated region were  $\tau_b = 0.17 \pm 0.08 \text{ N m}^{-2}$ , significantly larger than the critical stress threshold necessary for sediment entrainment

of  $0.04 \text{ N m}^{-2}$ . Within the eelgrass bed,  $\tau_b = 0.03 \pm 0.02 \text{ N m}^{-2}$  and stresses were below the critical stress threshold during 80% of the time period of measurement. Expansion of eelgrass within the coastal bay has thus altered the dynamics of the seafloor from an erosional environment to one that promotes deposition of suspended sediment, enhancing light penetration throughout the water column and creating a positive feedback for eelgrass growth.

## INTRODUCTION

Seagrass ecosystems have been viewed as depositional environments for sediment because the structure of the meadow serves to reduce flow and attenuate bottom shear stresses (Gruber and Kemp 2010; Koch et al. 2006; Ward et al. 1984). Studies of direct particle trapping by seagrasses and seagrass epiphytes confirm that seagrass meadows buffer against sediment resuspension and increase sediment retention, therefore reducing erosion in the coastal zone (Agawin and Duarte 2002; Gacia and Duarte 2001). When fluid flow encounters individual seagrass blades or a seagrass bed, drag is imparted on the flow and a velocity gradient develops, creating a boundary layer (Denny 1988). Momentum loss due to drag by the canopy leads to the reduction in resuspension; however, reduced resuspension and increased sediment accumulation may not occur at the same rate everywhere within the meadow, and are dependent upon local flow dynamics and sediment supply from within and outside the meadow (Chen et al. 2007). Whether bulk flow is able to move through the seagrass canopy or is diverted above or around it is dependent on shoot density and bed spatial heterogeneity (Fonseca and Koehl 2006; Nepf et al. 2007). Reduction in velocities within seagrass beds is often

accompanied by skimming flow, which increases velocities above the seagrass canopy relative to ambient flow conditions (Fonseca et al. 1982). This creates an inflection point of instability in the velocity profile, and shear layers are developed near the top of the canopy (Bouma et al. 2009; Widdows et al. 2008), which can locally enhance turbulent mixing into the canopy (Nepf and Vivoni 2000). Canopy friction exhibits a strong positive relationship to the percent of the water column occupied by the seagrass (Fonseca and Fisher 1986), and greater flow reductions are found inside canopies with increasing shoot density (Peterson et al. 2004). However, the impact of seagrass on within-canopy turbulence is less clear, and suggests that mixing rates and turbulent kinetic energy (TKE) are highly dependent upon seagrass density and morphology (Granata et al. 2001; Widdows et al. 2008; Worcester 1995).

Within shallow-water environments where seagrasses are abundant, local flow dynamics can be drastically altered depending on whether currents are dominated by tides, wind-generated waves, storm surge, or a combination of these factors (Fonseca and Cahalan 1992; Koch and Gust 1999; Koch et al. 2006). The increase in oscillatory flows caused by waves has been linked to enhanced turbidity (Granata et al. 2001). The nonlinear interaction between waves and currents leads to changes in the hydrodynamics and shear stresses imposed on the seafloor from those expected under either condition independently (Jing and Ridd 1996). Typically when waves are present in unvegetated seafloor regions, an oscillatory wave boundary layer develops that is more strongly sheared than the boundary layer formed under steady conditions alone (Grant and Madsen 1979). This wave boundary layer results in greater drag on the mean flow and increased bottom shear stresses. Sediment resuspension has been found to be

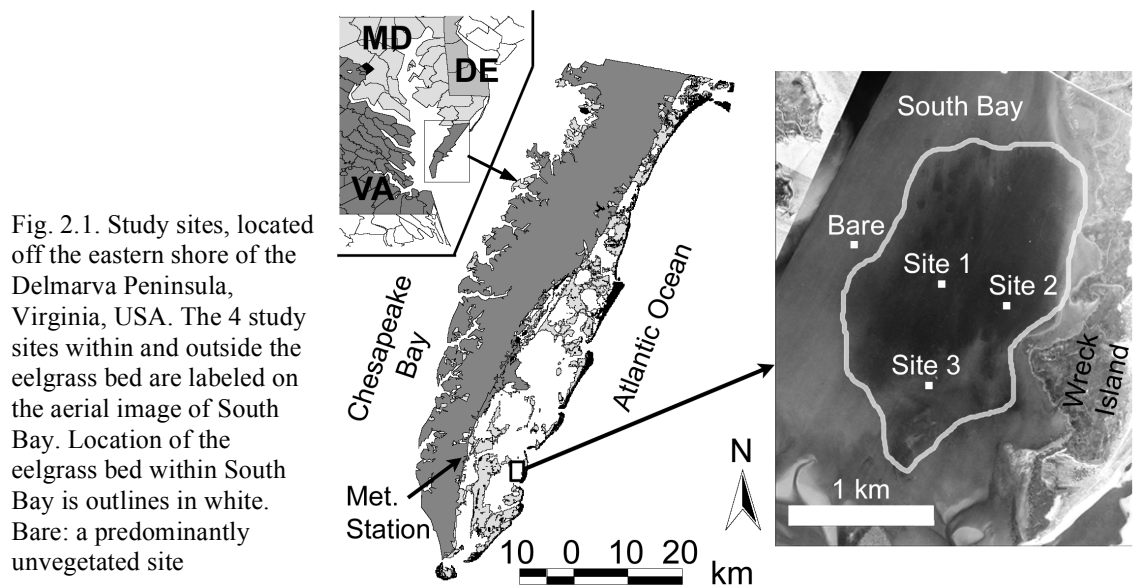
predominately controlled by waves in shallow coastal bays, occurring periodically and corresponding to high wind events (Lawson et al. 2007), suggesting sediment suspension is episodic in nature. Many studies have described how seagrasses attenuate waves (Bradley and Houser 2009; Fonseca and Cahalan 1992; Koch and Gust 1999); however, how this attenuation impacts bottom shear stresses and within-canopy turbulence, which are ultimately responsible for the suspension of sediments from the seafloor, is largely unknown.

Most studies that have addressed the impacts of seagrass density and morphology on flow and sediment dynamics have been based on laboratory flume experiments or numerical modeling (Bouma et al. 2009; Carr et al. 2010; Chen et al. 2007; Heller 1987). These studies have determined that the thickness of the shear layer at the top of the canopy is directly related to the vegetation density; as density is increased under a constant velocity, the exchange is reduced, as is the penetration depth of the mixed layer into the canopy (Ghisalberti and Nepf 2002). For waves that are typically generated in fetch-limited shallow coastal bays, wave energy decreases with depth, and the magnitude of wave energy that reaches the seafloor depends heavily on the wave period, wave height, and overall water depth (de Boer 2007). According to modeling efforts, wave energy attenuation increases with increasing shoot density (Chen et al. 2007), but the degree of flow reduction by the canopy can also be a function of distance from the edge of the canopy and the mean depth at which the seagrass resides below the surface (Fonseca and Fisher 1986; Verduin and Backhaus 2000). However, the lack of field studies on these interactions makes it difficult to understand the role of seagrass structure on near-bottom turbulence, bottom shear, and sediment dynamics (de Boer 2007).

Consequently, it is important to explore the dynamic interactions between seagrass meadows and fluid motion on multiple spatial and temporal scales.

Within the coastal bays of Virginia, USA, the once dominant seagrass species *Zostera marina* (eelgrass) virtually disappeared during the 1930s due to a pandemic infestation of a parasitic fungus, called wasting disease, combined with a destructive hurricane (Orth et al. 2006; Short et al. 1987). The discovery of several small, natural patches of eelgrass in the mid-1990s suggested that certain locations within the coastal bays were adequate for plant growth (Orth et al. 2006). Survival and expansion of these plots initiated an intensive, large-scale eelgrass seeding program to re-establish the Virginia coastal bays (Fig. 2.1) as a self-sustaining seagrass ecosystem (Orth et al. 2012). The shallow depths of Virginia coastal bays, typically < 2 m depth, make the bottom sediments susceptible to current- and wave- induced sediment suspension. These coastal bays also lack any significant riverine discharge, and therefore turbidity is primarily controlled by local resuspension (Lawson et al. 2007). In addition, low pelagic primary productivity in the coastal bays suggests that light attenuation is primarily controlled by non-algal particulate matter (McGlathery et al. 2001; Sand-Jensen and Borum 1991). High suspended sediment concentrations (SSC) can attenuate light penetration through the water column that can limit benthic primary production (Zimmerman et al. 1995). As a result, subsequent changes in the fluid environment due to the eelgrass expansion now being observed in these coastal bays (Orth et al. 2012) may improve water quality and reduce turbidity, thus increasing light penetration to the seafloor, which has been shown to have a positive feedback effect on seagrass growth (Carr et al. 2010; Madsen et al. 2001).

In coordination with the seagrass seeding program, the focus of the present study was on the relationships between physical and biological forces controlling water circulation, flow structure, and suspended sediment within the seagrass beds and the Virginia coastal bay system. The goals were to quantify: (1) the spatial variation of *Zostera marina* morphology across the meadow, (2) the velocity and turbulence levels above and within the *Z. marina* canopy, (3) the bottom shear stresses due to combined currents and waves, (4) and the response of the SSC to local turbulence and shear stress magnitudes. These parameters were compared to flow and sediment dynamics occurring in an adjacent unvegetated region.



## METHODS

Seagrass studies were performed in South Bay, one of the coastal bays within the Virginia Coast Reserve (VCR), where ongoing seagrass restoration efforts are being performed. The VCR is characterized by contiguous marsh, shallow bay, and barrier island systems and is a National Science Foundation – Long Term Ecological Research

(NSF-LTER) program site (Fig. 2.1). Reseeding of eelgrass *Zostera marina* in South Bay began in 2001 (Orth et al. 2012). Field studies were performed in May and June of 2010, with instrument deployments and field data collection occurring over a 72 h period at each site. Three seagrass sites were chosen of varying density, each surrounded by a *Z. marina* dominated area of at least 700 m<sup>2</sup>. During summer 2010, the total eelgrass cover in South Bay was estimated to be 1020 ha (Orth et al. 2012). A predominantly unvegetated site, containing only very few, small patches of eelgrass within the region, was also monitored as a reference for flow characteristics in the absence of any considerable benthic vegetation (“Bare” in Fig. 2.1). Eelgrass density was measured in the field via 0.25 m<sup>2</sup> quadrat shoot counts, while blade length and width were measured in the laboratory from eelgrass collected at each site (Table 2.1). The 3 sites, labeled Sites 1, 2, and 3 in Fig. 2.1, contained *Z. marina* of varying densities of 560 ± 70, 390 ± 80, and 150 ± 80 shoots m<sup>-2</sup>, respectively. Mean blade lengths ranged from 16 to 28 cm. Densities between each of the 3 sites, as well as mean blade lengths, were significantly different from one another (one-way ANOVA,  $p < 0.05$ ). Measurements were taken throughout 3 consecutive weeks from June to July 2010, a period in the growing season

Table 2.1. *Zostera marina*. Morphometrics during the summer of 2010 at 3 neighboring sites in South Bay, Virginia, USA. Eelgrass density was measured using *in situ* 0.25 m<sup>2</sup> quadrat shoot counts. Blade length is the mean length of all eelgrass blades measured, maximum length is the average of the longest 10% of all blades, and blade width was measured at the midpoint along the length of the blade. Values are ± SD. n<sub>blades</sub>: number of blades measured for length and width; n<sub>density</sub>: number of 0.25 m<sup>2</sup> quadrats measured

	Blade length (cm)	Max. Length (cm)	Blade width (cm)	n <sub>blades</sub>	Density (shoots m <sup>-2</sup> )	n <sub>density</sub>
Site 1	21 ± 8	33 ± 3	0.29 ± 0.08	158	560 ± 70	9
Site 2	28 ± 13	51 ± 3	0.41 ± 0.12	176	390 ± 80	8
Site 3	16 ± 9	34 ± 4	0.26 ± 0.07	73	150 ± 80	21

when the eelgrass is near peak biomass (Orth et al. 2006). Mean water depth at all study sites ranged between 1.4 and 1.8 m. Bathymetry for the coastal bays throughout the VCR is provided in Fagherazzi and Wiberg (2009).

### **Instrumentation**

A coordinated package of instrumentation was deployed at each site for a minimum of 72 h. Two Nortek Vector acoustic Doppler velocimeters (ADV) were deployed at each site, and velocity was quantified at a single point within a  $1 \text{ cm}^3$  sampling volume located 15 cm below each sensor. One ADV was located within the meadow with its sampling volume at  $z = 0.1$  m above the seafloor, and the other ADV was located above the meadow with its sampling volume at  $z = 0.5$  m. To measure velocities within the meadow, a small eelgrass patch of 15 cm diameter (the size of the instrument probe) was removed to prevent blades from blocking the sampling volume. In addition, values with poor correlation factors, often due to the probes being exposed at low tide, were removed. Velocities were measured at each site in 10 min bursts every 20 min at a sampling rate of 32 Hz. Each ADV was equipped with a pressure sensor, which was used to determine the water depth and characterize the wave climate. Wind data were obtained from a meteorological station in Oyster, Virginia, located approximately 4 km from South Bay (Fig. 2.1).

Sediment grain size distribution was characterized at each site using a laser diffraction particle size analyzer (Beckman Coulter LS I3 320). Sediment samples were sieved at 1 mm to remove large organic matter, such as eelgrass blades and roots, and then bleached to remove particulate organic matter. The size class distribution was found,

and  $D_{84}$ , the grain size diameter for which 84% of the sample grain diameters are smaller, was computed from the resulting size distribution curve. At least 2 samples were collected and analyzed from each site. Sediment  $D_{84}$  at the bare site was  $157 \pm 7 \mu\text{m}$ , while, at the eelgrass sites, sediments were finer at  $130 \pm 17 \mu\text{m}$ . SSCs were measured using 2 optical backscatter sensors (OBSs; Campbell Scientific OBS3+). One OBS was placed within the meadow to quantify SSC at  $z = 0.1 \text{ m}$ , and another, above the canopy at  $z = 0.5 \text{ m}$ , where  $z$  is the vertical distance above the seafloor. To perform laboratory calibrations of the OBS, sediment samples were collected, suspended, and known volumes of suspended sediment were mixed into 60 l of filtered seawater. Suspended sediment sample volumes were then dried and weighed, and a linear regression was formed between the backscatter intensity from the OBS and the SSC. Each calibration had an  $R^2 > 0.99$ .

### **Wave-turbulence decomposition**

Instantaneous velocity measurements were collected in the east-north-up (ENU) reference frame using the internal compass and tilt sensors of the velocimeters and were time-averaged independently for every 10 min burst interval. Velocities were then rotated for each burst interval into the dominant direction of horizontal flow,  $u$ . Mean velocity and turbulence statistics were computed along the dominant flow direction ( $u$ ), transverse direction ( $v$ ), and vertical direction ( $w$ ). The 10 min time interval was chosen because in statistical tests, 10 min often emerges as the best balance between obtaining convergence of the mean statistics while minimizing velocity drift due to changes in flow conditions (Gross and Nowell 1983).

In flows with both waves and currents, the variance in velocity associated with waves is often much larger than that associated with turbulence and some form of wave – turbulence decomposition must be performed (Trowbridge 1998). When waves and currents are present, the instantaneous horizontal and vertical velocities can be written as:

$$\begin{aligned} u &= u' + \tilde{u} + \bar{u} \\ w &= w' + \tilde{w} + \bar{w} \end{aligned} \quad (1)$$

where  $\bar{u}$  and  $\bar{w}$  are the horizontal and vertical components of the mean velocity,  $\tilde{u}$  and  $\tilde{w}$  are the wave-induced orbital velocities, and  $u'$  and  $w'$  are the turbulent velocities. To determine motions that contribute to the turbulent Reynolds stress,  $\overline{u'w'}$ , turbulent motions must be separated from that of waves. The method of wave-turbulence decomposition that was employed uses spectral decomposition, known as the phase method (Bricker and Monismith 2007), where the phase lag between the  $u$  and  $w$  components of the surface waves are used to interpolate the magnitude of turbulence under the wave peak. The wave stress is calculated through the spectral sum:

$$\overline{\tilde{u}\tilde{w}} = \int_{-f_{Nyquist}}^{f_{Nyquist}} S_{\tilde{u}\tilde{w}}(f) d(f) \quad (2)$$

where  $S_{\tilde{u}\tilde{w}}(f)$  is the 2-sided cross-spectral density (CSD) of the wave-induced orbital velocities,  $f$  is frequency and  $f_{Nyquist}$  is the Nyquist sampling frequency, which is half the sampling frequency of the discrete signal. The turbulence spectrum can be expressed as the difference between the spectrum of raw velocities and that of wave-induced orbital velocities such that:

$$S_{u'w'}(f) = S_{uw}(f) - S_{\tilde{u}\tilde{w}}(f) \quad (3)$$

The CSD of the spectra in Eq. (3) are then integrated to obtain the turbulent Reynolds stress:

$$\overline{u'w'} = \overline{uw} - \overline{\tilde{u}\tilde{w}} \quad (4)$$

$U_j = U(f_j)$  and  $W_j = W(f_j)$  are the Fourier transforms of  $u(t)$  and  $w(t)$  at the frequency  $f_j$  in the Fourier transform. For a finite data series, the integral of the wave stress becomes:

$$\overline{\tilde{u}\tilde{w}} = \sum_{j=-N/2}^{j=N/2} \tilde{U}_j \times \tilde{W}_j \quad (5)$$

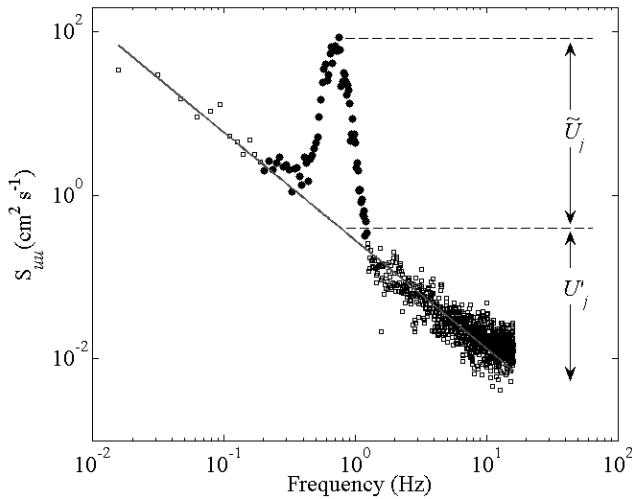


Fig. 2.2. Power spectral density (PSD) of the horizontal velocity,  $S_{uu}$ , for a 10 min representative data series computed at  $z = 0.1$  m at the bare site, where  $z$  is the vertical distance above the seafloor. Solid circles: region encompassing wave peak; squares: region of the spectra outside the wave domain. Grey solid line: least squares fit to the data outside the wave domain. The wave component of the stress is removed by subtracting the PSD formed above the grey line that encompasses the region of the wave peak

The same method is used to solve for  $\tilde{U}_j$ . The Fourier coefficients can be written in phasor notation as:

$$\overline{\tilde{u}\tilde{w}} = \sum_{j=wave\_peak} \tilde{U}_j \times \tilde{W}_j = \sum_{j=wave\_peak} |\tilde{U}_j| |\tilde{W}_j| \cos(\angle W_j - \angle U_j) \quad (7)$$

where  $N$  is the number of data points used in the Fourier transform and the magnitude of  $\tilde{W}_j$  is the difference between the raw  $W_j$  and the turbulence  $W'_j$  interpolated below the wave peak, via a least-squared fit straight line, as shown in Fig. 2.2.  $\tilde{W}_j$  is solved for by expressing the wave stresses in terms of power spectral density (PSD):

$$S_{ww_j} = \frac{1}{df} |W_j|^2 \quad (6)$$

where  $\angle W_j$  and  $\angle U_j$  are the phases of the Fourier coefficients. The wave stress is then found by integrating the wave component of CSD,  $S_{\tilde{u}\tilde{w}}(f)$ , over the width of the wave peak and subtracting it from the integral of the total stress,  $S_{uv}(f)$ , over the full frequency spectrum in order to obtain the Reynolds stress, as in Eq. (4).

### Wave orbital velocities

The spectral density of surface elevation,  $S_{\eta p}$ , was computed using the pressure signal from the ADV located at  $z = 0.5$  m as:

$$S_{\eta p} = \left[ \frac{\cosh(kh)}{\cosh(kz)} \right]^2 \frac{S_{pp}}{\rho^2 g^2} \quad (8)$$

where  $S_{pp}$  is the spectral density of the pressure,  $k$  is the wave number ( $\text{m}^{-1}$ ,  $=2\pi/L$  where  $L$  is wavelength),  $h$  is the mean water depth,  $z$  is the vertical distance above the seafloor,  $g$  is gravitational acceleration and  $\rho$  is density (Dean and Dalrymple 1991). Significant wave height ( $H_s$ ) and average period ( $T$ ) were then computed using the first ( $m0$ ) and second ( $m2$ ) moments from the  $S_{\eta p}$  power spectrum:

$$H_s = 4\sqrt{m0} \quad T = \sqrt{m0/m2} \quad (9)$$

where  $m0 = \int S_{\eta p}(f) d(f)$  and  $m2 = \int f^2 S_{\eta p}(f) d(f)$ .

To determine the interaction between eelgrass structure and wave-induced flows, wave orbital velocities were calculated and compared above and within the eelgrass meadow. Adjacent to the seafloor, vertical orbital velocity approaches zero and thus the horizontal component of the orbital velocity accounts for the majority of particle motion. The horizontal orbital velocity can be calculated from spectra of the horizontal velocity

components,  $u$  and  $v$ , by summing the contributions from wave spectra across each frequency component (Wiberg and Sherwood 2008):

$$u_{os}^2 = 2 \left[ \sum_j S_{\bar{u}\bar{u}_j} \Delta f_j + \sum_j S_{\bar{v}\bar{v}_j} \Delta f_j \right] \quad (10)$$

where  $u_{os}$  is equivalent to the root-mean-squared (rms) orbital velocity. Since only the wave spectra are used and not the full spectrum, this method removes water motion due to turbulence and currents driven by the tides. Eq. (10) can then be applied to velocities above and within the canopy to determine seagrass impacts on orbital wave motion.

## RESULTS

Physical characteristics of wind speed, water temperature and depth, as well as depth-averaged water currents, significant wave height, and SSCs measured at each *Zostera marina* site are shown in Fig. 2.3. The bay had a mean depth of approximately 1.6 m, and the average wind speed between May and June 2010 was  $2.3 \pm 1.2 \text{ m s}^{-1}$ . Over the course of the sampling period, water temperatures in the bay steadily increased from 21 to 30°C. The flow regime in South Bay was tidally dominated; therefore, water velocities were low at high and low tide and intensified during ebbing and flooding tides. In addition, flows were typically not symmetric, with ebbing tides characterized by slightly higher velocity magnitudes than flooding tides. Mean tidal amplitude and significant wave height at each site are shown in Fig. 2.4A. Tidal amplitudes ranged from 0.58 to 0.73 m, while  $H_s$  ranged from  $0.18 \pm 0.08 \text{ m}$  at the bare site to  $0.05 \pm 0.02 \text{ m}$  at eelgrass Site 3. Time-averaged velocities at  $z = 0.5$  and  $0.1 \text{ m}$  at each site are shown in Fig. 2.4B. The bare site showed a 40% reduction in velocity between  $z = 0.5$  and  $0.1 \text{ m}$

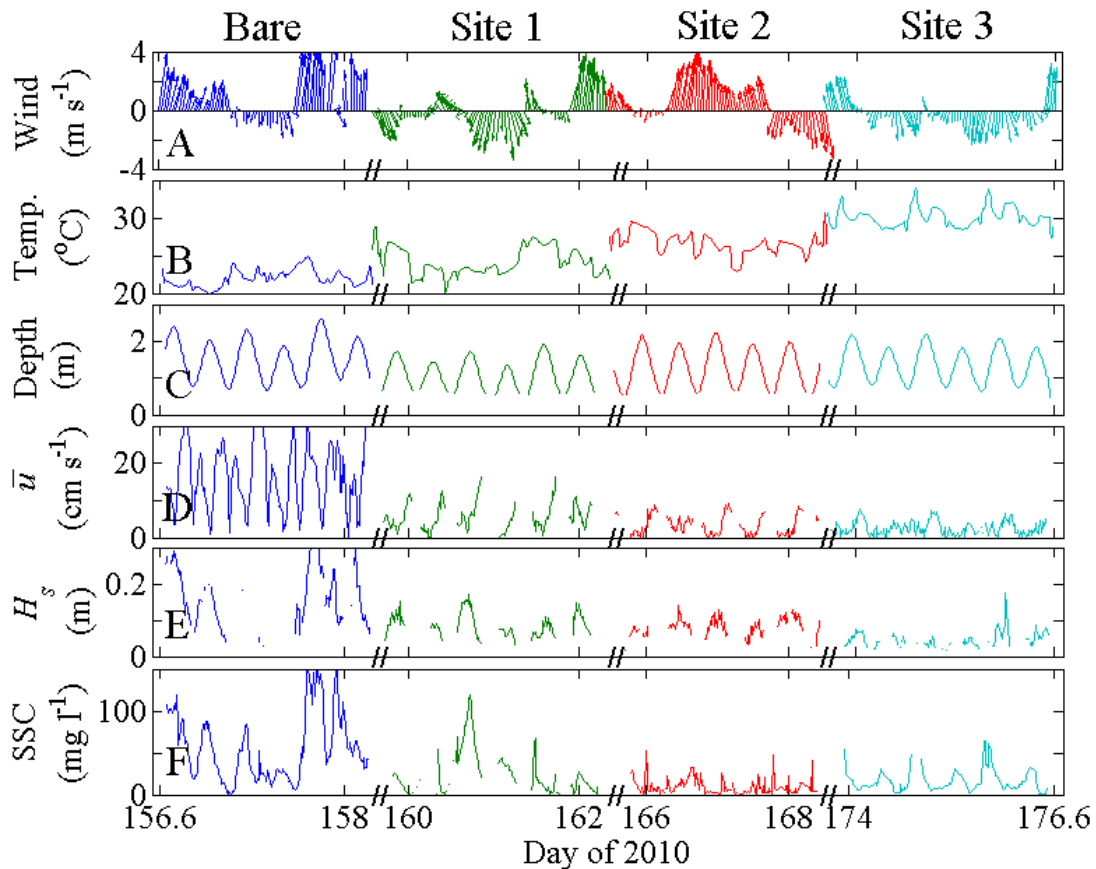


Fig. 2.3. (A) Wind magnitude and direction, (B) water temperature, (C) water depth, (D) magnitude of burst-averaged water speed ( $\bar{u}$ ) at  $z$  (vertical distance above the seafloor) = 0.5 m, (E) significant wave height ( $H_s$ ), and (F) suspended sediment concentration (SSC) at  $z = 0.1$  m. Locations of missing or no data correspond to time periods when velocimeters or sediment sensors has poor signal quality. Note the non-continuous time record, where days between successive monitoring of sites have been removed

due to frictional interaction with the seafloor. In comparison, velocities within the seagrass canopy ( $z = 0.1$  m) showed a 70% reduction in velocity compared to  $z = 0.5$  m due to the combined influence of friction by the seafloor and drag induced by the seagrass canopy.

Waves within these coastal bays were predominately formed by winds, the  $H_s$  of which is controlled by the fetch and bottom topography over which they propagate (Lawson et al. 2007). At the bare site, strong winds were mostly to the north. During these periods, wind-generated waves traveled over stretches of South Bay devoid of eelgrass, with average wind speeds ( $\pm 1$  SD) of  $2.6 \pm 1.4$  m s<sup>-1</sup>. At the eelgrass sites, there

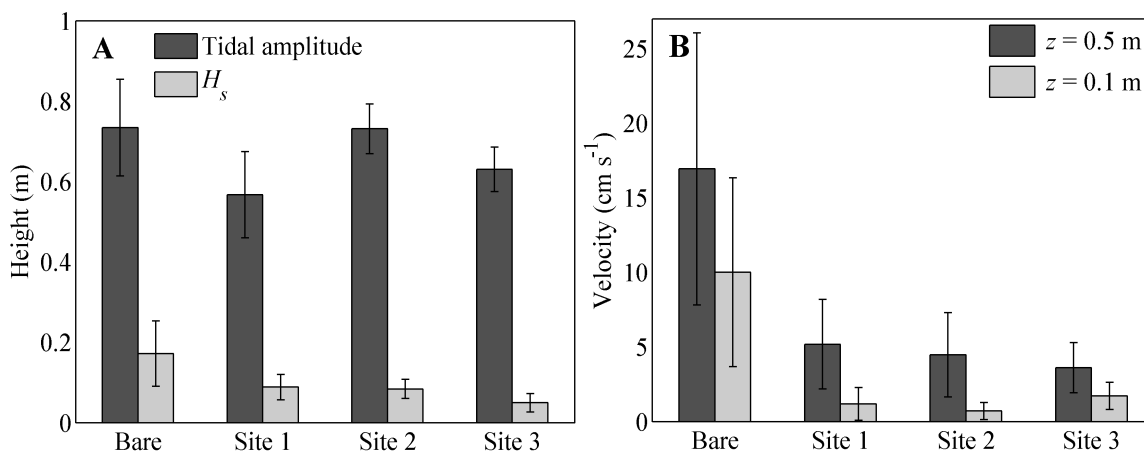


Fig. 2.4. (A) Average tidal amplitudes and significant wave heights ( $H_s$ ) with error bars representing  $\pm 1$  SD. The average across all sites was  $0.65 \pm 0.11$  m. (B) Time-averaged velocity magnitude of the study sites during tidally dominant flow conditions ( $\pm 1$  SD).  $z$ : vertical distance above the seafloor

were no consistent patterns in the wind direction, with winds oscillating from northward to southward (Fig. 2.3A). Average wind conditions at Sites 1, 2, and 3 were  $2.3 \pm 1.2$ ,  $2.4 \pm 1.1$ , and  $1.9 \pm 1.0$  m s<sup>-1</sup>, respectively. For all sites, there was a minimum of 5 km of fetch to both the north and south.  $H_s$  increased at all sites during periods surrounding high

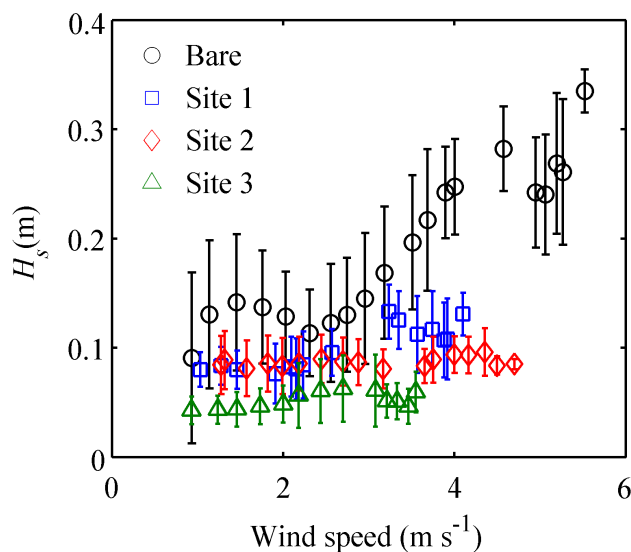


Fig. 2.5. Significant wave height ( $H_s$ ) as a function of mean wind speed. Bars represent  $\pm 1$  SD. Estimates of  $H_s$  were computed as running means over a  $\pm 0.5$  m s<sup>-1</sup> averaging window of wind speed

tide and was reduced during low tide (Fig. 2.3E). Overall, there was a 45 to 70% reduction in measured  $H_s$  at the eelgrass sites compared to the bare site, although changes in wind magnitude and direction during sampling played a factor in wave development and the overall amount of wave reduction (Fig. 2.5). In general, the rate of increase in  $H_s$  with

increasing wind speed was considerably smaller at the eelgrass sites than at the bare site.

### **Turbulent kinetic energy and Reynolds stress**

At each site, flows were separated into time periods where wave action was a significant contributor to the overall flow and those with minimal wave action where flows were dominated by tidally driven currents. Tidally dominated flows were those where the PSD of the wave component of the frequency spectrum,  $S_{\tilde{u}\tilde{w}}$ , constituted  $< 10\%$  of the overall power density,  $S_{uw}$ , measured at  $z = 0.5$  m. Overall, at the bare site, tidally dominated flows occurred 15% of the time, while, at the eelgrass sites, due to wave attenuation across the canopy, tidally dominated flows occurred approximately 25% of the time. There was no statistical difference in time-averaged mean velocity during periods in which tidally dominated or wave- dominated flows occurred. Both Reynolds stress ( $\overline{u'w'}$ ) and turbulent kinetic energy,  $TKE = 0.5(\overline{u'^2} + \overline{v'^2} + \overline{w'^2})$ , were computed at each site (Fig. 2.6), where  $u'$ ,  $v'$ , and  $w'$  are the turbulent velocity fluctuations in the dominant horizontal, transverse, and vertical directions, respectively. At the bare site during tidally dominated time periods, Reynolds stresses,  $\overline{u'w'}$ , were similar at the  $z = 0.5$  and 0.1 m elevations, whereas there was up to a 60% reduction in Reynolds stress magnitude at the eelgrass sites. Although standard deviations for TKE and Reynolds stress were large at all locations, this was primarily due to variations in velocity magnitude caused by waves and tides. Confidence intervals for mean estimates were typically quite small, and locations where significant differences were found between mean estimates of TKE and  $\overline{u'w'}$  at  $z = 0.1$  and 0.5 m are denoted with an asterisk in Fig. 2.6. Comparisons of  $\overline{u'w'}$  within the canopy versus that above the canopy at each site indicated that the largest reduction in  $\overline{u'w'}$  coincided with the most dense

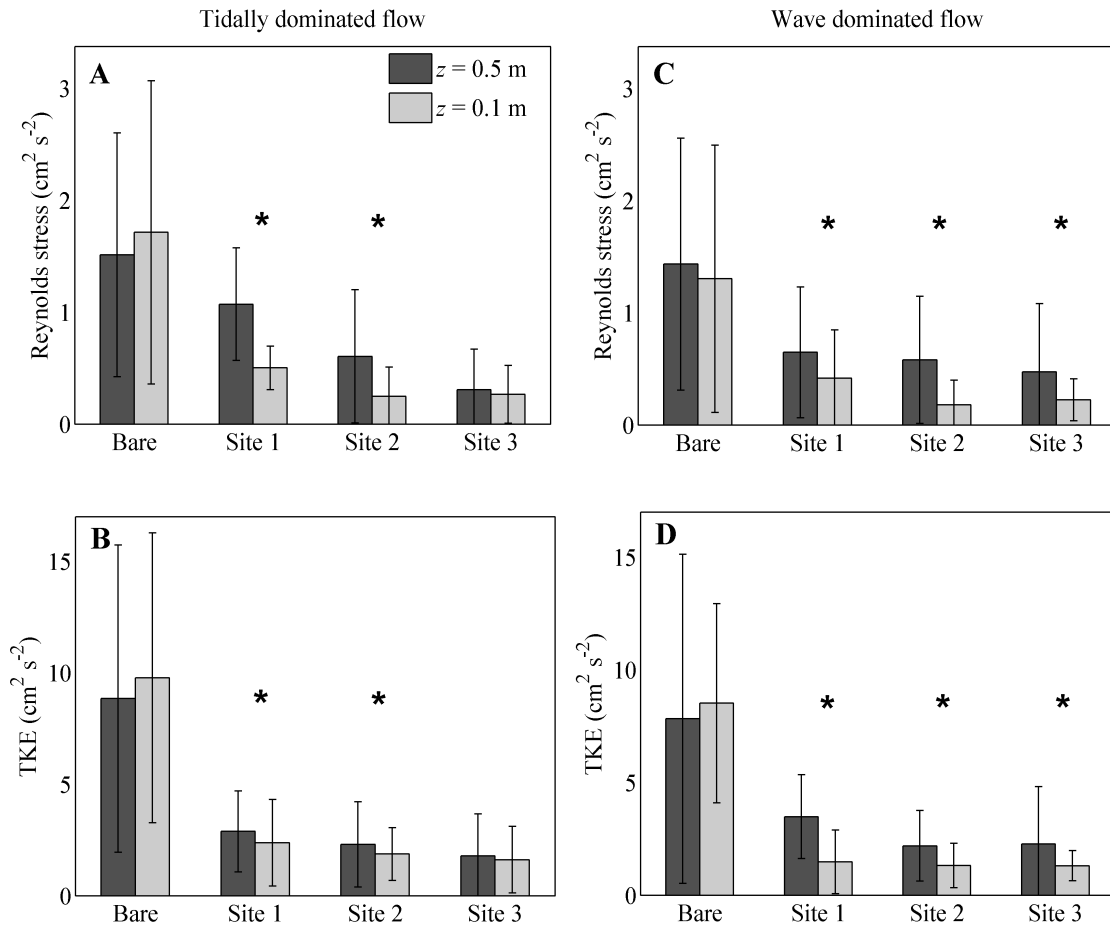


Fig. 2.6. (A) Reynolds stress ( $-\overline{u'w'}$ ,  $\pm 1 \text{ SD}$ ), (B) turbulent kinetic energy (TKE,  $\pm 1 \text{ SD}$ ) for tidally dominated flow conditions, (C) Reynolds stress and (D) TKE for wave-dominated flow conditions. \* Locations where confidence intervals of mean estimates were significantly different between  $z$  (vertical distance above the seafloor) = 0.1 and 0.5 m

eelgrass canopy, Site 1, followed by the mid-density, Site 2, and then the most sparse canopy, Site 3. TKE also showed reductions within the canopy versus above the canopy, but the magnitude of the reduction was significantly less than that of the Reynolds stress. This may be due to the added stem-generated TKE formed by flow interaction with the seagrass blades (Verduin and Backhaus 2000).

To compute Reynolds stress and TKE for wave-dominated flow conditions, the wave components of the PSD were first removed, as in Eq. (3), and then the remaining turbulent component of the PSD was integrated. Overall, the addition of waves did not

statistically alter the magnitude of Reynolds stress or TKE at either the bare site or eelgrass sites (Fig. 2.6C,D). Reynolds stress was typically reduced within the seagrass canopy compared to above the canopy although trends of greater reductions of within-canopy  $\overline{u'w'}$  with higher seagrass densities were not as evident under wave-dominated conditions as they were in tidally dominated flows.

### **Quadrant analysis of turbulence**

Quadrant analysis is a useful technique to describe how turbulent fluctuations contribute to the transport of momentum, sediment, and gases throughout the bottom boundary layer (Lu and Willmarth 1973). Depending upon the flow field, high-momentum fluid overlaying the seagrass canopy can be advected downwards into the canopy, or low-momentum fluid residing within the canopy can be advected upwards out of the canopy. Velocity fluctuations,  $u'$  and  $w'$ , were normalized by their respective standard deviations and were divided into 4 quadrants based on the sign of their instantaneous values. Contours of the turbulent probability distribution function (pdf) are shown in Fig. 2.7 for turbulent motions within and above the eelgrass bed at Site 1 during periods with no wave action. Quadrants are listed from Q1 to Q4. The 2 dominant quadrants responsible for momentum transfer are Q2 ( $u' < 0, w' > 0$ ), where turbulent ejections of low-momentum fluid are transported vertically upwards, and Q4, where sweeping events transport high-momentum fluid downward towards the seagrass meadow. These ejection/sweep phenomena result in intermittent flushing of water masses from within the canopy (Grass 1971). Typically, momentum transport is dominated by ejection and sweeping events and shows a predominance of values in Q2 and Q4, which

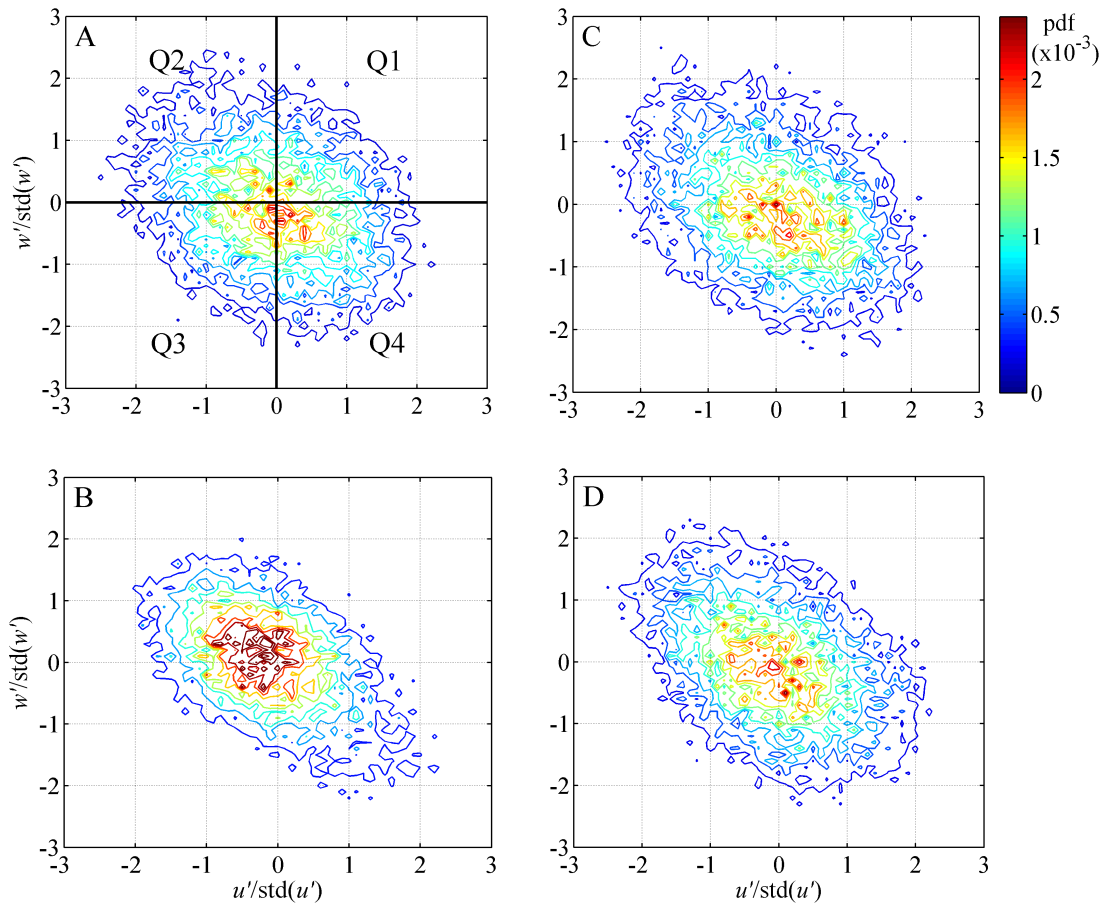


Fig. 2.7. Quadrant analysis of the probability density functions (pdf) of  $u'$  and  $w'$  distributions normalized by their standard deviation (std) at (A,B) *Zostera marina* Site 1 for (A)  $z$  (vertical distance above the seafloor) = 0.5 m and (B)  $z = 0.1$  m, showing the dominance of turbulent sweeping events in Quadrant 4 (Q4), and at (C,D) the bare site for (C)  $z = 0.5$  m and (D)  $z = 0.1$  m

held true for flows above the eelgrass canopy (Fig. 2.7A). The total contribution to Reynolds stress within each quadrant was found by summing the absolute value of the  $u'w'$  contributions within each quadrant and dividing by the total contribution from all quadrants: Q1 (15 %), Q2 (36 %), Q3 (15 %), and Q4 (34 %). This indicated that the combined Q2 and Q4 contributions accounted for approximately 70% of the total Reynolds stress, which is similar to results determined in other studies of flow over high-roughness topographies (Bennet and Best 1996; Lacey and Roy 2008). There was a fairly even distribution of stresses between Q2 and Q4, indicating that the turbulent ejection of

low-momentum fluid from near the top of the seagrass canopy was similar to that of sweeps of high-momentum fluid towards the canopy.

Within the seagrass canopy, at  $z = 0.1$  m, distinct changes in the contribution to the stress from various components occurred (Fig. 2.7B), where motions within Q4 were dominant. The total contribution to Reynolds stress within each quadrant was: Q1 (7 %), Q2 (32 %), Q3 (6 %), and Q4 (55 %). This signifies that the principal exchange of water masses within the canopy was driven by sweeps of high-momentum fluid from above the canopy downwards into the canopy. For the bare site (Fig. 2.7C,D), there was still dominance in Q2 and Q4, with 75 and 79% of the total Reynolds stresses found at  $z = 0.5$  and 0.1 m, respectively. However, there was a fairly even distribution of stresses between Q2 and Q4 at both elevations, similar to the flow structure formed above the seagrass canopy. For instance at  $z = 0.1$  m, contributions were: Q1 (11 %), Q2 (40 %), Q3 (10 %), and Q4 (39 %).

### **Velocity spectra and wave orbitals**

PSDs of the horizontal velocities during tidally dominated flow conditions at the bare site showed a distinct  $-5/3$  slope, indicative of an inertial subrange at both  $z = 0.1$  and 0.5 m (Fig. 2.8A). There was general agreement between the 2 elevations, with slightly higher energy at low frequencies ( $< 1$  Hz) for  $z = 0.5$  m, indicative of higher mean flows, but lower energy at higher frequencies ( $> 1$  Hz), indicating lower turbulent energy within the inertial subrange. Within the eelgrass meadow, there was a reduction in the magnitude of the PSD across all frequencies within the canopy compared to flow above the canopy (Fig. 2.8B).

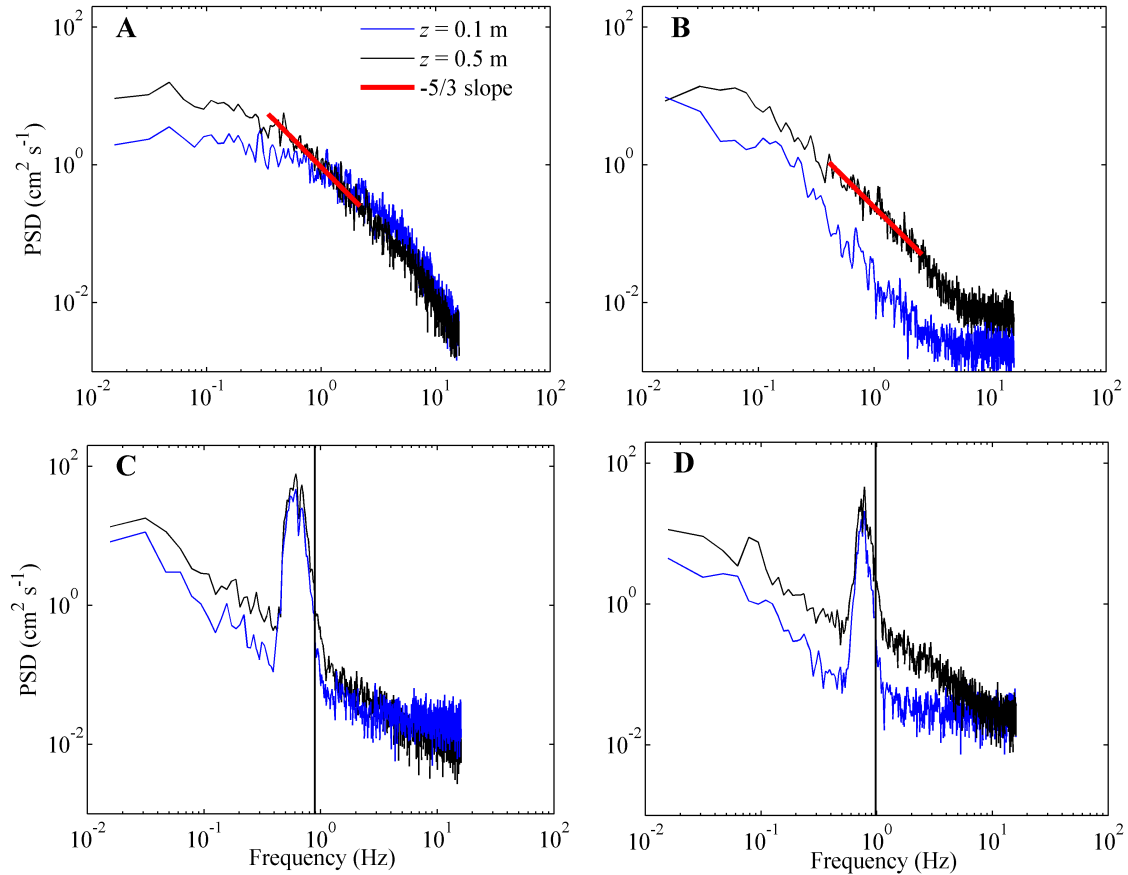


Fig. 2.8. Power spectral density (PSD) of horizontal velocity at the (A) bare site (horizontal component of the mean velocity  $[\bar{u}] = 9.7 \text{ cm s}^{-1}$ ) and (B) Site 2 ( $\bar{u} = 8.4 \text{ cm s}^{-1}$ ) during tidally-dominated flow conditions. Spectra are formed by averaging 9 independent spectra of  $n = 2048$  velocity records that occur within a 10 min time period. PSD for the (C) bare site ( $\bar{u} = 10.8 \text{ cm s}^{-1}$ , significant wave height  $[H_s] = 19 \text{ cm}$ ) and (D) mid-density eelgrass Site 2 ( $\bar{u} = 6.2 \text{ cm s}^{-1}$ ,  $H_s = 14 \text{ cm}$ ) during wave-dominated flow conditions. Vertical line represents the frequency at and above which wave motion is expected to be attenuated at  $z$  (vertical distance above the seafloor) = 0.1 m according to linear wave theory. Flattening of the power density at high frequencies ( $> 0.4 \text{ Hz}$  in Panels B, C, and D) indicates that the noise floor of the instrument has been reached and the velocity signal is indistinguishable from noise

PSD of wave-dominated flow conditions showed similar trends outside the wave domain of the frequency spectrum for both the bare and eelgrass sites. Within the wave domain at the bare site (Fig. 2.8C), there was little wave energy attenuation, indicating that oscillatory motion due to waves was effective at generating wave-induced orbital motions near the seafloor. Within the wave domain at the eelgrass site (Fig. 2.8D), wave energy was still able to penetrate the eelgrass canopy, with little reduction of wave

energy at  $z = 0.1$  m at frequencies smaller than the wave peak. However, at both the bare and eelgrass sites, but especially within the *Zostera marina* canopy (Fig. 2.8D), the bulk of energy loss occurred at wave frequencies within the wave domain at approximately  $f > 1$  Hz, where short period wave oscillations ( $T = 1/f$ ) attenuated before reaching the bottom. This agrees with wave theory that suggests waves will attenuate before reaching the seafloor for  $f = \sqrt{g/(4\pi h)}$  (Wiberg and Sherwood 2008). At a given elevation above the seafloor,  $z$ , waves with  $f = \sqrt{g/[4\pi(h - z)]}$  will be attenuated.

PSD for frequencies between 0 and 2 Hz for both horizontal and vertical velocities are shown for the bare site in Fig. 2.9. These plots include the tidally dominated contributions to the spectra at small frequencies (i.e.  $f < 0.3$  Hz), as well as the

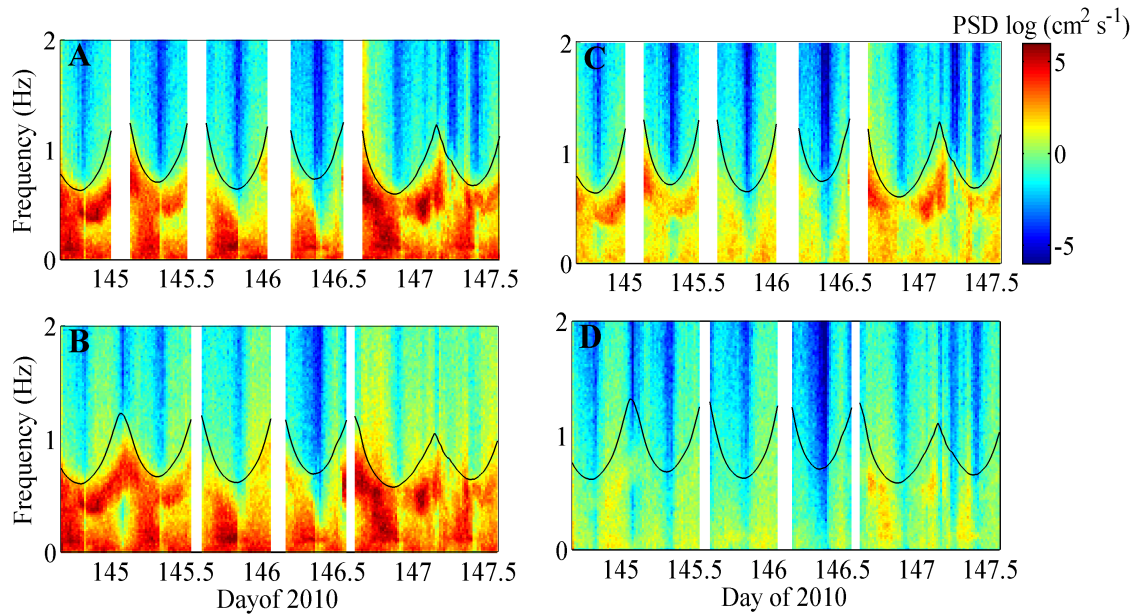


Fig. 2.9. Two-dimensional power spectral density (PSD) at the bare site of horizontal velocities (A)  $S_{uu}$  at  $z = 0.5$  m and (B)  $S_{uu}$  at  $z = 0.1$  m, showing only minor attenuation of the wave frequency band. Two-dimensional PSD of vertical velocities (C)  $S_{wv}$  at  $z = 0.5$  m and (D)  $S_{wv}$  at  $z = 0.1$  m, showing substantial attenuation of the wave frequency band, as predicted by wave theory. Black lines indicate  $f = \sqrt{g/[4\pi(h - z)]}$ , where  $g$  is gravitational acceleration,  $h$  is water depth,  $z$  is the vertical distance above the seafloor, and  $f$  is the frequency at and above which linear wave theory predicts wave motion is attenuated. Regions with no data are during low tide when velocimeters had poor signal quality

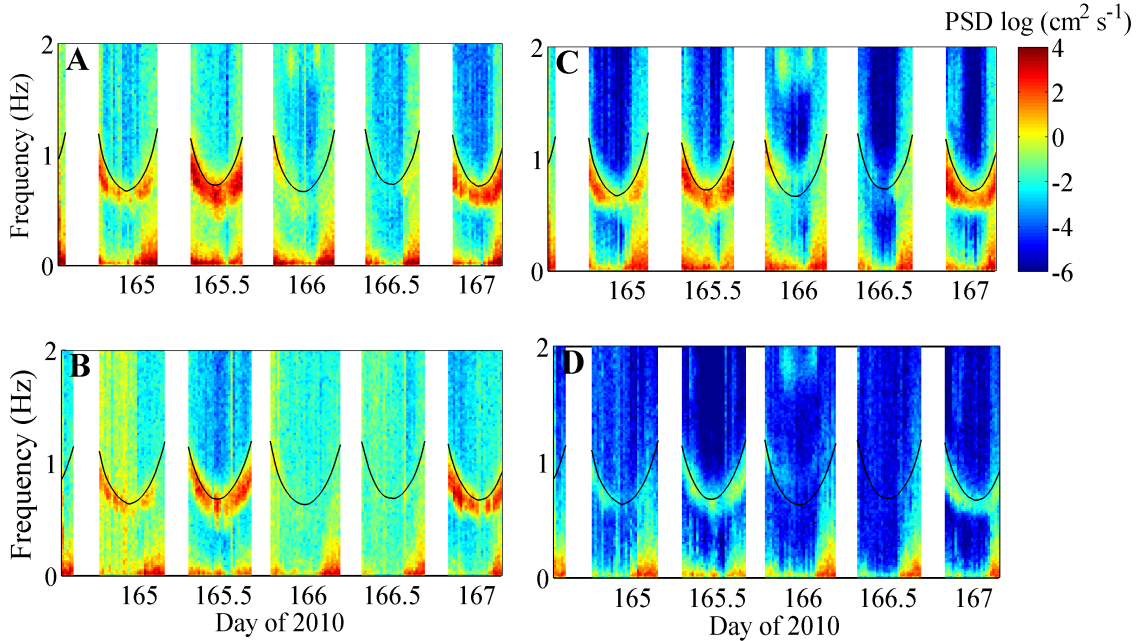


Fig. 2.10. Two-dimensional power spectral density (PSD) at the Site 2 of horizontal velocities (A)  $S_{uu}$  at  $z = 0.5$  m and (B)  $S_{uu}$  at  $z = 0.1$  m. Attenuation of the wave energy within the canopy primarily occurs at high frequency ( $f$ ) within the wave band of the spectrum. Two-dimensional PSD of vertical velocities (C)  $S_{wv}$  at  $z = 0.5$  m and (D)  $S_{wv}$  at  $z = 0.1$  m, showing substantial attenuation of wave energy at all  $f$ -values within the wave band. Black lines indicate  $f = \sqrt{g/[4\pi(h-z)]}$ , where  $g$  is gravitational acceleration,  $h$  is water depth,  $z$  is the vertical distance above the seafloor, and  $f$  is the frequency at and above which linear wave theory predicts wave motion is attenuated

wave component of the PSD, which typically spans the range  $0.3 < f < 1$  Hz. Frequency analysis within the wave domain of the frequency spectra for the bare site indicate that there was a general trend of a reduction of wave energy near the seafloor for the vertical velocity,  $S_{wv}$ , PSD, but a fairly uniform distribution of wave energy throughout the water column for the horizontal,  $S_{uu}$ , PSD. Peak wave frequency at high tide was approximately  $f = 0.5$  Hz ( $T = 2$  s), but as the water depth decreased, peak wave frequency increased to approximately  $f = 1$  Hz, indicating a reduction in the peak wave period to  $T = 1$  s.

For Site 2, similar trends emerged in a reduction of vertical wave energy ( $S_{wv}$ ) within the seagrass bed compared to flow above the canopy (Fig. 2.10). There were also reductions in wave energy within the horizontal component of the velocity,  $S_{uu}$ , due to the wave-dampening effect that the eelgrass had on the flow. However, as is also shown in

Fig. 2.8 for an individual spectrum, much of the reduction in wave energy occurred at the high frequencies within the wave band ( $f > 1$  Hz), which can be attributed both to attenuation due to the interaction with the seagrass and due to the natural attenuation of the waves with depth. The shorter period waves that formed over the seagrass bed (average  $T = 1.4 \pm 0.3$  s) tended to attenuate with depth to a greater extent than the longer period waves that formed over the bare site (average  $T = 1.7 \pm 0.4$  s), as predicted from linear wave theory. Also of note was the reduction in power density at low frequencies,  $f < 0.3$  Hz, indicating a reduction in the energy of the mean flow,  $u$ , within the canopy.

The wave-orbital velocity,  $u_{os}$ , at  $z = 0.5$  and  $0.1$  m was computed following Eq.

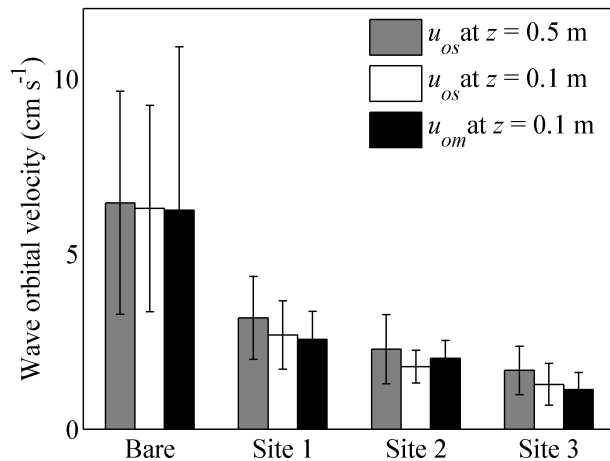


Fig. 2.11. Wave orbital velocities,  $u_{os}$  (Eq. 10), computed utilizing spectra of horizontal wave velocities,  $S_{\bar{u}\bar{u}}$  and  $S_{\bar{v}\bar{v}}$ , at  $z$  (vertical distance above the seafloor) =  $0.5$  m and  $z = 0.1$  m and wave orbital velocities,  $u_{om}$  (Eq. 12), at  $z = 0.1$  m, computed utilizing linear wave theory and estimates of free-surface displacements. Agreement between  $u_{os}$  and  $u_{om}$  at  $z = 0.1$  m suggests wave velocity decay is primarily due to wave attenuation of high-frequency wave motion with depth, and not from interaction with the eelgrass.

(10), and estimates for each site are shown in Fig. 2.11. At the bare site, there was only a 3% difference in measured  $u_{os}$  between the  $z = 0.5$  and  $0.1$  m elevations. At all 3 eelgrass sites there was an overall reduction in wave orbital motion by  $20 \pm 5\%$  within the canopy compared to above, and orbital velocities at the eelgrass sites were less than half that produced over the bare site. To determine the extent to which this

orbital wave reduction within the eelgrass canopy was due to natural attenuation with depth or due to interaction with the eelgrass bed, orbital velocities computed through

local velocity spectra (Eq. 10) were compared to estimates of bottom wave-orbital velocities using pressure sensor measurements of displacement of the free surface. Using linear wave theory for small-amplitude, monochromatic waves, the horizontal component of orbital velocity,  $u_o$ , can be computed as:

$$u_o = \frac{\pi H}{T} \frac{\cosh(kz)}{\sinh(kh)} \cos(kx - \omega t) \quad (11)$$

where  $H$  is the rms of wave height (m),  $\omega$  is the radian of wave frequency ( $\text{rad s}^{-1}$ ),  $x$  is the position in the wave orbital (m), and  $t$  is time (s). As the velocities vary sinusoidally with the  $x$ - and  $t$ -values throughout the wave period, the above equation can be simplified to the rms of the maximum orbital velocity when  $|\cos(kx - \omega t)| = 1$ :

$$u_{om} = \frac{\pi H}{T} \frac{\cosh(kz)}{\sinh(kh)} \quad (12)$$

Linear wave theory assumes the bed is frictionless; therefore, estimating wave velocity decay with depth using linear wave theory (Eq. 12) and comparing it to computed orbital velocities using local velocity measurements within the canopy (Eq. 10) should indicate the relative dampening of wave velocity due to frictional interaction with the seagrass canopy. Fig. 2.11 indicates there is good agreement between measured within-canopy orbital velocities and those estimated from linear wave theory, suggesting that within-canopy dampening of wave orbitals was primarily due to natural attenuation of high-frequency wave motion with depth and not from flow interaction with the eelgrass.

### **Bottom shear stresses and suspended sediment**

The total stress imparted to the seafloor was quantified using a combined bottom

shear stress,  $\tau_b$ , calculated as the square root of the sum of the squares of the shear stress due to currents,  $\tau_{current}$ , and due to waves,  $\tau_{wave}$  (Wiberg and Smith 1983) such that:

$$\tau_b = \sqrt{\tau_{wave}^2 + \tau_{current}^2} \quad (13)$$

Wave shear stresses were determined by:

$$\tau_{wave} = \frac{1}{2} f_w \rho u_b^2 \quad f_w = 0.04 \left[ \frac{u_b T}{2\pi k_b} \right]^{-0.25} \quad (14)$$

such that  $f_w$  is the wave friction factor,  $u_b$  is the bottom orbital velocity, which can be approximated as  $u_{os}$  measured near the seafloor (Wiberg and Sherwood 2008), and  $k_b$  is the characteristic roughness length of the bottom, which is defined as  $3D_{84}$  (Lawson et al. 2007).  $D_{84}$  is the sediment grain diameter such that 84% of grain diameters are smaller, and was measured to be 157  $\mu\text{m}$  at the bare site and 130  $\mu\text{m}$  within the seagrass canopy. Computation of the current shear stress within vegetation is not well described, especially in the presence of wave activity, but under unidirectional currents, a useful parameterization is through estimates of near-bottom TKE (Stapleton and Huntley 1995; Widdows et al. 2008):

$$\tau_{current} = \rho u_{*current}^2 = 0.19\rho(TKE) \quad (15)$$

Although waves can alter Reynolds stresses and TKE in the presence of a mean current (Grant and Madsen 1979), our findings within South Bay suggest only minor alteration in the magnitude of TKE in the presence of small-amplitude wind waves; therefore Eq. (15) can be reasonably applied.

Fig. 2.12 shows the magnitude of the total bottom shear stress at each site. At the bare site, median bottom shear stress was  $\tau_b = 0.17 \text{ N m}^{-2}$ , but within the eelgrass bed, median  $\tau_b \leq 0.035 \text{ N m}^{-2}$  at all sites. Although the critical shear stress that can initiate

sediment resuspension was not directly quantified in South Bay, estimates within Hog

Island Bay, which is directly adjacent to

South Bay in the VCR, were performed

by Lawson et al. (2007) and found to be

$\tau_{cr} = 0.04 \text{ N m}^{-2}$  over unvegetated sites

adjacent to seagrass beds. This value is

in relative agreement with  $\tau_{cr} = 0.05 \text{ N}$

$\text{m}^{-2}$  found by Widdows et al. (2008) for

sediments in the North Sea, where

adjacent *Zostera marina* beds had a

$\tau_{cr} = 0.07 \text{ N m}^{-2}$ . The increase in

sediment stabilization within the *Z. marina* bed was found to be due to increased

abundance of the microphytobenthos and lower densities of grazers. This suggests that

$\tau_{cr} = 0.04 \text{ N m}^{-2}$  is likely a reasonable estimate for unvegetated regions, and a

conservative estimate for the eelgrass bed in South Bay. At the 3 eelgrass sites, measured

$\tau_b$  was below the critical threshold for sediment entrainment during 80% of the sampling

time period. However,  $\tau_b$  at the unvegetated site was significantly larger than  $\tau_{cr}$ ,

suggesting that sediment resuspension was occurring during a significant fraction of the

sampling period.

OBSs were deployed at each site, measuring SSCs at  $z = 0.1$  and  $0.5 \text{ m}$ . SSC

estimates at these elevations were averaged to create a mean SSC within the water

column. Since flow and suspended sediment measurements were conducted at different

time periods at each site, direct cross-site comparisons of SSC for the same time periods

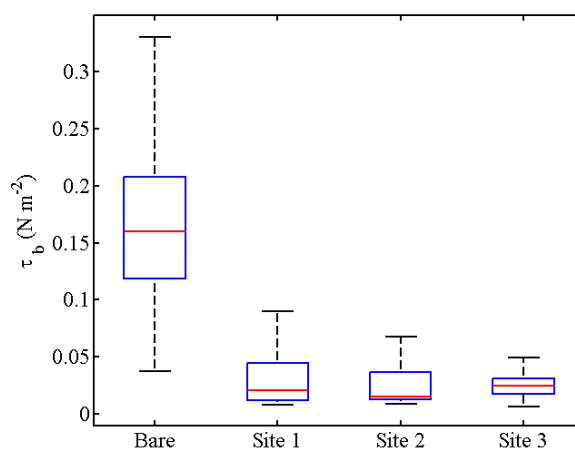


Fig. 2.12. Bottom shear stress ( $\tau_b$ ) at each site calculated as the square of the sums of the wave and current bottom stresses. Horizontal line within the box indicates median  $\tau_b$ , while the lower and upper edges of the box represent the 25<sup>th</sup> and 75<sup>th</sup> percentiles, respectively. Vertical lines extending from the box indicate the minimum and maximum measured  $\tau_b$ .

could not be conducted. Therefore, to determine if events of elevated magnitudes of bottom shear stress correlated to increases in SSC, a Pearson linear correlation was performed, which is defined as the covariance of the 2 variables divided by the product of their standard deviations. Elevated SSC events were determined by taking the temporal mean of the 72 h data set from each site and locating periods of time when  $\tau_b$  was greater than its mean. At the bare site (mean SSC = 56 mg l<sup>-1</sup>), there was a Pearson correlation coefficient of 0.72 between elevated levels of  $\tau_b$  and increased SSC. At Site 1 (mean SSC = 43 mg l<sup>-1</sup>), which is closest to the bare site, there was a correlation of 0.58, while at Site 2 (mean SSC = 23 mg l<sup>-1</sup>) and Site3 (mean SSC = 27 mg l<sup>-1</sup>) there were correlation coefficients of 0.26 and 0.23, respectively. Therefore, within the eelgrass meadow there was a decreased tendency for periods of high SSCs to correspond with periods of high bottom shear stress, suggesting that elevated levels of SSC within the seagrass bed were derived, in part, from non-local resuspension.

## DISCUSSION

*Zostera marina* beds in this Virginia coastal bay were found to substantially lower overall mean currents compared to adjacent bare site flow conditions. Average velocities were 2 to 3 times higher at the bare site than at the eelgrass sites, without a substantial change in tidal forcing. In addition, near-bed flows were dramatically reduced, with mean velocity at  $z = 0.1$  m at the bare site of 10.0 cm s<sup>-1</sup>, while average flows at the 3 eelgrass sites were 1.2 cm s<sup>-1</sup>, a 70% reduction compared to flow above the eelgrass canopy. Along the density gradient, ranging from 150 to 560 shoots m<sup>-2</sup>, the greatest flow reduction within the canopy compared to above the canopy occurred at Site 2, which was

the mid-density site with  $390 \pm 80$  shoots  $\text{m}^{-2}$ . The eelgrass at this site, however, also had a significantly higher mean (28 cm) and maximum blade length (51 cm) compared to the other two *Z. marina* sites. Although seagrass density has been found to play an important role in flow reduction (Ackerman and Okubo 1993), the blade length is also important in modifying the canopy friction (Fonseca and Fisher 1986), leading to a proportional reduction in fluid velocity (Gacia et al. 1999; Thompson et al. 2004). The smallest within-canopy flow reduction occurred at Site 3, which had the lowest eelgrass density and smallest average blade length. This suggests that both eelgrass density and blade length can have an impact on flow processes. Overall, the presence of seagrass structure serves to substantially reduce velocity magnitude as compared to the unvegetated seafloor (Hasegawa et al. 2008).

Tidally and wave-dominated flows were separated using the magnitude of the power density within the wave band of the frequency spectra. For tidally dominated flow conditions, the magnitude of the turbulent Reynolds stress typically decreased within the canopy compared to flow above, and within-canopy  $\overline{u'w'}$  reductions increased with increasing seagrass density. The highest relative turbulence levels within the eelgrass bed were found at the lowest eelgrass density, Site 3, and were of similar magnitude within and above the canopy. This transition from low turbulence in high-density beds to elevated turbulence in low-density beds agrees with findings within other seagrass systems and laboratory measurements, which indicate enhanced turbulence due to stem-generated wake turbulence (Nepf et al. 1997; Widdows et al. 2008). This enhanced turbulence can be intensified at the canopy–water interface (Abdelrhman 2003), where strong shear layers develop. Under wave-dominated flows, this relationship between

turbulence intensity and seagrass density became less apparent, but both Reynolds stresses and TKE values were of similar magnitude with and without the presence of wave action. Quadrant analysis indicated that much of the turbulent motions within the canopy were dominated by sweeping events, where high-momentum fluid was transported downward into the canopy. These sweeps constituted 55 % of the turbulent motion, compared to 32 % for ejections of low-momentum fluid transported upwards out of the canopy. Strong sweeping motions into the canopy were also observed by Ghisalberti and Nepf (2006), who found that sweeps were followed by weak ejection events ( $u' < 0, w' > 0$ ), which occurred at frequencies twice that of the dominant frequency of the coherent vortex formed at the top of the canopy.

### **Wave attenuation due to interaction with the seagrass canopy**

Significant wave heights and wave periods were computed from pressure records obtained from the ADVs at a sampling rate of 32 Hz. Wave periods at all sites ranged between 1 and 2 s, representing wind-generated gravity waves. There was a 45 to 70% reduction in average  $H_s$  at the eelgrass sites compared to the bare site. For both the bare and eelgrass sites, the majority of energy lost within the wave band occurred at high wave frequencies,  $\geq 1$  Hz. This is in general agreement with wave theory, which predicts that waves with  $f > \sqrt{g/(4\pi h)}$  will be attenuated before reaching the bottom (Wiberg and Sherwood 2008). Mean wave periods were  $T = 1.7 \pm 0.4$  s and  $T = 1.4 \pm 0.3$  s at the bare and eelgrass sites, respectively. As evident from PSD graphs, waves were not monochromatic and typically spanned a range of frequencies between  $f = 0.3$  and  $1 \text{ s}^{-1}$ . At the bare site, measured mean wave orbital velocities were within 3% of each other at

both  $z = 0.5$  and  $0.1$  m. With the presence of eelgrass structure, the horizontal orbital velocities were found to decrease by approximately 20% within the canopy versus above. That shorter period waves formed over the eelgrass canopy suggests that natural wave attenuation with depth was a major contributing factor in the measured reduction in orbital velocities within the canopy. However, little reduction in low-frequency wave motion within the canopy indicates that oscillatory flows were also effective at penetrating the eelgrass canopy for longer period waves. This suggests that storm events, which tend to increase  $H_s$  and  $T$  in combination with storm surge (Chen et al. 2005), may be effective in generating oscillatory flows through the seagrass canopy, increasing bottom shear stresses and ultimately leading to sediment resuspension. This agrees with the results of Bradley and Houser (2009), who found that the ability for seagrasses to attenuate wave energy decreases as wave heights increase, but that seagrasses also serve as a low-pass filter where higher frequencies in the spectra tend to be more attenuated. Their results also suggest that the rate of energy dissipation is not uniform over a range of wave frequencies, and waves at higher frequencies are attenuated, but waves at lower frequencies are less affected by the seagrass.

### **Bottom shear stress and sediment dynamics**

Total bottom shear stress was estimated by summing contributions from orbital wave motion due to waves and turbulence from the mean current. Overall, bottom shear stress at the bare site was found to be  $\tau_b = 0.17 \pm 0.08 \text{ N m}^{-2}$ , which was 5 times greater than at any of the eelgrass sites. Within the eelgrass canopy the mean  $\tau_b$  at the 3 sites ranged between  $0.025 \pm 0.02$  and  $0.032 \pm 0.03 \text{ N m}^{-2}$ . A conservative estimate of the

critical shear stress for sediment erosion was  $\tau_{cr} = 0.04 \text{ N m}^{-2}$ , which was measured in an adjacent coastal bay with similar water depth and sediment characteristics (Lawson et al. 2007). Bottom shear stress was found to be below the critical bottom stress threshold for erosion 80% of the time within the eelgrass meadow. In the absence of eelgrass, depth-averaged  $\text{SSC} = 56 \text{ mg l}^{-1}$ , and elevated levels of SSCs were well correlated throughout the water column with periods of high bottom shear stress (Pearson linear correlation coefficient = 0.72). However, with the addition of eelgrass structure, increases in depth-averaged suspended sediment were no longer well correlated with enhanced bottom shear stress. Correlation between  $\tau_b$  and elevated SSC occurred most closely at Site 1 (mean  $\text{SSC} = 43 \text{ mg l}^{-1}$ , correlation coefficient = 0.58), which is located closest to unvegetated sites within the bay and the edge of the eelgrass meadow (Fig. 2.1), where sediment resuspension is expected to be most pronounced. Further from regions devoid of eelgrass, correlations between elevated  $\tau_b$  and SSC drop considerably, where at Site 2 (mean  $\text{SSC} = 23 \text{ mg l}^{-1}$ ) and Site 3 (mean  $\text{SSC} = 27 \text{ mg l}^{-1}$ ) correlation coefficients were 0.26 and 0.23, respectively. This suggests that suspended sediment measured within the canopy was, to some magnitude, advected into the canopy from non-vegetated regions of the bay. Although wave activity has been shown to be a dominant driver initiating the suspension of sediment within these shallow coastal bays, previous studies have shown that wave activity alone does not necessarily induce the transport of sediment (Heller 1987). Rather, the combination of both waves and currents acts to distribute sediment throughout the seagrass bed. The stress exerted by wave motion acts to suspend sediment above the seafloor, but, ultimately, unidirectional currents will cause a net transport of

sediment, even if such a unidirectional current alone produces conditions below the threshold to initiate sediment suspension.

Overall, our results indicate that turbulence, wave heights, and wave orbital velocities were reduced in magnitude by the eelgrass canopy. This resulted in lowered suspended sediment within the eelgrass meadow as compared to adjacent unvegetated areas. In addition, between 2003 through 2009, monthly turbidity levels within the vegetated areas were found to be significantly lower than levels outside of the vegetated areas under summer conditions (Orth et al. 2012). Within the eelgrass canopy, SSC showed significant decreases over time, with median SSC decreasing approximately 75% between 2003 and 2009, and coincided with increased retention of fine sediments. These findings relate well with trends found in previous studies where flow reduction by seagrass meadows ranged from 25 to 80% (Koch and Gust 1999; Lacy and Wyllie-Echeverria 2011; Nepf 1999) and turbulence was reduced 30 to 50% (Granata et al. 2001). In a study by Gruber and Kemp (2010) with a similar current and wave regime as that in our study, reductions in SSC of up to 60% were found, which varied directly with seagrass biomass via seasonal senescence of a *Stuckenia pectinata* meadow. Our findings using different density sites within the same eelgrass bed suggest the opposite trend of lower SSC values at less dense seagrass sites. These opposing trends are likely due to site location within the meadow and local exposure to wind and wave activity. Locations that were further from the canopy edge and locations where waves propagated further distances across the eelgrass canopy had greater reductions in flow and suspended sediment. These findings suggest that seagrass density and meadow size both play roles in sediment suspension.

There is evidence to suggest that seagrass patches below a minimum size, and possibly locations close to the canopy edge, act to enhance near-bed turbulence and cause scouring (Fonseca and Koehl 2006; Heller 1987). Once the bed reaches a minimum density and patch width, turbulence reduction occurs, switching the local flow environment from erosional to depositional. Although it is still unclear what minimum size causes this transition, our findings suggest that the expansion of the eelgrass canopy within South Bay has altered the hydrodynamics from a net erosional environment to one that promotes deposition of suspended sediment. This has enhanced light penetration throughout the water column and created a positive feedback for eelgrass growth.

**ACKNOWLEDGEMENTS:** We thank E. Whitman, A. Schwarzschild, C. Buck, and D. Boyd for field assistance, and J. Bricker for helpful discussions regarding wave-turbulence decomposition. This research was funded by, and some data were provided by, a Virginia Coast Reserve Long-Term Ecological Research grant by the National Science Foundation (NSF-DEB 0621014, BSR-8702333-06, DEB-9211772, DEB-94118974, DEB-0080381). J.C.R.H. was supported through an NSF graduate research fellowship (DGE-0809128).

**CHAPTER 3:****Seasonal growth and senescence of a *Zostera marina* seagrass meadow alters wave-dominated flow and sediment suspension within a coastal bay\***

\*This chapter has been published, with citation: Hansen, JCR, and MA Reidenbach (2013) Seasonal growth and senescence of a *Zostera marina* seagrass meadow alters wave-dominated flow and sediment suspension within a coastal bay. *Estuaries and Coasts* doi: 10.1007/s12237-013-9620-5.

**ABSTRACT**

Tidally driven flows, waves, and suspended sediment concentrations were monitored seasonally within a *Zostera marina* seagrass (eelgrass) meadow located in a shallow (1 to 2 m depth) coastal bay. Eelgrass meadows were found to reduce velocities approximately 60% in the summer and 40% in the winter compared to an adjacent unvegetated site. Additionally, the seagrass meadow served to dampen wave heights for all seasons except during winter when seagrass meadow development was at a minimum. Although wave heights were attenuated across the meadow, orbital motions caused by waves were able to effectively penetrate through the canopy, inducing wave-enhanced bottom shear stress ( $\tau_b$ ). Within the seagrass meadow,  $\tau_b$  was greater than the critical stress threshold (= 0.04 Pa) necessary to induce sediment suspension 80 to 85% of the sampling period in the winter and spring, but only 55% of the time in the summer. At the unvegetated site,  $\tau_b$  was above the critical threshold greater than 90% of the time across all seasons. During low seagrass coverage in the winter, near-bed turbulence levels were

enhanced, likely caused by stem-wake interaction with the sparse canopy. Reduction in  $\tau_b$  within the seagrass meadow during the summer correlated to a 60% reduction in suspended sediment concentrations but in winter, suspended sediment was enhanced compared to the unvegetated site. With minimal seagrass coverage,  $\tau_b$  and wave statistics were similar to unvegetated regions; however, during high seagrass coverage, sediment stabilization increased light availability for photosynthesis and created a positive feedback for seagrass growth.

## **INTRODUCTION**

Seagrass meadows induce hydrodynamic drag on the flow that reduces water velocities and attenuates wave energy (Ackerman and Okubo 1993; Bryan et al. 2007; Carr et al. 2010; Gambi et al. 1990; Granata et al. 2001; Koch and Gust 1999; Peterson et al. 2004). These plants also serve to shelter the seafloor from hydrodynamic shear stresses (Bouma et al. 2009; Sand-Jensen 2008; Vogel 1981), which has been found to reduce the resuspension of sediments (Carr et al. 2010; Gacia and Duarte 2001; Granata et al. 2001; Ward et al. 1984). This has led to the view that seagrass meadows serve as depositional environments for sediment (Gacia et al. 1999; Gruber and Kemp 2010). Seagrasses require incident light radiation for growth (Duarte 1991); therefore, the stabilizing effect they have on sediments, and the corresponding increase in light penetration to the seafloor, creates a positive feedback for their growth (Carr et al. 2010). Since the relative amount of open space within a meadow influences the magnitude of bed shear reaching the seafloor, seagrass density can control the degree of sediment resuspension (de Boer 2007). Though meadows are often net depositional, spatial and

temporal variability within seagrass meadows can create localized enhancement of sediment suspension and transport. Recent findings support a more dynamic seagrass-sediment interaction, where sediment scouring occurs on the edge of meadows (Chen et al. 2007), and low densities of seagrass can actually enhance sediment suspension (Lawson et al. 2012). This switch from an erosional to depositional environment may depend on the development of skimming flow over the meadow, where a shift can occur from horizontal flow diversion around individual seagrass blades in low-density seagrass systems (i.e., blades per square meter of seafloor), causing scouring around individual shoots (Nepf 1999), to vertical diversion above the meadow, reducing water velocities and turbulence adjacent to the bed within a high-density seagrass canopy (Lawson et al. 2012).

In addition to seagrass density, the magnitude of fluid shear stresses impacting the seafloor in shallow-water environments can be controlled by whether flows are dominated by tidal currents or orbital wave motion. The interaction between waves and currents is nonlinear and leads to changes in the hydrodynamics and shear stresses imposed on the seafloor from those expected under either condition independently (Jing and Ridd 1996). Luhar et al. (2010) found that seagrasses caused only minor reductions of in-canopy oscillatory motions produced by waves, in contrast to unidirectional flows that can be significantly damped within a meadow. Typically, when waves are present, a thin, oscillatory wave boundary layer develops that is more strongly sheared than one formed under steady currents alone (Grant and Madsen 1979). This wave boundary layer induces greater drag on the mean flow and increased bottom shear stresses. For waves that are typically generated in fetch-limited shallow coastal bays, wave orbital motions

decrease with depth and the magnitude of wave energy that reaches the seafloor depends on the wave period, wave height, and water depth (de Boer 2007; Chen et al. 2007; Fagherazzi and Wiberg 2009). Although wave energy attenuation increases with increasing shoot density (Chen et al. 2007), the degree of flow reduction by the canopy can also be a function of distance from the edge, and the depth at which the seagrass resides below the surface (Fonseca and Fisher 1986; Verduin and Backhaus 2000).

Within a *Thalassia testudinum* seagrass meadow, the density of the canopy was important in controlling mixing across the canopy-water interface (Koch and Gust 1999), and with relative increases of wave- versus tidally-driven currents, near-bed velocities and shear stresses increased. With waves, orbital motions cause the canopy to oscillate, which limits the development of skimming flows, thereby enhancing the interaction of water masses across the canopy-water interface and increasing bed shear stresses (Koch and Gust 1999).

In temperate climates, *Zostera marina* meadows typically germinate in the fall, between mid-October to November in the coastal bays of Virginia, USA (Moore et al. 1993; Orth et al. 2012), and flowering shoots mature in late spring to early summer (May-June). The meadow reaches maximum blade density and coverage midsummer, begins senescence in late summer, and has sparse coverage over the winter (Orth et al. 2012). The sloughing of leaves in the senescent seagrass meadow effectively thins the meadow density and shortens the canopy height. Such changes to seagrass blade density and height have been shown to influence fluid velocities within meadows (Fonseca and Koehl 2006; Nepf et al. 2007), where canopy friction exhibits a strong positive relationship to the percent of the water column that is occupied by the seagrass (Fonseca

and Fisher 1986). In Gacia and Duarte (2001), resuspension of sediment was greatest with minimum canopy development, while deposition occurred under maximum above-ground canopy biomass conditions. Studies also show that mixing rates and turbulent kinetic energy are highly dependent upon seagrass density and areal cover of the canopy (Granata et al. 2001; Hansen and Reidenbach 2012). These findings suggest that throughout the year, the hydrodynamic regime and physical forces will vary greatly, altering the rates and dynamics of sediment erosion and deposition.

Though flow dynamics in seagrass meadows have been investigated in a number of studies; to date, most research has focused on observations conducted during the summer under full-growth conditions, while few studies have considered how structural and morphological changes that occur in seagrasses throughout the seasons of the year impact flow and sediment suspension. In order to determine the effects of seasonal growth and senescence of a seagrass meadow on hydrodynamics and sediment suspension, a *Z. marina* meadow in South Bay, Virginia, was monitored in summer, fall, winter, and spring conditions from June 2010 to June 2011 and compared to flow and sediment dynamics occurring at an adjacent, primarily unvegetated region. The goals of

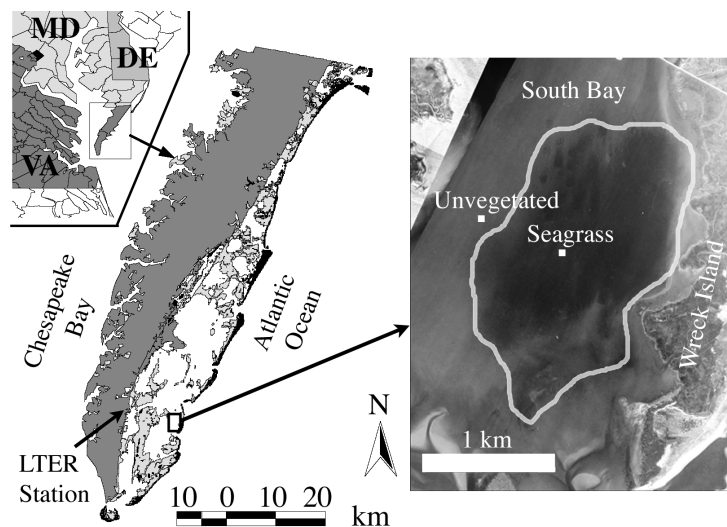


Fig. 3.1. Delmarva Peninsula, USA showing the landmass, barrier islands (grey), and coastal bays. Labeled points represent the Long-Term Ecological Research (LTER) station where wind data were gathered, the unvegetated reference site (unvegetated), and the seagrass site (seagrass) within the large *Z. marina* meadow in South Bay, Virginia

this study were to quantify the (1) seasonal variability of *Zostera marina* morphology within a coastal bay, (2) flow and turbulence structure within and above the seagrass meadow due to the combined influence of waves and tidally driven flows, and (3) response of suspended sediment concentrations to variations in the magnitude of bed shear stresses.

## **METHODS**

### **Study area**

Field studies were performed within a *Z. marina* seagrass (eelgrass) meadow in South Bay, Virginia, USA (Fig. 3.1); a coastal bay within the Virginia Coast Reserve (VCR) where ongoing seagrass restoration efforts are being performed (Orth and McGlathery 2012). The VCR is characterized by contiguous marsh, shallow coastal bay, and barrier island systems and is a National Science Foundation Long-Term Ecological Research site. South Bay lacks any significant riverine discharge, and therefore turbidity is primarily controlled by local resuspension. The shallow depth of South Bay, typically < 2 m, makes the bed sediments susceptible to suspension from both wind waves and tidal currents (Hansen and Reidenbach 2012). In addition, low pelagic primary productivity in the coastal bays suggests that non-algal particulate matter primarily controls light attenuation (McGlathery et al. 2001).

A high-density seagrass site and an adjacent unvegetated reference site within South Bay were examined in June 2010 (summer), October 2010 (fall), January 2011 (winter), March 2011 (spring), and June 2011 (summer). Mean air temperature during sampling within each season was 21, 20, 0, 7, and 24 °C, respectively. During June 2010,

the total *Z. marina* cover in South Bay was estimated to be 1,020 ha (Orth et al. 2012).

The unvegetated site, located adjacent to the meadow containing very few, small patches of seagrass, was monitored as a reference for flow characteristics in the absence of any considerable benthic vegetation.

During each season, seagrass shoot density was measured in the field, while blade length and the number of blades per shoot were measured in the lab from seagrass collected at each site (Table 3.1), and canopy height was calculated as the average of the longest  $2/3$  of the seagrass blade lengths (Koch et al. 2006). Blade width and the spacing between blades were obtained via image analysis in ImageJ from pictures captured during each season. In order to quantify the meadow structure, a metric was developed incorporating the blade area and meadow density. Following Nepf (2012), frontal area is defined as  $ah$ , where  $a = d/\Delta S^2$ ,  $d$  is blade width,  $\Delta S$  is the spacing between canopy elements (i.e., seagrass blades), and  $h$  is the canopy height. Values for each season are listed in Table 3.1.

Table 3.1. *Zostera marina* seagrass morphometrics for South Bay Virginia.  $n$  represents the number of samples for each average. Values represent the mean and standard deviations. Canopy height represents the average of the longest  $2/3$  of the seagrass blades sampled and frontal area is calculated as  $ah$ , where  $a = d/\Delta S^2$ ,  $d$  is blade width,  $\Delta S$  is the spacing between canopy elements, and  $h$  is the canopy height

	blade length (cm)	$n$	canopy height (cm)	$n$	density (shoots $m^{-2}$ )	$n$	blade width (cm)	$n$	blades/shoot	$n$	frontal area
Jun 2010	21±8	158	25±5	105	560±70	9	0.3±0.1	19	4.8±1.3	33	2.9±1.3
Oct 2010	19±7	59	23±5	39	350±50	6	0.2±0.1	25	3.0±0.9	20	0.7±0.3
Jan 2011	13±7	52	16±5	34	310±60	4	0.2±0.1	20	2.6±1.0	20	0.3±0.1
Mar 2011	12±5	91	15±3	60	350±90	6	0.2±0.1	20	4.0±1.4	20	0.5±0.3
Jun 2011	23±11	93	29±8	62	440±140	10	0.2±0.1	82	4.2±1.2	22	1.3±0.9

## Instrumentation

Two acoustic Doppler velocimeters (ADV, Nortek® Vector), coupled with optical backscatter sediment sensors (OBS, Campbell Scientific® OBS 3+), were placed at  $z = 0.5$  and  $0.1$  m above the seafloor at the seagrass and unvegetated sites to quantify velocity and suspended sediment concentrations for a 72-h period. Measurement heights were chosen to obtain fluid velocities and sediment concentrations both within and above the seagrass meadow. In order to prevent seagrass from interfering with the measurements, a 0.15-m diameter patch of grass was removed from below each sensor head. Velocities were measured at each site in 10-min bursts every 20 min at a sampling rate of 32 Hz. Instantaneous velocity measurements were collected in the east, north, and up reference frame using the internal compass and tilt sensors of the velocimeters, and then rotated for each burst interval to align the flow along the dominant flow direction,  $u$ , while minimizing flow in the transverse direction,  $v$ , and leaving the vertical direction,  $w$ , unchanged. Each ADV was equipped with a pressure sensor, which was used to determine the water depth and characterize the wave climate with parameters such as significant wave height ( $H_s$ ), average wavelength ( $L$ ), and wave period ( $T$ ) using linear wave theory (Dean and Dalrymple 1991). To obtain general flow characteristics at each site, a high-resolution Nortek Aquadopp© acoustic Doppler current profiler (ADCP) measured water velocities in 3-cm bins, between 0.2 and 1.0 m above the bottom at a sampling rate of 1 Hz for 10-min bursts every 20 min. During each season, two ADVs along with two OBSs were placed within the seagrass meadow for 72 h, then moved to an adjacent unvegetated seafloor for 72 h. During instrument deployments within the seagrass meadow, an additional ADCP and OBS sediment sensor were simultaneously

deployed at the unvegetated site to collect water velocities, water depth, and suspended sediment concentrations. Wind data were obtained from a meteorological station in Oyster, VA, USA located approximately 4 km from South Bay.

Calibrations to relate backscatter intensity obtained from the OBS to suspended sediment concentrations were performed using sediment collected from the seagrass meadow and unvegetated site (technique described in Hansen and Reidenbach 2012). Sediment grain size distributions were characterized using a laser diffraction particle size analyzer (Beckman Coulter LS I3 320).  $D_{84}$ , the grain size diameter for which 84% of the sample grain diameters are smaller, at the unvegetated site was  $157 \pm 7 \mu\text{m}$ ; while at the seagrass site, sediments were finer at  $130 \pm 17 \mu\text{m}$ .

### **Wave-turbulence decomposition**

In flows with both currents and waves, the covariance in velocity associated with waves is often larger than that associated with turbulence, and a wave-turbulence decomposition must be performed. When waves and currents are present, the instantaneous horizontal and vertical velocities can be written as:

$$\begin{aligned} u &= u' + \tilde{u} + \bar{u} \\ w &= w' + \tilde{w} + \bar{w} \end{aligned} \tag{1}$$

where  $\bar{u}$  and  $\bar{w}$  are the horizontal and vertical components of the mean velocity,  $\tilde{u}$  and  $\tilde{w}$  are the wave-induced orbital velocities, and  $u'$  and  $w'$  are the turbulent velocities. Most methods of wave-turbulence decomposition rely on two or more spatially separated velocity sensors to decouple wave motion from that of turbulence (Trowbridge 1998), or use simultaneous free surface displacement and velocity measurements to estimate wave

motion at depth (Benilov and Filyushkin 1970). Although these methods work well over relatively smooth beds, neither technique can be applied where bed topography significantly alters oscillatory flow structure outside the relatively thin wave-boundary layer.

A method of wave-turbulence decomposition that can be employed within seagrass systems uses a spectral decomposition, known as the Phase method (Bricker and Monismith 2007), where the phase lag between the  $u$  and  $w$  components of the surface waves

from one velocity sensor are used to interpolate the magnitude of turbulence under the wave peak. In this method, the turbulent Reynolds stress can be quantified as the difference between the total stress and the wave stress (Hansen and Reidenbach 2012):

$$\overline{u'w'} = \overline{uw} - \overline{\tilde{u}\tilde{w}} \quad (2)$$

Both the total stress and wave stress can be computed from the Fourier transforms of the individual velocity components,  $u$  and  $w$ . For example, the wave stress becomes:

$$\overline{\tilde{u}\tilde{w}} = \sum_{j=-N/2}^{j=N/2} \tilde{U}_j^* \tilde{W}_j \quad (3)$$

where  $U_j = U(f_j)$  is the Fourier transform of  $u(t)$  at the frequency  $f_j$  and  $*$  denotes the complex conjugate of  $U_j$ , which is multiplied by  $W_j$ , the Fourier transform of  $w(t)$  at the

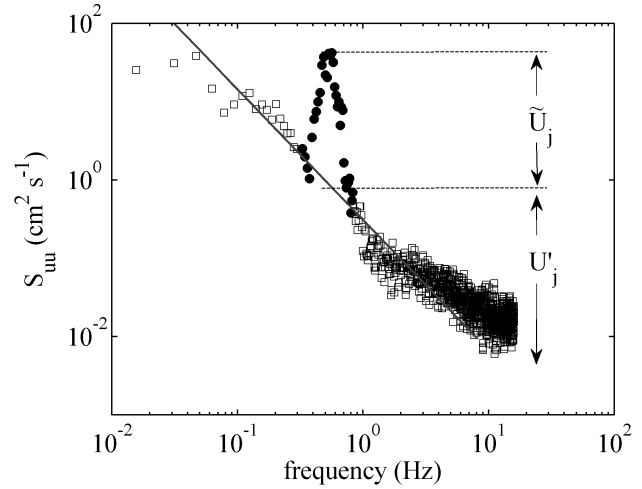


Fig. 3.2. Power spectral density (PSD) of the horizontal velocity,  $S_{uu}$ , for a 10-min representative data series computed at  $z = 0.5$  m at the seagrass site. The region encompassing the wave peak is denoted by the solid circles, while the squares represent the region of the spectra outside the wave domain. The grey solid line represents the least squares fit to the data outside the wave domain. The wave component of the stress,  $S_{\tilde{u}\tilde{w}}$ , is removed by subtracting the PSD formed above the grey line that encompasses the region of the wave peak

frequency  $f_j$ . Equation 3 assumes that waves and turbulence do not interact, and the magnitude of  $\tilde{U}_j$  is the difference between the raw  $U_j$  and the turbulence  $U'_j$  that is interpolated below the wave peak via a least squares fit straight line, as shown in Fig. 3.2. The same method was used to solve for  $\tilde{W}_j$ . Since waves dominate the spectra under the wave peak, this method also assumes that the phase difference between  $u$  and  $w$  is dominated by the wave flow. Estimates for  $\overline{uw}$  were computed in a similar manner as Eq. 3 by using the full spectrum  $U_j$  and  $W_j$ . Estimates of  $\overline{u'w'}$  from the Phase method were compared to the Benilov and Filyushkin (1970) method outside regions impacted by the seagrass canopy and agree to within  $\pm 10\%$   $\overline{u'w'}$ .

For time periods when waves were present, the horizontal wave orbital velocity,  $u_{os}$ , was calculated by summing the contributions from wave spectra across each frequency component of the horizontal and transverse velocity,  $u$  and  $v$  (Wiberg and Sherwood 2008).  $u_{os}$  is equivalent to the root mean squared orbital velocity and was computed both at  $z = 0.5$  and  $0.1$  m. Techniques for wave-turbulence decomposition and estimating  $u_{os}$  are described more fully in Hansen and Reidenbach (2012).

### **Bottom shear stress**

The total bed shear stress,  $\tau_b$ , was calculated as the square root of the sum of the squares of the bed stress due to waves,  $\tau_{wave}$ , and currents,  $\tau_{current}$  (Wiberg and Smith 1983), from wave orbital velocity and turbulent kinetic energy measured at  $z = 0.1$  m above the seafloor:

$$\tau_b = \sqrt{\tau_{wave}^2 + \tau_{current}^2} \quad (4)$$

Bottom shear stress due to waves was calculated from Fagherazzi and Wiberg (2009):

$$\tau_{wave} = \frac{1}{2} f_w \rho u_b^2 \quad f_w = 0.04 \left[ \frac{u_b T}{2\pi k_b} \right]^{-0.25} \quad (5)$$

where  $f_w$  is the wave friction factor,  $k_b$  is the characteristic roughness length estimated as  $3D_{84}$  (Lawson et al. 2007), and  $u_b$  is the bottom orbital velocity, which was approximated using estimates of  $u_{os}$  computed at  $z = 0.1$  m. The current shear stress was estimated as (Stapleton and Huntley 1995; Widdows et al. 2008):

$$\tau_{current} = \rho u_{*current}^2 = 0.19\rho(TKE) \quad (6)$$

where TKE is the turbulent kinetic energy calculated from the turbulent portion of the velocity spectrum:

$$TKE = 0.5(\overline{u'^2} + \overline{v'^2} + \overline{w'^2}) \quad (7)$$

Values of TKE were used to estimate shear stress instead of Reynolds stress (where  $\tau = -\rho \overline{u'w'}$ , commonly called the covariance method) because the covariance method assumes a logarithmic velocity profile has formed within an equilibrium boundary layer, which is rarely observed within a seagrass canopy. Although waves can alter Reynolds stress and TKE in the presence of a mean current (Grant and Madsen 1979), previous findings within South Bay (Hansen and Reidenbach 2012) suggest only minor alteration in the magnitude of TKE in the presence of small-amplitude wind waves, and therefore Eq. 6 can be reasonably applied.

## RESULTS

Average blade length and canopy height for each season are listed in Table 3.1,

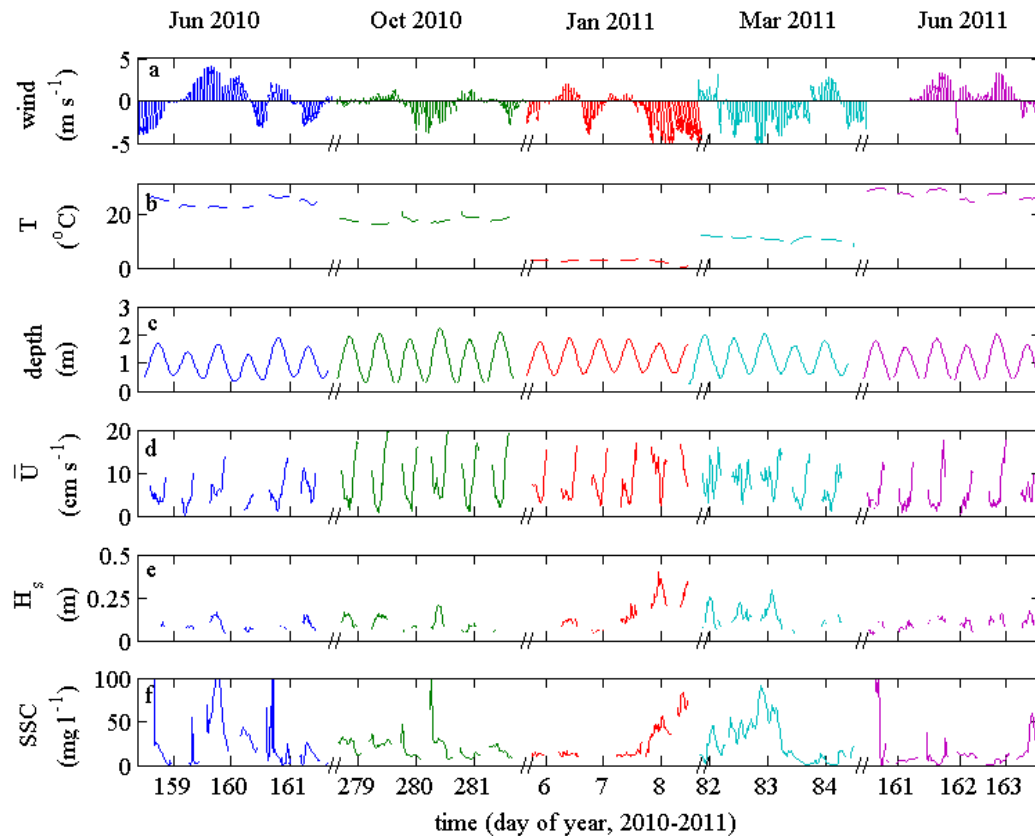


Fig. 3.3 (a) Wind speed, arrows denote the direction toward which the wind is blowing, with northward up and eastward to the right; (b) water temperature; (c) water depth at the seagrass site; (d) root mean square horizontal water velocities averaged over 10-min burst intervals at  $z = 0.5$  m above the seafloor at the seagrass site; (e) significant wave height ( $H_s$ ) over the seagrass meadow; and (f) near-bed suspended sediment concentrations (SSC) within the seagrass meadow at  $z = 0.1$  m. Breaks in data represent periods when the instrument was out of the water, or in (e) when waves were not present

and were statistically greater in the summer (June) and fall (October) than in January and March (one-way ANOVA with Bonferroni multicomparison,  $p < 0.05$ ). Both the shoot density (shoots per square meter) and blades per shoot were statistically lower in winter than summer, creating a more patch-like distribution (one-way ANOVA with Bonferroni multicomparison,  $p < 0.05$ ). The blade frontal area decreased from a maximum value of  $2.9 \pm 1.3$  during June 2010 to a minimum value of  $0.3 \pm 0.1$  in January 2011.

Physical characteristics at the seagrass site for each season are shown in Fig. 3.3. Hourly wind speeds ranged between  $0.1$  and  $8.2 \text{ m s}^{-1}$ , while wind speeds averaged over

the 3-day deployments varied from 1.7 to 3.3 m s<sup>-1</sup> between seasons (Fig. 3.4). The

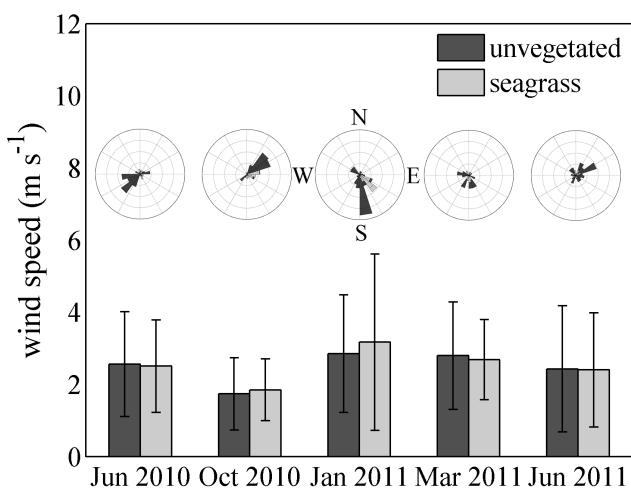


Fig. 3.4. Average wind speed ( $\pm 1$  standard deviation) and direction at both the unvegetated and seagrass sites for each season. Compass plots are histograms of wind direction with concentric rings each representing 20 vector samples and chords at 30° intervals

unvegetated site was 0.8 km to the northwest of the seagrass site, and fetch distances from each site to surrounding barriers were mapped at 30° intervals. Wind directions were variable between seasons, and depending upon wind direction, fetch length ranged from 1 to 15 km at the seagrass site and 0.9 to 16 km at the unvegetated site. The range of fetch

lengths was not significantly different between sites (one-way ANOVA,  $p > 0.6$ ). Water temperature throughout the year ranged from 2.6°C during January 2011 to 28.1°C during June 2011. Dominant tidal flow was along a northeast/southwest direction at both the seagrass site and adjacent unvegetated site for all seasons. Mean depth at the seagrass site was 1.1 m and at the unvegetated site was 1.4 m, while tidal amplitude ranged from 0.5 to 0.8 m (Table 3.2). Significant wave heights at the unvegetated site ranged on average from  $0.13 \pm 0.05$  to  $0.21 \pm 0.07$  m throughout the year. At the seagrass site, significant wave heights ranged from  $0.10 \pm 0.03$  m during June to  $0.18 \pm 0.09$  m during January.

Seasonal variations in mean velocities above ( $z = 0.5$  m) and within ( $z = 0.1$  m) the seagrass canopy and adjacent unvegetated reference site ( $z = 0.5$  m) are shown in Fig. 3.5a. Mean velocities at the unvegetated site did not vary significantly at  $z = 0.5$  m

Table 3.2. Temporal averages of suspended sediment concentration (SSC),  $\pm 1$  standard error, water depth, and tidal amplitudes ( $\pm 1$  standard deviation) during seasonal deployments at both an unvegetated reference site and over the seagrass meadow

	Seagrass SSC (mg l <sup>-1</sup> ) <i>z</i> = 0.5 m	Seagrass SSC (mg l <sup>-1</sup> ) <i>z</i> = 0.1 m	Unvegetated SSC (mg l <sup>-1</sup> ) <i>z</i> = 0.1 m	Seagrass Depth (m)	Seagrass Tidal Amplitude (m)	Unvegetated Depth (m)	Unvegetated Tidal Amplitude (m)
Jun 2010	33±3	26±2	57±3	0.99±0.43	0.57±0.11	1.49±0.55	0.73±0.12
Oct 2010	16±1	19±1	15±2	1.04±0.59	0.83±0.08	1.44±0.49	0.62±0.11
Jan 2011	21±2	33±3	17±1	1.07±0.42	0.59±0.04	1.38±0.57	0.81±0.05
Mar 2011	23±2	27±2	25±2	1.15±0.49	0.65±0.09	1.27±0.41	0.52±0.03
Jun 2011	21±2	17±2	50±1	1.04±0.49	0.67±0.09	1.50±0.51	0.68±0.06

between seasons (one-way ANOVA,  $p = 0.18$ ). Within the seagrass meadow, velocities were significantly smaller during the summer (June 2010, 2011) than at any other time of year (one-way ANOVA with Bonferroni multicomparison,  $p < 0.05$ ). In addition, there was a significant difference between the velocities measured at the seagrass and unvegetated sites during every season (one-way ANOVA with Bonferroni multicomparison,  $p < 0.05$ ), with the greatest reduction in flow between the two sites occurring during the summer (55 to 60% at  $z = 0.5$  m) and least reduction during winter (40% at  $z = 0.5$  m). Figure 3.5b shows that as frontal area increases, so does the percent velocity reduction within the canopy (at  $z = 0.1$  m) compared to above (at  $z = 0.5$  m). Average velocity reduction across all seasons between  $z = 0.1$  and 0.5 m at the unvegetated site was 44%. At the unvegetated site, a logarithmic flow profile developed throughout the entire bottom boundary layer. However, at the seagrass site, greater attenuation of velocity occurred adjacent to the seafloor due to flow interaction with the

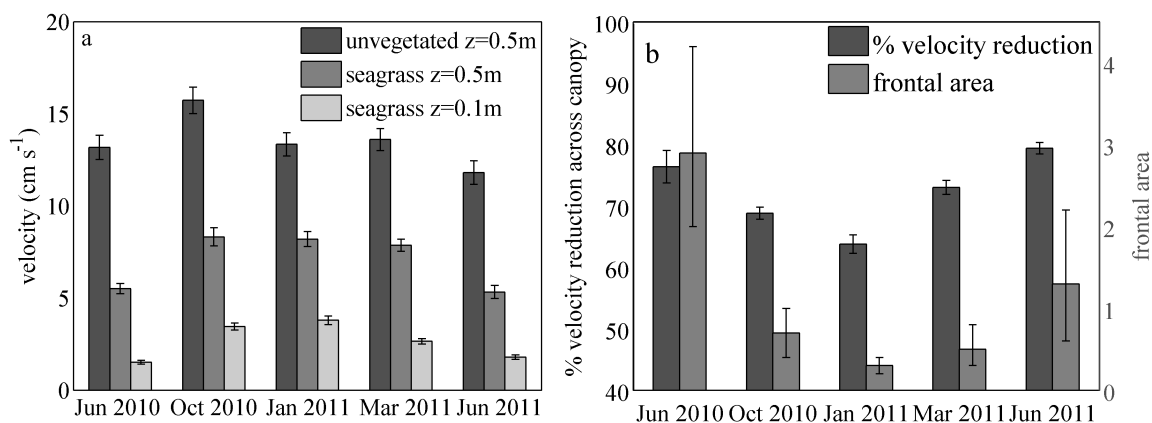


Fig. 3.5. (a) Average velocities ( $\pm 1$  standard error) at  $z = 0.5$  m above the seafloor at the unvegetated reference site, at  $z = 0.5$  and  $0.1$  m at the seagrass site, measured simultaneously. (b) Percent velocity reduction ( $\pm 1$  standard error) within the seagrass canopy (at  $z = 0.1\text{m}$ ) compared to above the canopy (at  $z = 0.5\text{m}$ ). Secondary y-axis represents the seagrass canopy frontal area per unit area of seafloor ( $\pm 1$  standard deviation)

meadow, creating an inflection point in the velocity profile at the top of the seagrass canopy (Fig. 3.6), which was strongest during summer.

### Waves and orbital motion

Waves in South Bay were locally developed wind waves with average wave periods ( $T$ ) ranging from 1.4 to 1.9 s. Significant wave heights ( $H_s$ ) ranged from 0.10 to 0.21 m during sampling at both sites, but were smaller over the seagrass meadow than the unvegetated seafloor for all seasons except winter, even

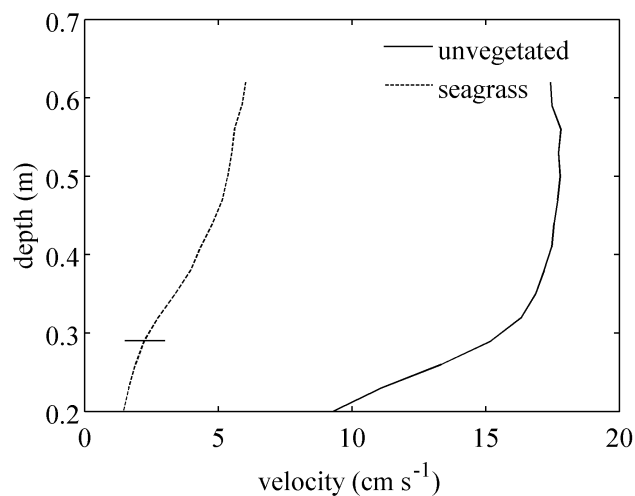


Fig. 3.6. Vertical profiles of horizontal velocity averaged over a single ebbing tide at the unvegetated and seagrass sites during simultaneous deployments in June 2011. Horizontal line represents the canopy height

though wind speeds were statistically similar within each season (Fig. 3.7, one-way

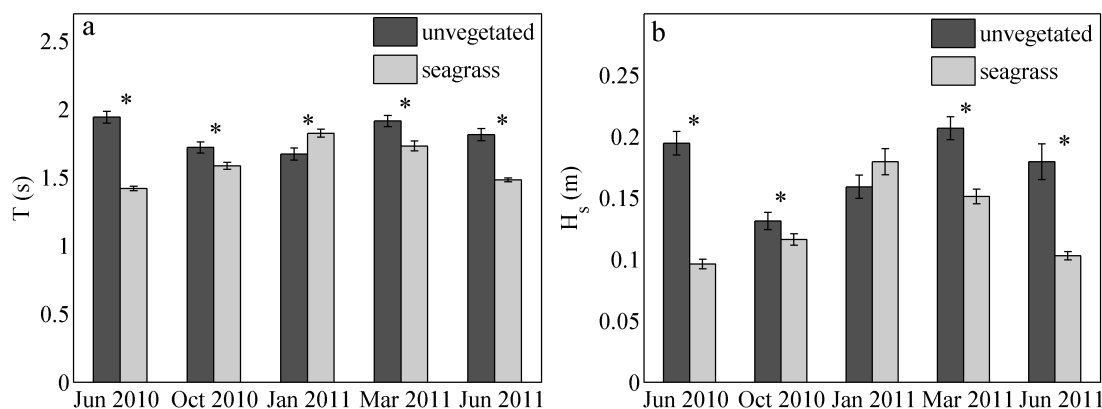


Fig. 3.7. (a) Significant wave period,  $T$ , and (b) significant wave height,  $H_s$ , for each season calculated from linear wave theory ( $\pm 1$  standard error). Asterisks (\*) above graphs indicate values are statistically different between the unvegetated and seagrass sites within the season

ANOVA,  $p > 0.08$ ). In addition, the reduction of  $H_s$  and  $T$  in the seagrass meadow scaled with increased seagrass canopy area, where the largest difference in  $H_s$  and  $T$  between the seagrass meadow and unvegetated site occurred during the summer. Wave development depends not only on frictional interaction with benthic vegetation, but also on wind speed and water column depth. Significant wave height and period plotted against wind speed (Fig. 3.8a,b) show that waves were larger and had longer periods over the unvegetated seafloor than over the seagrass meadow for any given wind speed except for weak wind conditions ( $\leq 2 \text{ m s}^{-1}$ ) where there was no statistical difference in  $H_s$  (one-way ANOVA,  $p > 0.05$ ). Additionally, both significant wave height and wave period were lowest for the fully developed meadow in the summer for all wind speeds. Wave height and period also increased with increasing water depth, but for any given water depth, waves were larger and had longer periods at the unvegetated site than compared to the seagrass site for all seasons of the year (Fig. 3.8c,d) except for January. In general, wave dynamics within the seagrass canopy matched the unvegetated site most closely during January, when seagrass cover was minimal.

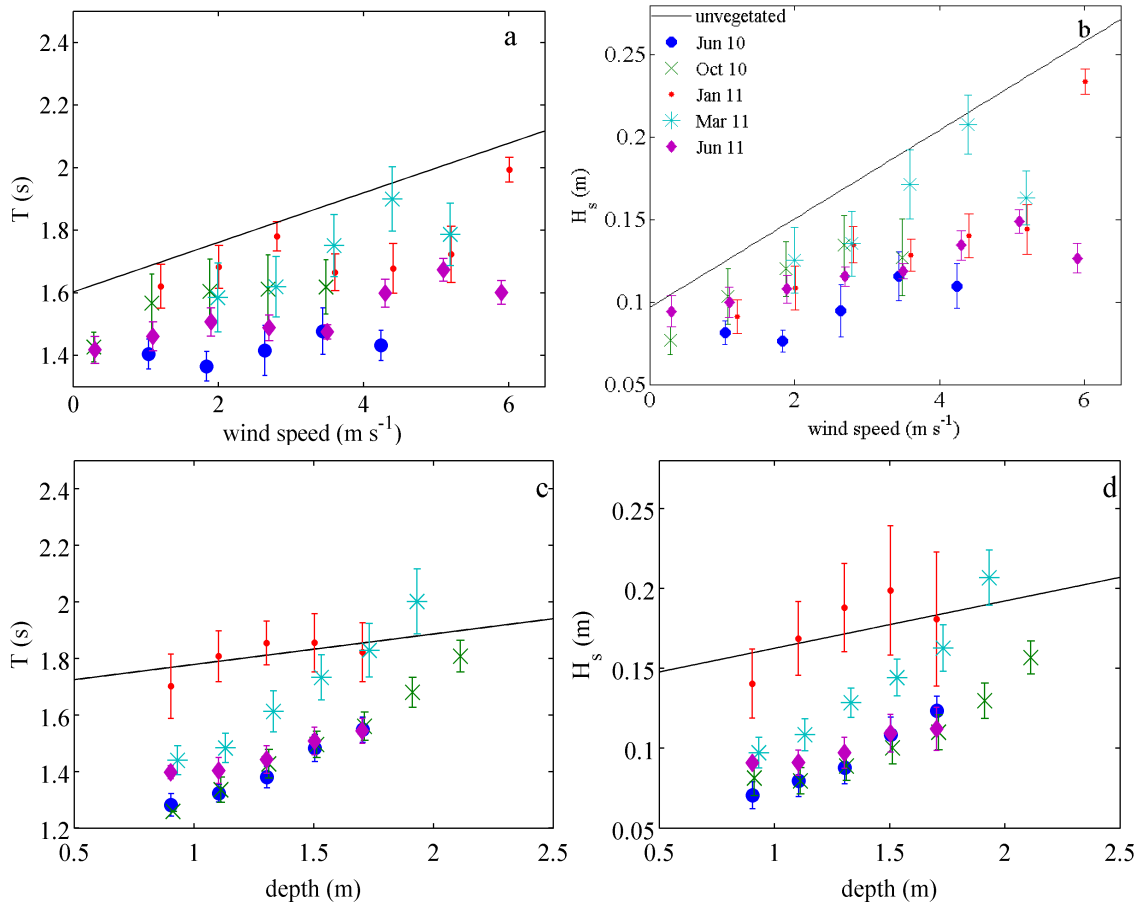


Fig. 3.8. (a) Average wave period,  $T$ , and (b) significant wave height,  $H_s$ , plotted as a function of wind speed ( $\pm 1$  standard error). (c) Average wave period,  $T$ , and (d) significant wave height,  $H_s$ , plotted as a function of water depth ( $\pm 1$  standard error). Data collected at the seagrass site during each season were averaged using a running mean with a  $0.8 \text{ m s}^{-1}$  averaging window for wind speed and  $0.2 \text{ m}$  for water depth. Solid black line represents best-fit line for all seasons at the unvegetated site

Horizontal orbital velocities ( $u_{os}$ ) above and within the meadow were computed using spectra of the horizontal wave motions. As expected, during all seasons orbital motions were greater at  $z = 0.5 \text{ m}$  than at  $z = 0.1 \text{ m}$  due to natural attenuation of short-period waves with depth (Fig. 3.9). Orbital motions were highest within the seagrass meadow in January and March when larger waves were able to develop due to the low percent cover of the seagrass. In January, the absence of seagrass cover also allowed longer period waves to develop (shown in Fig. 3.7a). In summer (June 2010 and June

2011), wave periods and orbital velocities were decreased, suggesting that the significant seagrass structure attenuated wave development over the meadow.

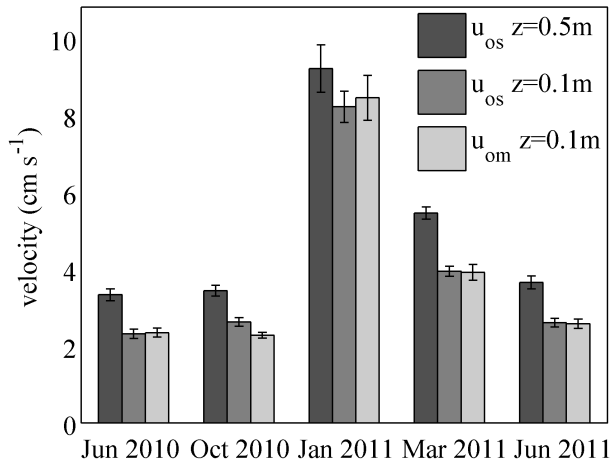


Fig. 3.9. Horizontal orbital velocities,  $u_{os}$ , above ( $z = 0.5$  m) and within ( $z = 0.1$  m) seagrass meadows from spectral analysis, as well as expected orbital velocities,  $u_{om}$ , calculated via linear wave theory. Linear wave theory predictions were never significantly greater than horizontal orbital velocities measured from spectral analysis (one-way ANOVA,  $p < 0.05$ ). Error bars represent  $\pm 1$  standard error

To determine the extent to which reduction of wave orbital velocities within the seagrass canopy was due to natural attenuation with depth or interaction with the seagrass blades, orbital velocities ( $u_{os}$ ) computed through velocity spectra

were compared with estimates of wave orbital velocities ( $u_{om}$ ) using pressure sensor measurements from the ADV. From linear wave theory for small

amplitude, monochromatic waves, the horizontal component of orbital velocity,  $u_{om}$ , was computed as (Dean and Dalrymple 1991):

$$u_{om} = \frac{\pi H_s \cosh(kz)}{T \sinh(kh)} \quad (8)$$

where  $H_s$  is the significant wave height,  $k$  is the wave number such that  $k=2\pi/L$  where  $L$  is the wavelength,  $T$  is wave period,  $z$  is the location above the seafloor, and  $h$  is the water column depth. The wavelength,  $L$ , was calculated according to linear wave theory

for intermediate waves as:  $L = L_\infty \sqrt{\tanh(\frac{2\pi h}{L_\infty})}$ , where  $L_\infty = \frac{g}{2\pi} T^2$ .

Linear wave theory assumes the bed is frictionless and therefore, estimating wave orbital velocity decay with depth using linear wave theory (Eq. 8) and comparing it to

computed orbital velocities using local velocity measurements within the canopy ( $u_{os}$ ) should indicate the relative dampening of wave orbital velocity due to frictional interaction with the seagrass canopy. At the seagrass site, the orbital motion predicted by linear wave theory at  $z = 0.1$  m within the seagrass canopy was not significantly greater than that quantified through velocity spectra during any season of the year (one-way ANOVA,  $p > 0.05$ ), suggesting that seagrass did not have a significant impact on the attenuation of wave orbital motion with depth (Fig. 3.9). This suggests that although seagrass attenuates the amplitude of waves as they propagate across the meadow, orbital motions are not attenuated due to direct interaction with the seagrass blades within the canopy.

The power spectral density (PSD) of horizontal velocities,  $S_{uu}$ , was examined to quantify the relationship between meadow structure, wave period, and turbulence intensity (Fig. 3.10). The velocity time series from each season was first filtered to select for wave-influenced periods, where the wave portion of the PSD accounted for greater than 10% of the total energy. The frequency spectrum was then averaged over the remaining time series to obtain the average frequency distribution in each season. Figure 3.10a shows spectra comparing the unvegetated and seagrass sites in June 2011 while Fig. 3.10b shows spectra for January 2011. Although velocity measurements were not measured simultaneously within the seagrass and unvegetated sites, winds were comparable within each season, and therefore, wave statistics can be generally compared. The reduced magnitudes of  $S_{uu}$  within the seagrass meadow were indicative of lower turbulent energy compared to the unvegetated site, with greater reductions in  $S_{uu}$  occurring in the summer. Peaks in the spectra that occur between  $f = 0.2$  and 1 Hz were

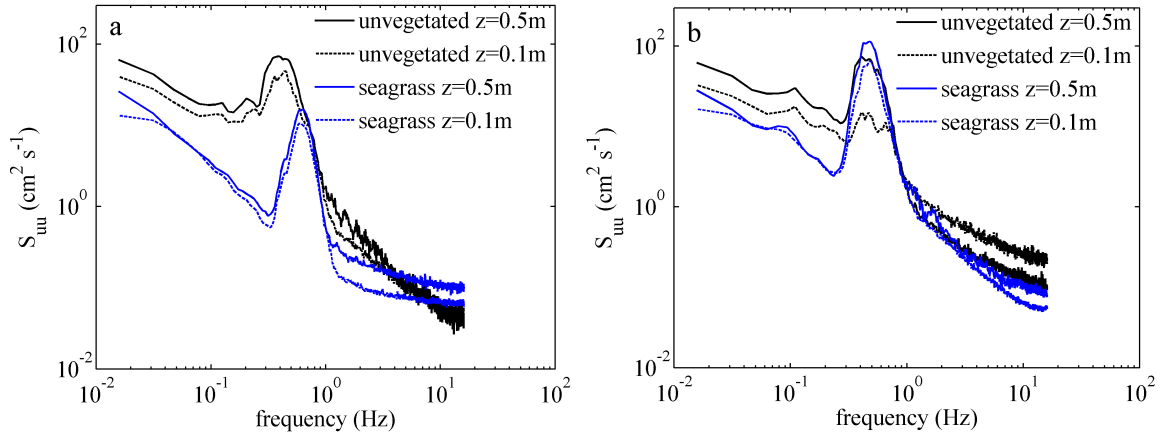


Fig. 3.10. Power spectral density (PSD),  $S_{uu}$ , for periods with wave activity for (a) June 2011 and (b) January 2011. Spectra were formed by averaging individual spectra, of length  $n = 2048$  velocity records, over time periods when the wave portion of the PSD accounted for greater than 10% of the total energy of the flow. Peaks in the PSD between frequencies ( $f$ ) of  $0.2 \leq f \leq 1$  Hz represent water motion due to waves. Flattening of the spectra at high frequencies ( $f > 5$  Hz to 10 Hz) represents the noise floor of the instrument

due to orbital wave motion and indicated that wave energy was reduced within the meadow during June compared to the unvegetated site (one-way ANOVA,  $p < 0.05$ ), but was not significantly reduced during January (one-way ANOVA,  $p = 0.98$ ). In addition, wave motion at low frequencies was reduced within the seagrass meadow in June ( $0.3 < f < 0.6$  Hz) compared to the unvegetated site, but was not substantially altered during January; all suggesting that under high seagrass meadow development, both wave heights and wave periods were reduced.

### Turbulence and momentum transport

After removal of orbital motions due to waves, Reynolds stresses were calculated from the turbulence portion of the velocity spectrum at  $z = 0.5$  and  $0.1$  m within the seagrass meadow (Fig. 3.11). Reynolds stress was then normalized by  $\Delta U^2$ , which is defined as the difference between velocities measured at  $z = 0.5$  and  $0.1$  m ( $\Delta U = U_{0.5m} - U_{0.1m}$ ). The greatest reduction of within-canopy Reynolds stress occurred in June, when

the canopy frontal area was greatest. In October, during initial senescence of the meadow, turbulence levels increased within the canopy, and in January and March, when the meadow frontal area was minimal, enhanced turbulence within the canopy was measured relative to above (at  $z = 0.5$  m). Compared to the unvegetated site, the most dramatic reductions of within-canopy Reynolds stress occurred in summer, with enhanced Reynolds stresses in winter. The absolute magnitude of Reynolds stress followed these same normalized trends throughout the seasons at both the unvegetated and seagrass sites.

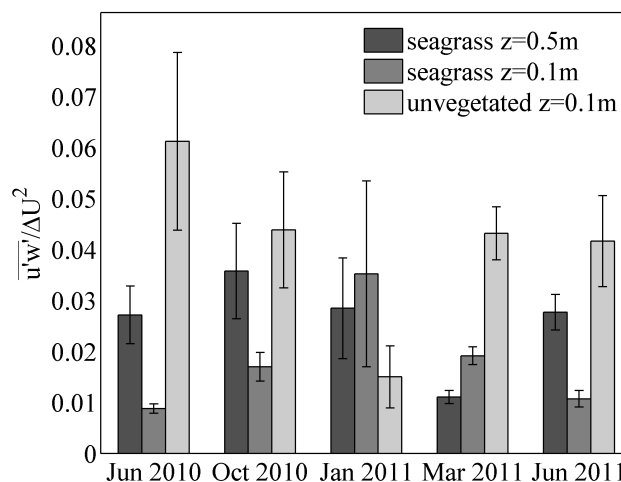


Fig. 3.11. Reynolds stress for turbulence portion of velocity spectrum above ( $z = 0.5$  m) and within ( $z = 0.1$  m) the seagrass meadow and at the unvegetated site ( $z = 0.1$  m). Reynolds stress is normalized by  $\Delta U^2$ , which is defined as the difference between mean velocities measured at  $z = 0.5$  m and  $0.1$  m,  $\Delta U = U_{0.5m} - U_{0.1m}$ . Error bars represent  $\pm 1$  standard error

To determine how turbulent fluctuations contribute to the transport of momentum throughout the bottom boundary layer, quadrant analysis was performed. Velocity fluctuations,  $u'$  and  $w'$ , were normalized by their respective standard deviations and divided into four quadrants based on the sign of their instantaneous values (Lu and Willmarth 1973). The two dominant quadrants responsible for momentum transfer are quadrant 2 (Q2), where turbulent ejections of low momentum fluid are transported vertically upward ( $u' < 0$ ,  $w' > 0$ ), and quadrant 4 (Q4), where sweeping events transport high momentum fluid downward towards the seafloor ( $u' > 0$ ,  $w' < 0$ ). These ejections and sweeps lead to periodic mixing across the seagrass canopy-water interface.

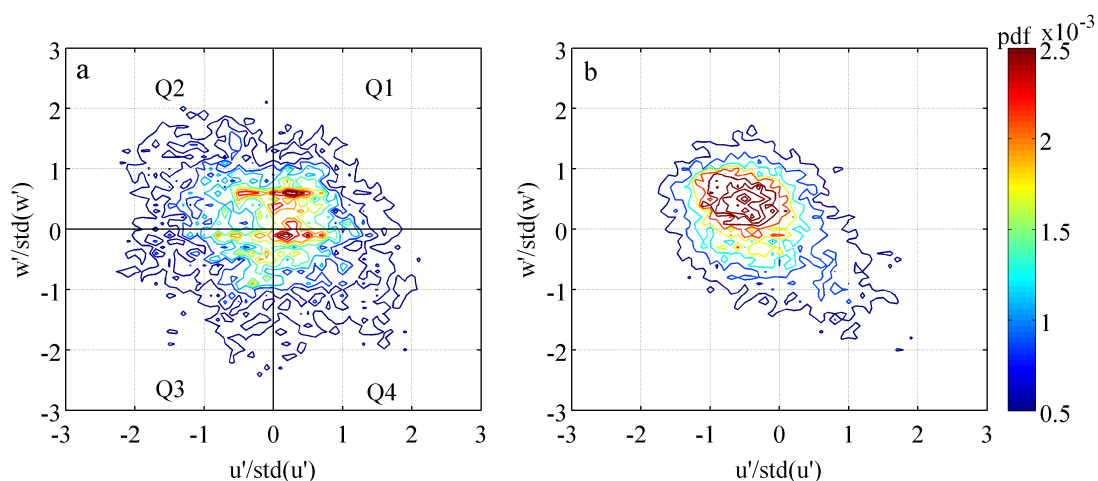


Fig. 3.12. Quadrant analysis of the probability density functions (pdfs) of  $u'$  and  $w'$  distributions normalized by their standard deviation at (a)  $z = 0.1$  m above the seafloor at the unvegetated site and (b)  $z = 0.1$  m at the seagrass site, which shows the dominance of turbulent sweeping events in quadrant 4

Contours of the turbulent probability distribution function (pdf) are shown in Fig. 3.12 for turbulent motions at  $z = 0.1$  m at the unvegetated and seagrass sites in June 2011 during periods with no wave action (i.e., energy within the wave portion of the PSD accounted for less than 10% of the total energy). At the unvegetated site, the distribution of momentum was balanced between Q2 and Q4 with Q1 (16%), Q2 (33%), Q3 (16%), and Q4 (35%). In comparison, at the seagrass site, the distribution was Q1 (11%), Q2 (26%), Q3 (10%), and Q4 (53%). These sweeping events transport high momentum fluid down into the meadow from the overlying water. The combined Q2 and Q4 contributions accounted for 79% of the total Reynolds stress in the seagrass canopy, compared to 68% at the unvegetated site. This indicates that though Reynolds stress was smaller within the seagrass canopy, turbulent motions were more efficient in the vertical transport of momentum compared to the unvegetated site. The increasing shift toward motion in Q2 and Q4 also correlated with increasing canopy frontal area. In January and March, combined Q2 and Q4 shifts are 74 and 73%, respectively, at  $z = 0.1$  m. With increased

seagrass canopy development in the summer, contributions to Q2 and Q4 increased to 87 and 79% during June 2010 and 2011.

### Bottom shear stress and suspended sediment dynamics

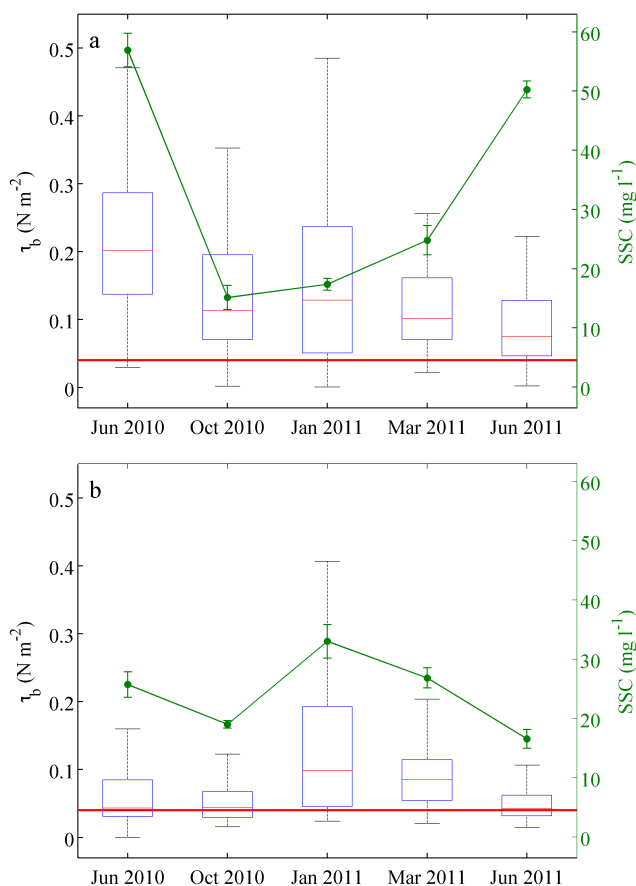


Fig. 3.13. Bed shear stress,  $\tau_b$ , at the (a) unvegetated site and (b) seagrass meadow. Horizontal line within the box indicates median  $\tau_b$ , while the lower and upper edges of the box represent the 25<sup>th</sup> and 75<sup>th</sup> percentiles, respectively. Whiskers extending from the box indicate the minimum and maximum measured  $\tau_b$ . Horizontal red line across both plots represents the critical stress threshold for the suspension of sediment. Average suspended sediment concentrations ( $\pm 1$  standard error) measured at  $z = 0.1$  m above the seafloor are plotted in green with the secondary y-axis

The total stress imparted to the seafloor was quantified using a combined bottom shear stress,  $\tau_b$  (Eq. 4), calculated as the square root of the sum of the squares of the shear stress due to waves,  $\tau_{wave}$  (Eq. 5), and due to currents,  $\tau_{current}$  (Eq. 6; Wiberg and Smith 1983). Over the unvegetated seafloor, shear stress was consistently greater than that produced within the seagrass meadow (Fig. 3.13a). At the seagrass site,  $\tau_b$  was largest during January (Fig. 3.13b) and lowest in the summer.

Although the critical shear stress that can initiate sediment resuspension was not directly quantified in South Bay, estimates

within Hog Island Bay, which is directly adjacent to South Bay in the VCR, were performed by Lawson et al. (2007) and found to be  $\tau_{cr} = 0.04 \text{ N m}^{-2}$  over unvegetated sites adjacent to seagrass meadows. This value is in agreement with  $\tau_{cr} = 0.05 \text{ N m}^{-2}$  found by Widdows et al. (2008) for unvegetated seafloor sediments in the North Sea, where adjacent *Z. marina* meadows had a  $\tau_{cr} = 0.07 \text{ N m}^{-2}$ . Increased abundances of microphytobenthos and lower densities of grazers were found to be the cause for increased sediment stabilization within the *Z. marina* meadow. This suggests that  $\tau_{cr} = 0.04 \text{ N m}^{-2}$  is likely a reasonable estimate for unvegetated regions and a conservative estimate for the eelgrass meadow in South Bay. To determine the influence of the meadow on sediment suspension, shear events with magnitudes greater than this critical shear stress necessary for sediment suspension were isolated. At the unvegetated site, greater than 90% of the deployment times had bed shear that was sufficient for initiating sediment suspension. Within the seagrass meadow, bed shear was greater than critical shear stress for 55% of the deployment time period in the summer and fall, while winter and spring had bed shear stresses that exceeded the critical stress threshold 80 to 85% of the time. Corresponding reductions in suspended sediment concentrations (SSC) at the seagrass site, as compared to the unvegetated site, were highest during the summer (60% reduction). During the spring, the magnitude of SSC within the canopy was not significantly different than that near the seafloor at the unvegetated site (at  $z = 0.1 \text{ m}$ , one-way ANOVA,  $p > 0.48$ ). Interestingly, in winter SSC was significantly enhanced, up to two times (one-way ANOVA,  $p < 0.05$ ) in the seagrass meadow compared to the adjacent unvegetated site (Table 3.2).

A two-dimensional PSD of horizontal velocities is shown for the seagrass site in

Fig. 3.14a for frequencies between 0 and 2 Hz. This plot includes the tidally-dominated contributions to the spectra at small frequencies (i.e.,  $f < 0.3$  Hz), as well as the wave

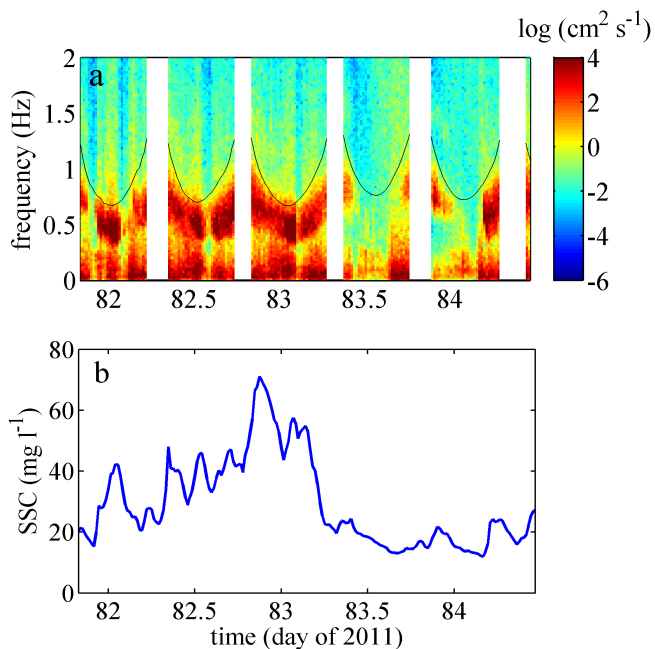


Fig. 3.14. (a) Two-dimensional power spectral density of horizontal velocities at  $z = 0.1$  m above the seafloor at the seagrass site during March 2011. Black lines indicate  $f = \sqrt{g/[4\pi(h-z)]}$ , the frequency ( $f$ ) at and above which linear wave theory predicts wave motion is attenuated due to water depth. Regions with no data were during low tide when the velocimeter had poor signal quality. (b) Corresponding suspended sediment concentrations (SSC) at  $z = 0.1$  m, indicating correlation between periods of high wave activity and increased SSC

component of the PSD, which typically span the range  $0.3 < f < 1$  Hz. Peak wave frequency at high tide was approximately  $f = 0.5$  Hz ( $T = 2$  s), but as the water depth decreased, peak wave frequency increased to approximately  $f = 1$  Hz, indicating a reduction in the peak wave period to  $T = 1$  s. Time periods with highest wave energy (i.e., high PSD in the wave band  $0.3 < f < 1$  Hz), corresponded closely to time periods with enhanced SSC (Fig. 3.14b). A Pearson linear correlation

factor, defined as the covariance of two variables divided by the product of their standard deviations, was computed to determine the relationship between suspended sediment and orbital motion near the seafloor. At the seagrass site, SSC values near the seafloor ( $z = 0.1$  m) were positively correlated with wave orbital velocities in all seasons, with correlation factors ranging from 0.47 to 0.67 ( $p < 0.05$ ). However, enhanced SSC values were not significantly correlated to enhanced mean currents, indicating waves were the dominant mechanism initiating sediment resuspension.

## DISCUSSION

*Z. marina* meadows within a Virginia coastal bay were found to substantially lower overall mean currents compared to an adjacent unvegetated site's flow conditions during all seasons of the year. Average velocities were 1.6 to 2.4 times lower at the seagrass site than at the unvegetated site even though tidal amplitude was statistically similar (average tidal amplitude during deployments at the seagrass site was  $0.67 \pm 0.10$  m and at the unvegetated site was  $0.67 \pm 0.11$  m; Table 3.2).

Near-bed flows within the seagrass meadow were dramatically reduced, but varied seasonally in response to seagrass canopy area as expected. Yearly averaged, mean velocity at  $z = 0.1$  m at the unvegetated site was  $9.2 \text{ cm s}^{-1}$ , while mean flow at the seagrass site was  $2.6 \text{ cm s}^{-1}$ . The greatest flow reduction within the canopy compared to above occurred during June, while the smallest within-canopy flow reduction occurred in January. This agrees with predicted shear layer development, where shear layers are expected to form when  $ah > 0.1$  (Nepf 2012). In shear layers, velocity profiles above the meadow become logarithmic (Kaimal and Finnigan 1994), while velocities rapidly decrease within the canopy, creating an inflection point near the canopy-water interface. Due to seasonal changes in seagrass cover, altering both the canopy height and canopy frontal area, the precise location of an inflection point could not always be determined. However,  $ah > 0.1$  occurs during all seasons of the year, with  $ah > 1$  in the summer. For sparse canopies, a coherent canopy shear layer is not formed, rather, characteristics of both shear layer and rough-wall boundary layers are present, with reduced shear layer development occurring as flow velocity increases (Lacy and Wyllie-Echeverria 2011).

When  $ah > 1$ , the canopies become essentially cutoff from overlying flow (Luhar et al. 2008), dramatically reducing within-canopy velocities.

Tidally- and wave-dominated flows were separated using the magnitude of power density within the wave band of the frequency spectra. In the fully developed canopy in the summer, normalized Reynolds stress within the canopy was reduced by 75 to 85% compared to measurements at the same elevation of  $z = 0.1$  m at the unvegetated site. The highest turbulence levels within the seagrass meadow were found at the lowest seagrass canopy frontal area, and Reynolds stress was greater within the canopy than above in the winter and spring. Turbulence enhancement can be caused both by reduced stem density that can increase stem-generated wake turbulence (Nepf et al. 1997; Widdows et al. 2008), or by a reduction in meadow height, causing an intensification of turbulence closer to the seafloor from the fluid shear layer formed at the top of the canopy (Abdelrhman 2003; Gambi et al. 1990). Additionally, in sparse canopies, significant turbulence can be generated by flow interaction with the seafloor (Lacy and Wyllie-Echeverria 2011). Both blade length and density contribute to changes in frontal area. Luhar et al. (2008) found that when frontal area is substantially greater than  $\sim 0.1$ , the canopy acts as a dense canopy. In dense canopies, within-canopy turbulence and flow are significantly reduced and roughness length-scales decrease with increasing frontal area due to the mutual sheltering of individual canopy elements (Luhar et al. 2008). When the frontal area reaches approximately  $\geq 1$ , flow is almost entirely displaced above the canopy, substantially limiting turbulence that can contribute to sediment resuspension (Luhar et al. 2008). Luhar et al. (2008) also noted that by reducing the momentum penetration, a dense canopy shelters itself from high flow, which is critical during extreme events such

as floods, and the reduction in bottom stress associated with dense canopies can stabilize the bed and improve water clarity. Our results indicate that under summer conditions, the Virginia seagrass meadow was acting as a dense canopy (frontal area of 1.3 to 2.9), which both reduced bottom stress and stabilized sediments compared to the unvegetated seafloor. Although there is a transition region for canopies with frontal areas between 0.1 and 0.5, Luhar et al. (2008) found when frontal area is less than  $\sim 0.1$ , the canopy acts as a sparse canopy. In sparse canopies, the flow penetrates throughout the entire canopy and turbulence intensities increase with frontal area, as stem-wake flow interactions are enhanced (Raupach et al. 1996). Our results in winter (frontal area of  $0.3 \pm 0.1$ , within the transitional region) agree with conditions found for a sparse canopy, which include flow penetration through the canopy and increased turbulence intensities contributing to enhanced bottom shear stress and sediment suspension compared to the unvegetated site.

Quadrant analysis indicated that during all seasons, turbulent motion within the meadow was dominated by sweeping events of momentum, suggesting turbulence was generated at the shear layer at the top of the canopy and momentum transport occurred into the canopy. Although the magnitude of turbulence within the canopy was reduced with increased seagrass coverage, the efficiency of momentum transport increased, as evident from the greater relative contributions from both ejection and sweep motions of turbulent eddies transporting momentum into the canopy. Strong sweep motions into the canopy were also observed by Ghisalberti and Nepf (2006), who found that sweeps were followed by weak ejection events ( $u' < 0$ ,  $w' > 0$ ) that occurred at frequencies twice that of the dominant frequency of the coherent vortex formed at the top of the canopy.

### Wave interaction with the seagrass canopy

Wave periods and significant wave heights were computed from pressure records obtained from the ADVs at a sampling rate of 32 Hz. Wave periods at all sites ranged between 1 and 4 s, representing wind generated gravity waves. Over the year, there was a 35% reduction in  $H_s$  at the seagrass site compared to the unvegetated site. Most of this reduction occurred during the summer, with no statistical difference in  $H_s$  during the winter. As evident from PSD graphs (Fig. 3.10), waves were not monochromatic and typically spanned a range of frequencies between  $f = 0.3$  to 1 Hz. When comparing attenuation of wave energy within this wave portion of the PSD, the largest reductions in wave motion within the seagrass bed compared to the unvegetated site occurred at low frequencies during the summer. Bradley and Houser (2009) found that waves at  $T \sim 2.6$  s were relatively unaffected by seagrass, but higher frequency waves ( $T \sim 1.5$  s) caused seagrass blade movement that tended to be out of phase with wave motion, increasing frictional drag and wave energy attenuation. Waves in our study tended to be of shorter period, and most of the attenuation in wave energy occurred between wave periods of  $T = 1.4$  to 2.0 s. Although blade movement was not quantified in our study, this attenuation is within the same frequency range as that found by Bradley and Houser (2009).

The ratio of wave orbital excursion length ( $A$ ) to blade spacing ( $\Delta S$ ) can also be used to indicate the significance of wave orbital motion reduction within the canopy (Lowe et al. 2005a). As per Lowe et al. (2005a),  $A = u_{os}/\omega$ , where  $u_{os}$  is the wave orbital velocity and  $\omega = 2\pi/T$ , is the radian wave frequency estimated directly above the canopy at  $z = 0.5$  m. For  $A/\Delta S > 1$ , the attenuation of orbital motion within the canopy is significant. Our measurements show that  $A/\Delta S$  ranged between 0.5 during summer and

0.75 during winter. This indicates that orbital motions are not significantly altered due to direct interaction with the seagrass blades, and although tidally driven flows may be damped, oscillatory motion was able to effectively penetrate the seagrass canopy. This finding is similar to laboratory measurements of flow structure within and above a model *Z. marina* meadow (Luhar et al. 2010), which found that although unidirectional flows were reduced within the meadow, in-canopy orbital velocities were not significantly altered. This suggests that throughout the year, storm events, which tend to increase  $H_s$  and  $T$  (Chen et al. 2005), may be effective at generating oscillatory flows through the seagrass canopy. However, since attenuation in wave amplitudes across the seagrass meadow is least effective during time periods of low canopy area, this may ultimately lead to seasonal increases in sediment resuspension during winter, as sediment suspension within the meadow was sensitive to wave oscillatory motion. Overall, at minimum frontal area in winter, average velocities were reduced, but the meadow behaved similarly to an unvegetated seafloor in regard to significant wave height, orbital velocities, and bottom shear stress. This agrees with findings from Bradley and Houser (2009) that attenuation of wave energy across a seagrass meadow is the result of the high density of seagrass blades and the aerial extent of the canopy, not the drag induced by flow interaction with individual blades.

### **Sediment suspension**

Overall, seasonal changes in the meadow frontal area strongly influenced wave development, bed shear stress, and subsequent sediment suspension in the seagrass meadow. During the summer, SSC at the unvegetated site was roughly double that within

the seagrass canopy, while similar SSC were found in March and October within and outside the seagrass meadow. Many studies have also found that with increasing seagrass density, sediment resuspension is limited and sediment deposition occurs (Granata et al. 2001; Ward et al. 1984). Likely, this is caused by a transition from dense canopy cover during summer, where the canopy is essentially cutoff from the overflow, to a more sparse canopy cover, where the flow, vertical momentum, and mass transport is more vigorous (Luhar et al. 2008). In addition, under low canopy development in winter, although the magnitude of bottom shear was similar within the seagrass meadow and the adjacent unvegetated site, sediment suspension was enhanced within the meadow. This agrees with previous studies that have shown at low densities, seagrass enhanced sediment suspension through scouring (Bouma et al. 2009). Finer sediment grain sizes were also found within the meadow, likely caused by enhanced deposition in summer. Since finer-grained particles typically resuspend at lower critical shear stresses than larger particles, this may have contributed to greater wintertime resuspension compared to unvegetated sites under similar bed shear stress conditions.

Although seasonal changes occur, Gacia and Duarte (2001) concluded that seagrass meadows often reduce resuspension rather than enhance deposition, as deposition only occurred during the summer and was only slightly increased. In yearly studies within a seagrass canopy undergoing restoration along the Virginia coast, turbidity levels during June-July, when the meadow was at peak biomass, showed significant reductions over a 10-year period with increased seagrass blade density and overall canopy size (Orth et al. 2012). *Z. marina* meadows also depend on seed production and germination in order to expand cover (Orth et al. 2006). Increased orbital

motion, turbulence, and flow through the canopy can serve to distribute seeds in the spring (Orth et al. 2012), and the transport of seeds and other resources may be particularly important within the meadow's transition periods of senescence in the fall and growth in the spring/summer. During summer, flow reduction and sediment stabilization can serve to decrease turbidity and enhance the available light for photosynthesis (Carr et al. 2010, 2012), creating a positive feedback for seagrass growth.

**ACKNOWLEDGEMENTS:** We thank A. Schwarzschild, C. Buck, B. Rodgers, and D. Boyd for field assistance, and J. Bricker for helpful discussions regarding wave-turbulence decomposition. This research was funded by the National Science Foundation (NSF-DEB 0621014, BSR-8702333-06, DEB-9211772, DEB-94118974, and DEB-0080381) to the Virginia Coast Reserve Long-Term Ecological Research program and by NSF-OCE 1151314. J.C.R. Hansen was supported through an NSF graduate research fellowship (DGE-0809128).

**CHAPTER 4:****Fine-scale mixing and momentum transport within a *Thalassia testudinum* seagrass meadow****ABSTRACT**

Seagrasses serve an important function in the ecology of Florida Bay, providing critical nursery habitat and a food source for a variety of organisms. They also create significant benthic structure that induces drag, altering local hydrodynamics that can influence mixing and nutrient dynamics. The seagrass *Thalassia testudinum* was investigated to determine how shoot density and morphometrics alter turbulence and wave effects on mixing processes and fluid retention times. The spatial structure of velocity and turbulence was determined using an *in situ* particle image velocimetry (PIV) system. Fluid retention times were calculated by measuring the passage of a dye plume both above and through the seagrass meadows using a fluorometer. Sparsely vegetated and densely vegetated meadows were monitored, with shoot densities of  $260 \pm 25$  and  $485 \pm 80$  shoots  $m^{-2}$ , respectively. Results of flow structure show that a typical logarithmic boundary layer does not form; instead a shear layer with an inflection point of instability forms at the top of the seagrass canopy. This shear layer imparts substantial turbulent mixing, and the depth of penetration of the turbulence into the seagrass meadow is a function of blade morphology and shoot density. Flow velocity was reduced within the canopy compared to ambient values, with 44% and 52% reductions in velocity at the sparse and dense canopies, respectively. Reynolds stress was reduced 16% across the canopy-water interface of the dense canopy, compared to a 10% vertical reduction at the

unvegetated site, while enhanced Reynolds stress was present within the sparse canopy. Fluid retention times within the canopy were found to vary with shoot density. However, oscillatory motion due to waves generated flow within the canopy that penetrated to a greater extent than unidirectional currents. Both shoot density and flow conditions were important drivers controlling mixing across the canopy-water interface.

## **INTRODUCTION**

Significant aboveground biomass is created by seagrass meadows, which serves as an obstruction to flow, altering local hydrodynamics that influence the meadow's productivity (Peralta et al. 2006; Schanz and Asmus 2003), photosynthetic rates (Koch 1994), nutrient uptake (Cornelisen and Thomas 2009; Thomas et al. 2000), and sediment dynamics (Bouma et al. 2009; Hansen and Reidenbach 2012, 2013; Koch 1999; Ward et al. 1984). Aquatic plant communities rely on the delivery of nutrients from the surrounding water column (Taylor et al. 1995), which must cross the canopy-water interface. This is particularly important in Florida Bay, where uptake of nutrients occurs near the mass-transfer limit (Cornelisen and Thomas 2009), and nutrient concentrations in the water column tend to be low due to the subtropical environment. Canopy-scale hydrodynamics are also important for the recruitment of larvae into suitable habitats (Eckman 1983; Grizzle et al. 1996) and the reproduction and distribution of seagrass meadows through the exchange of pollen across the canopy (Ackerman 1997; Ackerman 2002; Gaylord et al. 2004).

At the top of the seagrass canopy, significant drag is imparted to the flow, creating a discontinuity and displacing the logarithmic velocity profile vertically above the canopy into the water column (Ghisalberti and Nepf 2004). At the canopy-water interface, the discontinuity creates an instability point in the flow and a shear layer is developed (Nepf 2012). These shear layers grow to a finite thickness (Ghisalberti and Nepf 2002) effectively separating the canopy into an upper region of exchange, driven by turbulent transport, and a lower region of limited transport, driven by stem-generated turbulence (Lacy and Wyllie-Echeverria 2011). In the upper region, transport occurs through the development of Kelvin-Helmholtz vortices created by the velocity profile instability (Raupach et al. 1996). These eddy structures not only carry momentum across the canopy-water interface, but also promote the exchange of dissolved gasses (Anderson and Charters 1982) and nutrients (Cornelisen and Thomas 2009).

The density of the seagrass meadow will also influence the turbulence and shear layer structure. As the density of the seagrass meadow increases, energy generated by the Kelvin-Helmholtz vortices in the shear layer is lost more rapidly, shortening the penetration depth of turbulence into the canopy (Ghisalberti and Nepf 2004). Within sparsely vegetated canopies, velocity profiles can be logarithmic (Nepf 2012) or resemble disturbed boundary layers (Cornelisen and Thomas 2009) where turbulence is enhanced (Lacy and Wyllie-Echeverria 2011; Hansen and Reidenbach 2013; Lawson et al. 2012) due to stem-wake interactions with individual seagrass blades. In contrast, dense canopies resemble mixing layers (Cornelisen and Thomas 2009), which are formed when velocities in two adjacent regions flow at different speeds separated by a shear region

containing an inflection point (Raupach et al. 1996). Typically, turbulence below the mixing layer is negligible (Finnigan 2000; Lacy and Wyllie-Echeverria 2011).

Expected biophysical interactions are altered in the presence of waves. Oscillatory motion leads to movement of the seagrass blades, enhancing exchange (Koch and Gust 1999) and nutrient uptake (Lowe et al. 2005a). Low frequency waves penetrate the meadow (Bradley and Houser 2009; Hansen and Reidenbach 2012), while high frequency oscillatory flows are attenuated by the relative motion of the seagrass blades (Bradley and Houser 2009). This reduces the ability of the meadow to attenuate flow velocity and enhances turbulence at the canopy-water interface leading to greater mixing (Koch and Gust 1999). Enhanced fluid penetration under oscillatory flows also increases mass transfer in benthic canopies (Lowe et al. 2005b). Further, the interaction of the canopy with wave-induced flows is density-dependent (Hansen and Reidenbach 2012), and the ability for seagrass canopies to reduce within-canopy turbulence is decreased in wave dominated flows (Hansen and Reidenbach 2012). Lowe et al. (2005b) determined not only that oscillatory flow enhances mass transfer, but as shoot density increases, increases in mass transfer become more pronounced relative to unidirectional flows. Therefore, in both sparse and dense seagrass canopies, oscillatory flows should enhance turbulence, mixing, and mass transport.

Seagrass meadows in Florida Bay, USA suffered a large die-off event in 1987 (Zieman et al. 1999), which resulted in the loss of more than 4,000 ha (Robblee et al. 1991) due to changes to the freshwater supply that increased hypoxia (Robblee et al. 1991), sulfide toxicity (Borum et al. 2005; Carlson et al. 1994), and salinity (Zieman et al. 1999). The removal of seagrass leads to major changes in flow patterns (Fonseca and

Fisher 1986), and therefore, in light of historic and proposed future alterations to the Everglades and Florida Bay ecosystems, understanding the biophysical interactions within the seagrass meadows that control mixing across the vegetated canopy is critical to understanding their persistence in this environment. This study aims to investigate mixing parameters by quantifying flow and turbulence development in relation to the seagrass shoot density, as well as the vertical structure and efficiency of momentum transport. An *in situ* particle image velocimetry (PIV) system was employed under both wave- and current-dominated forcing. In the presence of waves, velocity data was analyzed using a spectral wave-turbulence decomposition method (Hansen and Reidenbach 2012) to obtain spatial velocity maps of the turbulence structure across varying density seagrass canopies. Velocity, Reynolds stress, and the turbulent kinetic energy (TKE) budget were quantified across two different density *Thalassia testudinum* seagrass canopies in Florida Bay under both unidirectional and oscillatory flow conditions.

## **METHODS**

### **Study area**

Florida Bay is characterized as a shallow basin, bordered by the Florida Keys, which separate the bay from the Atlantic Ocean to the east and the Gulf of Mexico to the west, with small island keys present throughout the bay. The study area was contained within the Everglades National Park, which has an area of 1800 km<sup>2</sup> with 1660 km<sup>2</sup> of seagrass; with *Thalassia testudinum* being the major species of seagrass in the area (Zieman et al. 1989).

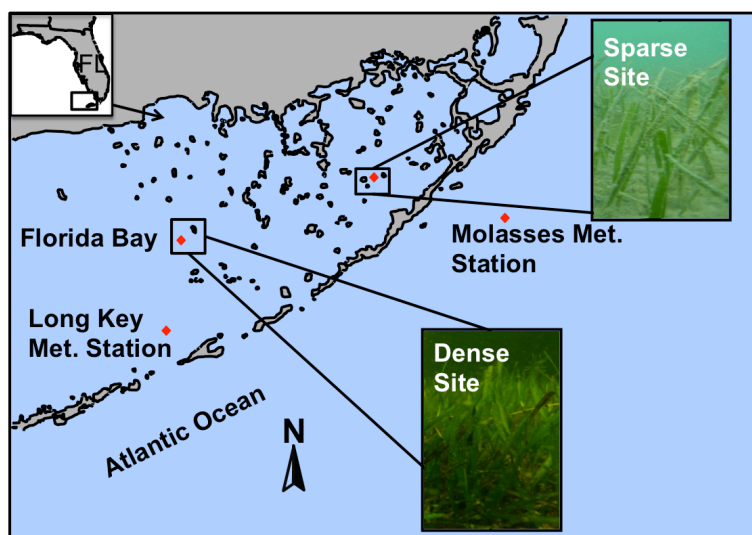


Fig. 4.1. Study sites, located in Everglades National Park, near Bottle Key and within Rabbit Key Basin in Florida Bay, FL, USA. Two separate *T. testudinum* meadows, labeled Sparse and Dense, and an additional unvegetated site as a comparison to flows in the absence of benthic structure, located near the sparse site, were monitored. Wind data was obtained from two NOAA data buoy meteorological stations, labeled Long Key Met. Station and Molasses Met. Station. Florida Keys map adapted from NOAA NGDC coastline extractor

Three locations within Florida Bay were chosen as study sites, two seagrass sites of different seagrass shoot densities, and an unvegetated site to serve as a comparison point for local flow conditions in the absence of considerable benthic structure (Fig. 4.1). The northeast portion of Florida bay tends to have sparse, patchy *T. testudinum* seagrass beds, while further South mixed beds of *T. testudinum* and *Halodule wrightii* are present (Zieman et al. 1989). The unvegetated site and the sparsely vegetated *T. testudinum* seagrass sites were 0.22 km apart, near Bottle Key, with the dense mixed *T. testudinum* and *H. wrightii* seagrass site located 29.8 km to the Southwest, in Rabbit Key Basin. Within the mixed bed, *T. testudinum* shoot density was approximately double that of *H. wrightii*. This is similar to the historic ratio of *H. wrightii* to *T. testudinum* (before the 1987-1991 die-off), reported as 1:1.31 across Florida Bay, which was reduced to 1:13.31 by 1994 (Hall et al. 1999). Further, the projected frontal area (defined as  $ah$ , where  $a = d/\Delta S^2$ ,  $d$  is blade width,  $\Delta S$  is the spacing between canopy elements (i.e., seagrass blades), and  $h$  is the canopy height; Nepf et al. 2012) of *H. wrightii* in this study was only 2.3% of that provided by *T. testudinum* where they co-exist, and therefore the impact of *H.*

*wrightii* on the flow dynamics is expected to be minimal. Shoot densities reported in this study represent that of the *T. testudinum* only. Experiments at each site were conducted during consecutive weeks in September 2009.

Table 4.1. *Thalassia testudinum*. Morphometrics of two seagrass meadows in Florida Bay, FL. Density was measured *in situ* via shoot counts within 0.25 m<sup>2</sup> quadrats. Canopy height, blade width, and inter-blade spacing were measured in the lab through image analysis using ImageJ software on pictures taken in the field

	Canopy Height (cm)	n	Density (shoots m <sup>-2</sup> )	n	Blade Width (cm)	n	Inter-Blade (cm)	n
Sparse	15.2±2.0	66	259±26	10	0.74±0.27	50	1.28±0.62	200
Dense	37 ± 4.8	50	484±78	10	0.80±0.19	40	1.13±0.55	160

### Seagrass morphometrics

Seagrass density was measured at each site by counting the number of seagrass shoots per 0.25 m<sup>2</sup> quadrat placed on the seafloor. Seagrass blade length, blade width, canopy height, and the spacing between blades were measured via image analysis of the canopy with ImageJ software. Canopy height was defined as the average of the longest 2/3 of the blade lengths as per methodology in Koch et al. (2006). The seagrass meadows had significantly different densities of  $260 \pm 25$  shoots m<sup>-2</sup> and  $485 \pm 80$  shoots m<sup>-2</sup> (one-way ANOVA,  $p < 0.05$ ), which will therefore be referred to as the sparse and dense seagrass sites to represent their relative shoot densities, and significantly different lengths with averages of  $33 \pm 7$  cm and  $14 \pm 2$  cm (one-way ANOVA,  $p < 0.05$ ), respectively (Table 4.1). This “dense” site is on the lower range of that present within Florida Bay; average short-shoot density across the Bay in 1994 was  $565.7 \pm 50.5$  ( $\pm$ SE) (Hall et al. 1999), between 1989 and 1995 short-shoot density was between  $518 \pm 49$  and  $768 \pm 33$  ( $\pm$ SE) (Zieman et al. 1999), and in 2005 it was reported to range from  $665 \pm 139$  to  $1533 \pm 137$ , with shoot density near Rabbit Key at  $1233 \pm 190$  (Borum et al. 2005). Since shoot

densities were on the lower range of what may be expected in Florida Bay, but both had frontal areas greater than would be characteristic of a “dense” meadow ( $ah > 1$ ), the designation of “sparse” and “dense” was used to represent their relative densities in this study.

### **Instrumentation**

Water velocities were measured using two Nortek Vector© acoustic Doppler velocimeters (ADV<sub>s</sub>), and located with their 1 cm<sup>3</sup> sampling volume at  $z = 0.35$  m and  $z = 0.15$  m above the bed at the unvegetated site,  $z = 0.3$  m and  $z = 0.1$  m above the bed ( $z/h = 2.0$  and  $0.7$ , where  $h$  is canopy height) at the sparse seagrass site, and  $z = 0.5$  m and  $z = 0.3$  m above the bed ( $z/h = 1.4$  and  $0.8$ ) at the dense seagrass site. This ensured that when seagrass was present, the sample volumes were placed at the same position relative to the top of the canopy for each of the two seagrass sites, with one placed 0.15 m above and the other 0.05 m below the canopy. Velocity and pressure were recorded at 32 Hz for 10 min bursts every 20 min over a 72 hr period in order to obtain high-resolution temporal data. The 10 min time interval was chosen as the best balance between convergence of mean statistics, while minimizing drift due to changes in flow conditions (Gross and Nowell 1983). Data were rotated in post-processing from earth coordinates, east, north, and up, to align with dominant horizontal flow direction,  $u$ , minimizing the transverse direction,  $v$ , while leaving the vertical,  $w$ , unchanged. Velocity values with poor correlations were removed, often due to interference from drifting wrack or from fish swimming below the sensors.

Wind data was obtained from the National Data Buoy Center C-MAN stations at Molasses Reef, FL (MLRF1) and Long Key, FL (LONF1). The Molasses Reef station was located 19.75 km from the bare and sparse seagrass sites, and the Long Key Station was 13.65 km from the dense seagrass site. Using a two-year data set (from 1989-1991), Wang et al. (1994) analyzed wind data from Miami Airport, Key West, Flamingo, and Molasses Reef and determined that wind is spatially coherent in Florida Bay. Therefore, the large spatial scale of the wind data presented in this paper is likely representative of overall wind speed and direction at the different sites. Wind direction and magnitude were reported once every 10 min for each site.

### **Particle image velocimetry**

In order to investigate physical processes occurring at the seagrass canopy-water interface, small-scale velocity fields were examined using an underwater particle image velocimetry (PIV) system (Liao et al. 2009). A 532nm, 300mW laser (Laserglow Technologies), and a high definition video camera (Sony HDR-HC7), equipped with a  $530 \pm 10$  nm bandpass filter (Omega Optical 530BP10) to remove ambient light, were used to capture particle motion. A convex lens was used to spread laser light into a 2 mm thick sheet oriented parallel to the flow. The water was seeded with neutrally buoyant 100  $\mu\text{m}$  clay particles. Particle motion was recorded by the video camera over a 12 cm by 6 cm viewing window at 30 frames per second.

High definition videos were first translated into individual images, then sequential image pairs were processed using a cross-correlation analysis to track particle motions over time using MatPIV, a PIV analysis software program written for Matlab® (Sveen

and Cowen 2004). Particle tracking relies on pattern recognition between sequential frames determined via Fast-Fourier transform:

$$R(s, t) = \sum_{m=0}^{M-1} \sum_{n=0}^{N-1} I_1^{i,j}(m, n) \times I_2^{i,j}(m-s, n-t) \quad (1)$$

such that  $I_1$  and  $I_2$  represent two sequential images, which have been divided into sub-windows represented by  $i$  and  $j$ ,  $s$  is the position of the particles, and  $t$  is the time between images (Sveen 2004). Horizontal,  $u$ , and vertical,  $w$ , velocities are solved for each 32x32 pixel interrogation window with 50% overlap such that the final resolution is on a 16x16 pixel scale. Accuracy of the PIV measurements was found to be relative to the mean velocity of the flow  $U$ , with an overall accuracy of  $\pm 6\%U$  (Reidenbach et al. 2008). Ideal particle seeding concentration for achieving high accuracy ( $\sim 1\%$ ) typically ranges from about 5 – 10 particles per interrogation window (Bertuccioli et al. 1999; Keane and Adrian 1990); Bertuccioli et al. (1999) found 4.2 particle pairs per 64x64 interrogation window was sufficient in a natural environment. Particle seeding for PIV data collected in the seagrass meadows of Florida Bay, FL, ranged from 0 to 10 - 15 particles per 0.2x0.2 cm subwindow. Due to the planar nature of the PIV measurements, turbulence, velocity, and vorticity can be measured in the boundary layer independent of the typical flow structure assumptions of a logarithmic velocity profile, a constant stress layer, or an inertial subrange within the turbulence spectra (Bertuccioli et al. 1999). This allows for measurement in inhomogeneous flows, and the investigation of spatial variations in turbulence without the use of Taylor's frozen hypothesis (Nimmo Smith et al. 2002).

Turbulence magnitude is calculated by subtracting the temporal mean velocity ( $\bar{u}$ ,  $\bar{w}$ ) from each instantaneous horizontal ( $u$ ) and vertical ( $w$ ) component of velocity,  $u = \bar{u} + u'$  and  $w = \bar{w} + w'$  (Cowen et al. 2001). The cross-correlation of the

fluctuations from the mean are averaged over the time series to quantify turbulence magnitude,  $\overline{u'w'}$ . Turbulent kinetic energy (TKE) is calculated as:

$$q'^2 = \overline{u'u'} + 2.3\overline{w'w'} \quad (2)$$

Since only the horizontal and vertical velocity components are measured with PIV, the third component of velocity,  $\overline{v'v'}$ , is estimated as  $1.3\overline{w'w'}$  (Raupach et al. 1991).

Turbulence production ( $P$ ) is equal to the turbulence magnitude multiplied by the velocity gradient,  $P = -\overline{u'w'} \frac{\partial U}{\partial z}$ . Turbulent dissipation was calculated according to Zhu et al.

(2006):

$$\varepsilon_D = \frac{15}{7} \nu \left[ 2 \left\langle \frac{\partial u^2}{\partial x} \right\rangle + 2 \left\langle \frac{\partial w^2}{\partial z} \right\rangle + \left\langle \frac{\partial u^2}{\partial z} \right\rangle + \left\langle \frac{\partial w^2}{\partial x} \right\rangle + 2 \left\langle \frac{\partial u}{\partial z} \frac{\partial w}{\partial x} \right\rangle \right] \quad (3)$$

where  $\nu$  is the kinematic viscosity and brackets denote ensemble averages. Under equilibrium conditions, turbulent production and dissipation tend to be in balance.

However, in non-equilibrium, turbulent kinetic energy will be transported, either through turbulent transport or pressure driven transport (Reidenbach et al. 2010). Turbulent transport ( $T_t$ ) is computed from the vertical gradient in TKE, such that:

$$T_t = - \frac{\partial(\overline{0.5q'^2 w'})}{\partial z} \quad (4)$$

### Wave-turbulence decomposition

When waves and currents are both present, velocity fluctuations are associated with both waves and turbulence, and some sort of wave-turbulence decomposition must be performed (Trowbridge 1998). Instantaneous horizontal and vertical velocities can be written as:

$$u = \bar{u} + u' + \tilde{u} \quad w = \bar{w} + w' + \tilde{w} \quad (5)$$

such that  $u'$ ,  $w'$  are fluctuations in velocity due to turbulence,  $\tilde{u}$ ,  $\tilde{w}$  are fluctuations due to waves, and  $\bar{u}$ ,  $\bar{w}$ , are the mean velocity. To separate the contributions due to waves and turbulence a spectral decomposition, the Phase method (Bricker and Monismith 2007), was utilized on velocity data obtained via PIV. The phase lag between the  $u$  and  $w$  components of surface waves were used to interpolate the magnitude of turbulence under the wave peak (Hansen and Reidenbach 2012). The wave stress was then calculated through the spectral sum of motions within the wave band of the velocity spectrum:

$$\overline{\tilde{u}\tilde{w}} = \int_{-f_{Nyquist}}^{f_{Nyquist}} S_{\tilde{u}\tilde{w}}(f) d(f) \quad (6)$$

where  $S_{\tilde{u}\tilde{w}}(f)$  is the two-sided cross-spectral density (CSD) of the wave-induced orbital velocities and  $f$  is the frequency.  $S_{uw}(f)$  was computed from the full spectrum and integrated in a similar manner as Eq. 6 to quantify  $\overline{uw}$ . The turbulent Reynolds stress was then found as the difference between the total stress and the wave stress:

$$\overline{u'w'} = \overline{uw} + \overline{\tilde{u}\tilde{w}} \quad (7)$$

Further details of this technique can be found in Hansen and Reidenbach (2012).

### Quadrant analysis

Quadrant analysis describes the vertical transport of momentum (Lu and Willmarth 1973), where fluctuations for horizontal and vertical velocities,  $u'$  and  $w'$ , were normalized by their standard deviations and divided into the four Cartesian quadrants based on the sign of their instantaneous values. The total contribution to Reynolds stress within each quadrant was found by summing the absolute value of the  $u'$

and  $w'$  contributions for each quadrant and dividing by the total contribution from all quadrants. Quadrants 2 and 4 are responsible for the vertical momentum transfer across the seagrass canopy, and are termed turbulent ejections and sweeps, respectively. Typically, momentum transport is dominated by these ejection and sweeping events, which advect low momentum fluid vertically upwards out of the meadow or transfer high momentum fluid vertically downward toward the seafloor. Contours of the turbulent probability distribution function (pdf) were plotted, and the percent of the distribution in each quadrant was calculated both within and above the canopy. Within the seagrass bed this analysis aids in determining how turbulent motions contribute to momentum flux across the canopy. Only time periods with no waves were analyzed.

## RESULTS

### Site characterization

Physical characteristics of each site are reported in Fig. 4.2. Winds were of greater magnitude on average during the deployment at the sparse site, and further increased during the deployment at the dense site (one-way ANOVA with Bonferroni multicomparison,  $p < 0.05$ ). Prevailing wind direction during the deployment at the bare site was toward the Southwest, while winds during the sparse and dense deployments were toward the Northwest (Fig. 4.2A). The fetch length at each of the sites was similar (one-way ANOVA on fetch lengths at 30 degree intervals,  $p = 0.9$ ); therefore wave development was primarily dependent on wind magnitude. Water temperature was consistent throughout the deployment period, with temperature ranges of 29 to 31 °C (Fig. 4.2B).

Average water column depths ( $\pm$  tidal amplitude) were  $2.5 \pm 0.04$ ,  $2.4 \pm 0.03$ , and  $2.6 \pm 0.10$  m at the bare, sparse, and dense sites, respectively. Water flow within the Northeastern portion of Florida Bay is restricted from the tidal influences of the neighboring Atlantic Ocean and the Gulf of Mexico by the numerous keys and shallow banks (Wang et al. 1994); therefore, in this area wind driven currents dominate (Holmquist et al. 1989). Thus, both the bare and sparse sites had small tidal amplitudes, though their water depths were statistically different (one-way ANOVA with Bonferroni multicomparison,  $p < 0.05$ ). The dense seagrass site was deeper and more influenced by tides from the Atlantic Ocean, resulting in significantly greater tidal amplitudes (one-way ANOVA with Bonferroni multicomparison,  $p < 0.05$ ). This also resulted in faster water velocities at the dense site compared to the unvegetated or sparse seagrass sites (Fig.

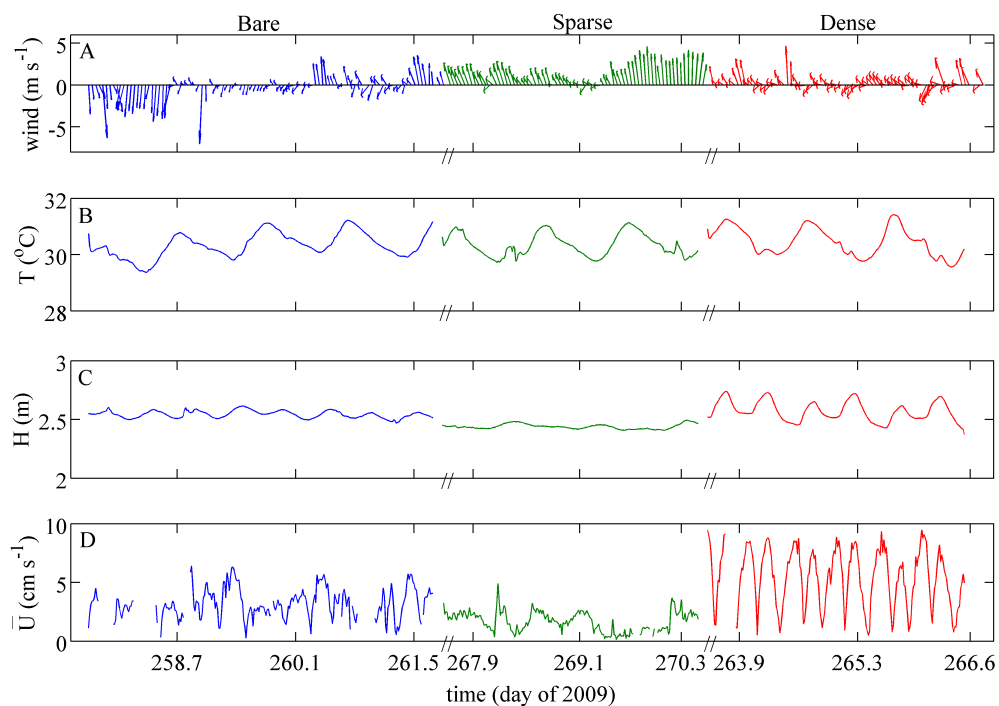


Fig. 4.2. (A) Wind magnitude and direction, arrows denote the direction toward which the wind is blowing with Northward up and Eastward to the right, (B) water temperature,  $T$ , (C) water depth,  $H$ , and (D) horizontally averaged velocity,  $U$ , above the seagrass meadow. Note discontinuous time record between successive monitoring of the sites

4.2D). Therefore, to isolate differences in fluid parameters influenced by the seagrass canopy structure, data comparisons between sites were via a percent reduction from ambient conditions (above the canopy) or through normalization. Data was normalized either by the maximum velocity in a vertical profile, or the shear velocity ( $u_*$ ) obtained from a logarithmic best-fit to velocity data above the seagrass canopy using the law-of-the-wall approximation (Fig. 4.3).

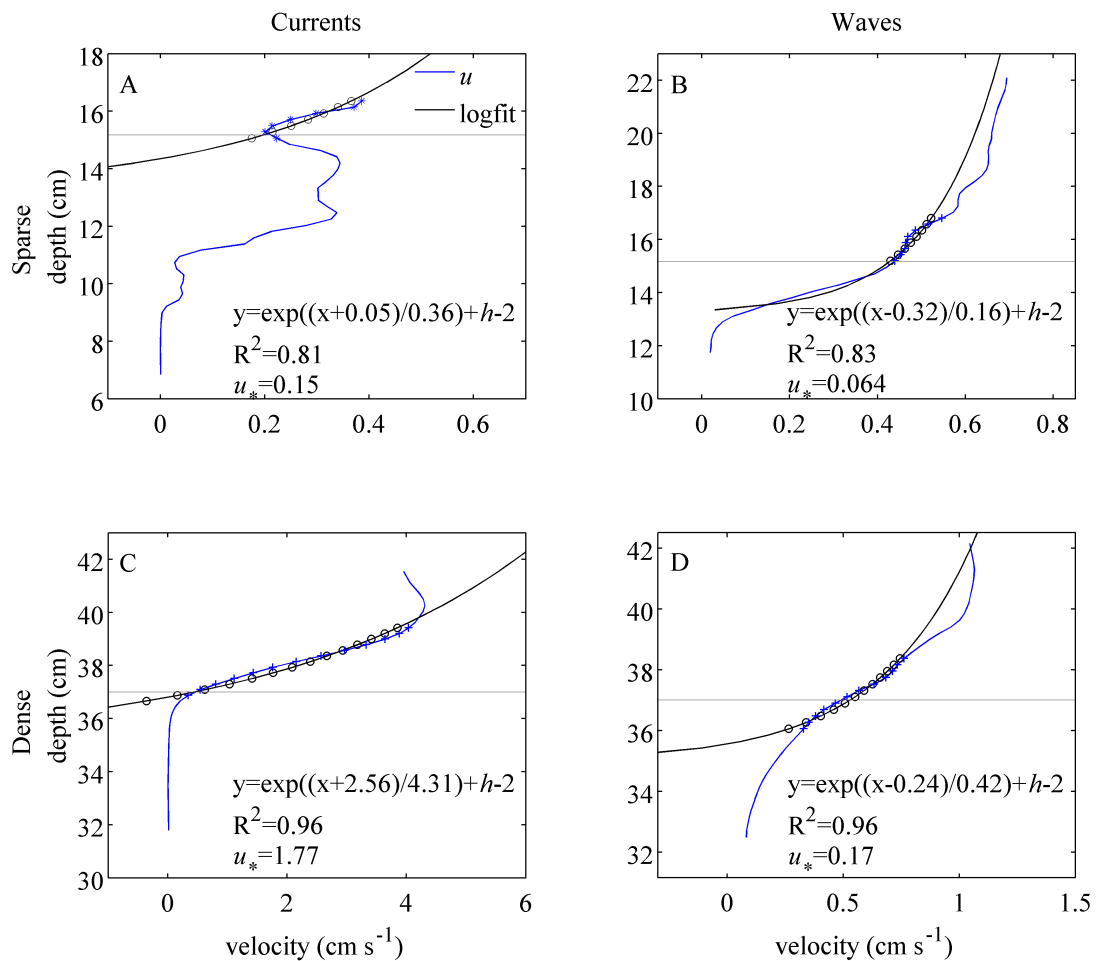


Fig. 4.3. Logarithmic best-fit to vertical profiles of horizontal velocity under unidirectionally- (A,C) and wave- (B,D) dominant flow conditions at the sparse (A,B) and dense (C,D) seagrass meadows. Equations represent the fit using the law-of-the-wall approximation.

## Velocity structure

The vertical velocity gradient in the water column was determined for each site from the ADV measurements. Within canopy velocities were reduced 44% and 52% at the sparse and dense site, respectively, compared to above the canopy. These reductions were significantly greater (one-way ANOVA with Bonferroni multicomparison,  $p < 0.05$ ) than the 22% reduction in near-bed flows at

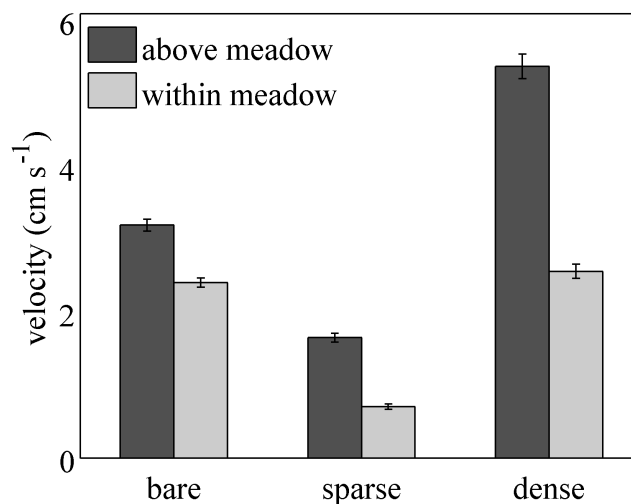


Fig. 4.4. Time averaged velocity,  $\pm$  standard error, taken at the same relative positions above and within the seagrass canopy

the bare site (Fig. 4.4). Overall, velocities were reduced throughout the water column at the sparsely vegetated site compared to the unvegetated site.

Velocities, measured at 2 mm spatial resolution across the seagrass canopy, were

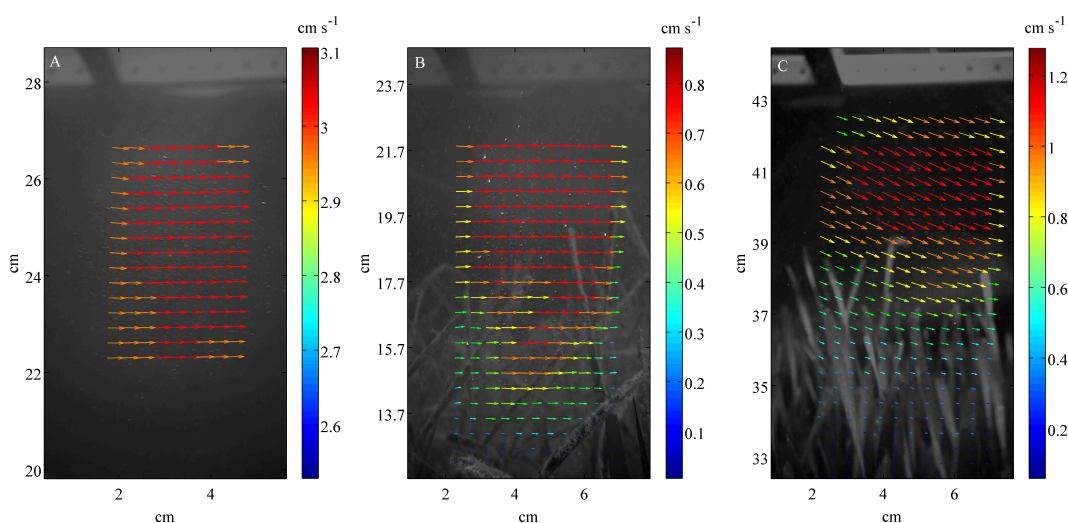


Fig. 4.5. Mean velocity vectors at the bare site (A), sparse seagrass site (B), and dense seagrass sites (C) under wave dominated flows. Length of the vector arrows indicates magnitude and arrowheads indicate direction. Y axis is distance (cm) above seafloor, for the sparse site  $z/h = 0.9 - 1.6$  and the dense site  $z/h = 0.89 - 1.16$

obtained from particle image velocimetry (PIV). At the bare site, unidirectional flow existed through the water column that contained low mean-shear (Fig. 4.5A). At the sparse site, unidirectional flows showed low shear above the meadow but a shear layer developed near the top of the meadow. At both the sparse and dense sites, flow was reduced within the seagrass canopy compared to above (Fig. 4.5B,C), but stronger mean velocity shear developed within the dense canopy. Additionally, at the dense site, negative mean vertical velocities indicate flow into the meadow from the overlying water column, which may suggest that within canopy transport is dependent upon vertical exchange across the canopy.

Shear layers developed due to the presence of the seagrass structure, which included an inflection point of instability at the canopy-water interface (Fig. 4.6). Normalized velocity profiles showed low vertical velocity gradients ( $dU/dz$ ) above the canopy, but high shear at the top of the canopy, which increased with increasing seagrass shoot density (Table 4.2). When waves were present, the shear velocity,  $u_*$ , decreased (Table

4.2). During these periods, normalized wave dominated flows produced much higher velocities within the dense meadow than under current-dominated flows (Fig. 4.6). The profile development under wave-dominated flows was similar over both density

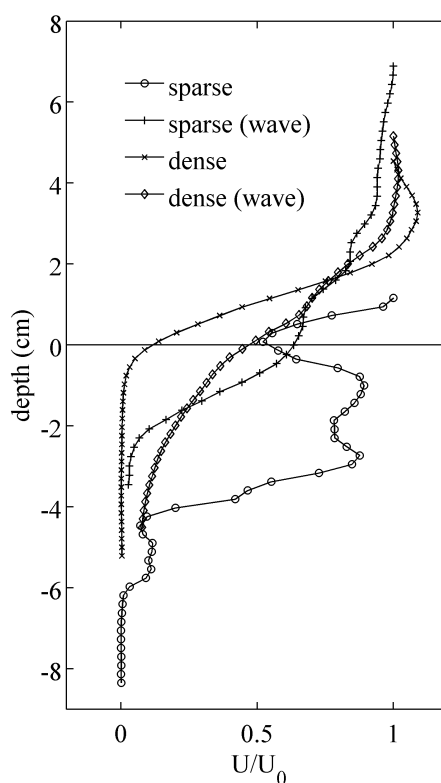


Fig. 4.6. Velocity profiles at the sparse and dense seagrass sites normalized by the velocity at the top of each profile. Horizontal gray line represents the seagrass canopy. Mean estimates were formed by averaging horizontally across all the PIV velocity vectors

meadows. Further, normalized velocity profiles show enhanced flow penetration into the sparse meadow as compared to the dense meadow (Fig. 4.6).

### Velocity spectra and orbital motion

Power spectral densities (PSDs) of horizontal velocities during current- and wave-dominated flow conditions were determined for each site at two locations in the water column, one above and the other within the seagrass canopy (Fig. 4.7), and compared to equivalent elevations at the bare site. At the bare site, there was general agreement in the spectra at both locations for each flow condition (Fig. 4.7A). The turbulence portions of the spectra were also similar under current- and wave-dominated conditions. At the sparse site, the differentiation between wave-dominant and current-dominant flows was less distinct and a slight wave-peak can be seen both above and within the canopy under both flow conditions (Fig. 4.7B). Across the dense canopy, there is a reduction in the wave peak of the spectrum and a significant decrease in turbulence within the meadow (Fig. 4.7C). This reduction in the turbulence spectrum occurs at the canopy-

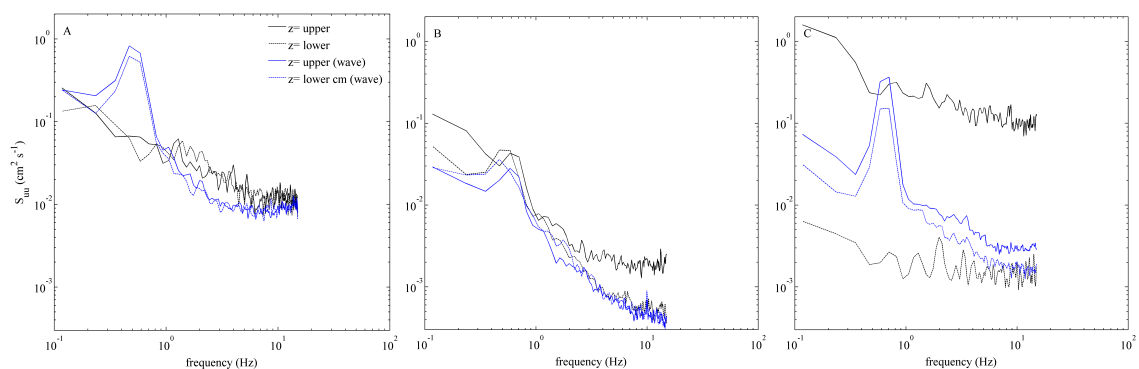


Fig. 4.7. Velocity spectra at two locations in the water column at the bare (A), sparse (B), and dense (C) sites for current- and wave-dominated flow periods (black and blue lines, respectively). Two vertical locations in the water column, denoted upper and lower, were separated by 2 cm. At the seagrass meadow sites, measurements were taken from 1 cm above (upper) and 1 cm below (lower) the canopy

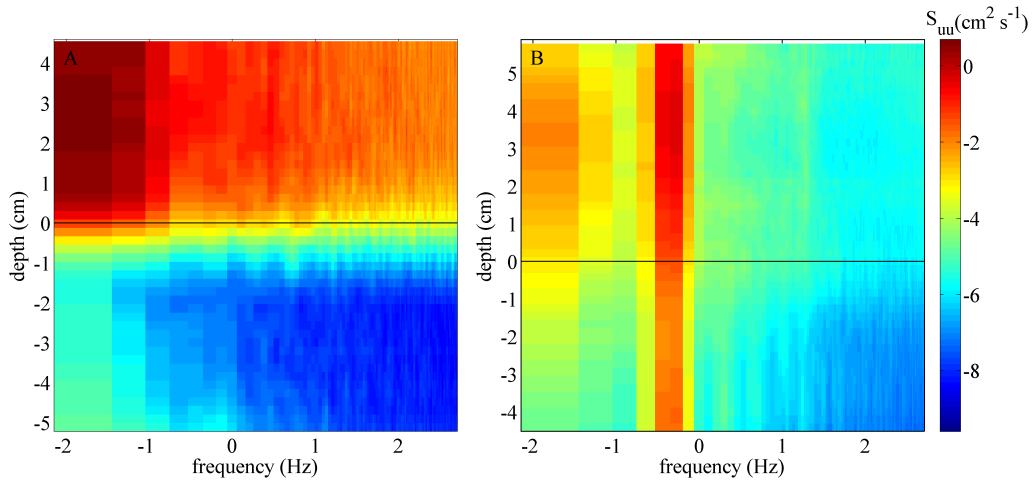


Fig. 4.8. Variations in the natural logarithm of power spectral density (PSD) for horizontal velocity,  $S_{uu}$ , with depth at the dense seagrass site, where warmer colors represent greater PSD, under unidirectional (A) and wave-dominated (B) flows. The depth range from -5 to 5 cm across the canopy represents  $z/h = 0.9 - 1.14$ . Horizontal black line is the canopy height

water interface (Fig. 4.8A). Reduction in the wave spectrum also coincides with the canopy-water interface; however, the gradient in the PSD is much smaller and is confined to a narrow frequency band indicating the prevalence of the wave signature (Fig. 4.8B). Further, under current-dominated flow, the turbulence spectral energy is much greater than under wave-dominated flow conditions (Fig. 4.8).

Wave orbital velocities and peak wave periods were determined from the PSD of horizontal velocity. Horizontal orbital velocity was calculated according to Wiberg and Sherwood (2008):

$$u_{os} = \sqrt{2 \sum_j S_{\tilde{u}\tilde{u}_j} \Delta f_j} \quad (8)$$

where  $u_{os}$  is equivalent to the root-mean-squared (rms) orbital velocity,  $S_{\tilde{u}\tilde{u}}$  is the wave portion of the velocity spectra, and  $f$  is the frequency. Profiles of orbital velocities were obtained by averaging horizontally across the PIV viewing window and normalized by velocity at the top of each profile. For both the sparse and dense seagrass meadows, rms

orbital velocities were greater than average flow velocity. Further, rms orbital motion was greater at the sparse site than at the dense site.

### Turbulent kinetic energy

Turbulent kinetic energy (TKE) produced across the top of the seagrass canopies was quantified using the spatial information of the velocity vectors obtained from the PIV technique. The TKE budget can be represented by the following equation (Townsend 1976):

$$\frac{-\partial(\overline{0.5q'^2})}{\partial x} + \frac{-\partial(\overline{0.5q'^2})}{\partial z} = -\overline{u'w'} \frac{\partial U}{\partial z} - \frac{\partial(\overline{0.5q'^2 w'})}{\partial z} - \frac{1}{\rho} \frac{\partial(\overline{w'p'})}{\partial z} - \varepsilon \quad (9)$$

where the terms on the left are advective flow terms, and on the right are production ( $P$ ), turbulent transport ( $T_t$ ), pressure driven transport ( $T_p$ ), and dissipation ( $\varepsilon$ ), respectively. In fully developed shear flows, the left hand side equals zero. Under equilibrium conditions, production and dissipation are equal and in nonequilibrium conditions, TKE is transported, either through pressure driven transport or turbulent transport. TKE dissipation can also be calculated through the temporal data series obtained from the PIV data as:

$$S_{uu}(k) = \frac{9}{55} \left( \frac{4 - \cos^2(\theta)}{3} \right) 1.56 \varepsilon^{2/3} f^{-5/3} (k)^{2/3} \quad (10)$$

where  $S_{uu}(k)$  is the power spectral density as a function of the wave number,  $k$ ,  $\theta$  is the phase angle,  $\varepsilon$  is dissipation,  $f$  is frequency, and  $u$  is horizontal velocity (Reidenbach et al. 2007). Using Taylor's frozen turbulence hypothesis (Kundu 1990), wavenumber space was converted to frequency space as  $f = Uk/(2\pi)$ . Dissipation was then estimated through Eq. 10 by determining the spectral intensity  $S_{uu}$  at a given frequency,  $f$ , within the inertial

subrange, isolated via a least squares fit straight line to the velocity spectrum in frequency space.

To confirm the dissipation data, results from these two methods were compared (Fig. 4.9). Overall, vertical profiles of dissipation were similar, reflecting the accuracy of the PIV data. Differences between resulting profiles can be attributed, in part, to the filtering of spatial TKE dissipation values based on the divergence between the magnitudes of instantaneous dissipation and production (where production magnitudes <

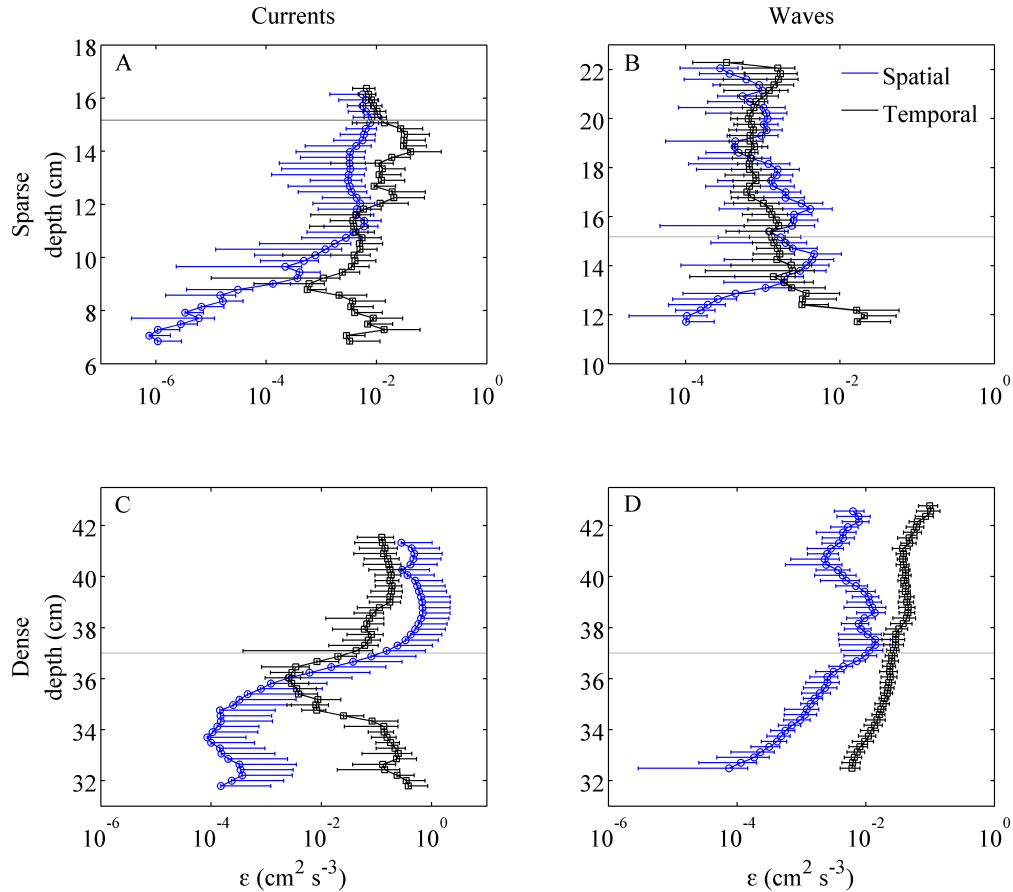


Fig. 4.9. Vertical profiles of TKE dissipation,  $\epsilon$ , under unidirectionally- (A,C) and wave- (B,D) dominant flow conditions at the sparse (A,B) and dense (C,D) seagrass meadows. Dissipation was calculated via two methods, (1) using the spatial matrix of velocity (blue lines) and (2) using the  $-5/3$  slope characteristic of turbulence on time series of velocity translated into frequency space (black lines),  $\pm 1$  standard deviation on data averaged horizontally across the spatial matrix. Horizontal gray lines represent the canopy height.

10% of dissipation magnitudes were removed). Based on this filtration technique, the average spatial resolution of the PIV data ranged from 0.2 to 1.9 cm. This compared to eddy length scales for both density meadows under all flow conditions that ranged from 0.5 to 2 cm. Eddy length scale was computed through a modification of the integral time scale, where the normalized autocorrelation function of the horizontal velocity was computed on the horizontal spatial scale of the PIV for each time step and measurement height. The autocorrelation series was then integrated to obtain the horizontal spatial distance over which velocity remains highly correlated, reflecting the eddy scale. The overlap in the eddy scale and spatial resolution scales suggests the data resolution is on the order necessary to resolve locally developed turbulence eddies within the seagrass meadows.

TKE production and dissipation were much greater above the dense seagrass canopy than the sparse canopy due to the fully developed shear layer and larger ambient velocities (Fig. 4.10). This strong shear over the dense canopy led to large production and dissipation values between 1.5 and 3.5 cm ( $z/h = 1.04 - 1.09$ ) above the canopy-water interface (Fig. 4.10B). The peak in production at 1.5 cm above the canopy ( $z/h = 1.04$ ) is matched by large turbulent transport values suggesting redistribution of TKE above the meadow, away from the shear layer (Reidenbach et al. 2010). Approximately 3 cm from the canopy-water interface ( $z/h = 1.08$ ), values return to equilibrium flow conditions where dissipation and production are balanced and there is a net loss in turbulent transport. These shear dynamics suggest enhanced vertical exchange above the canopy.

The open nature of the sparse canopy led to greater TKE dissipation within the canopy where velocity gradients were enhanced by flow penetration below the top of the

canopy (Fig. 4.10A). Peaks in production, dissipation, and turbulent transport occurred adjacent to the top of the canopy as well, at about 1 to 1.5 cm below the median seagrass blade length ( $z/h = 0.80 - 0.83$ ). Across the sparse canopy the shear region is less well defined and turbulent transport occurs over a larger vertical extent throughout the canopy.

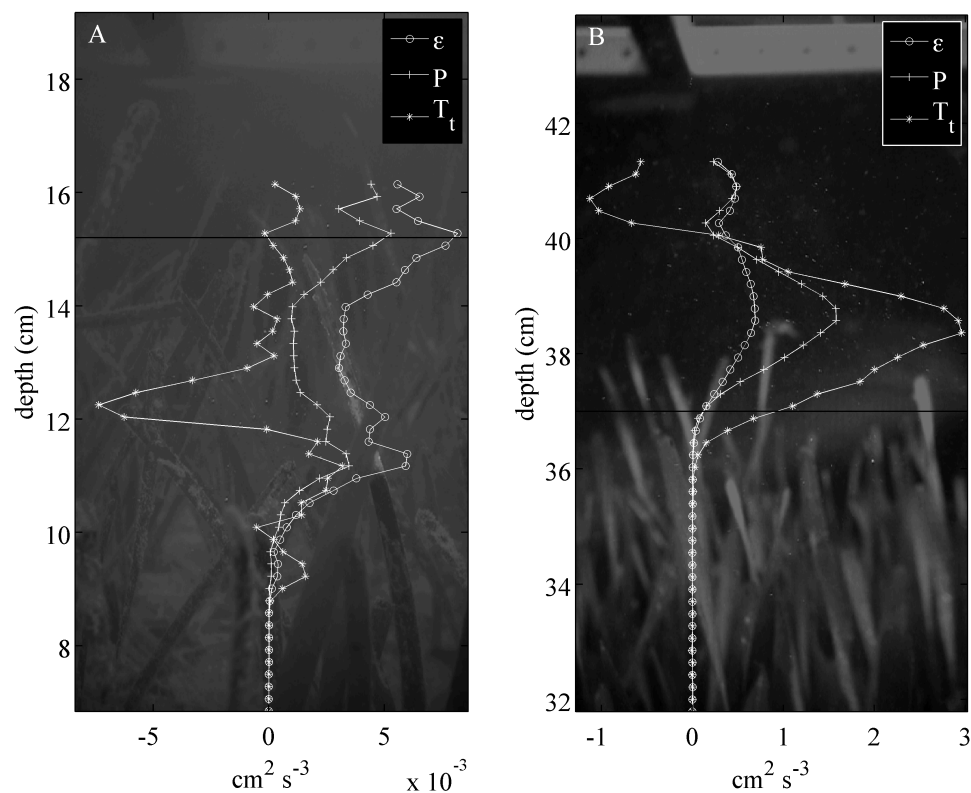


Fig. 4.10. Vertical profiles of turbulent kinetic energy (TKE) dissipation, production, and turbulent transport across sparse (A) and dense (B) seagrass canopies during current dominated flows. Horizontal black lines represent the canopy height. Normalized depth,  $z/h$ , at the sparse site were 0.53 – 1.18 and at the dense site, 0.86 – 1.4

Turbulence dynamics within the meadows were also quantified during periods of wave dominant flows (Table 4.2). After removal of motion due to waves, TKE production and dissipation were quantified and non-dimensionalized for comparison across different ambient flow conditions. Normalization was performed by dividing  $P$  and  $\varepsilon$  by  $u_*^4 / \nu$ , where  $u_*$  is the shear velocity, and  $\nu$  is kinematic viscosity. At the dense site, production and dissipation were enhanced 1 to 2 orders of magnitude, respectively,

above the canopy, which resulted in greater dissipation than production of TKE. Above the sparse seagrass canopy, dissipation was enhanced 5 to 13 times and production 2 to 6 times in wave-dominated flows. The presence of waves also shifted peaks in production and dissipation toward the seafloor through the limitation of shear layer development (Table 4.2).

Table 4.2. Maximum values and locations ( $z/h$ ) of normalized turbulent kinetic energy (TKE) production ( $P$ ) and dissipation ( $\mathcal{E}$ ) at a sparse and dense *Thalassia testudinum* canopy, and shear velocities ( $u_*$ ) from vertical profiles obtained with particle image velocimetry (PIV). Measurements were taken during periods of both wave and current dominated flows, separated below, and normalized by concurrent shear velocity and kinematic viscosity to non-dimensionalize values for comparison

	$P$	$\mathcal{E}$	$z/h$	$u_*$ ( $\text{cm s}^{-1}$ )	$P$ (wave)	$\mathcal{E}$ (wave)	$z/h$	$u_{*wave}$ ( $\text{cm s}^{-1}$ )
Sparse	9.20E-2	1.42E-1	1.01	0.15	5.70E-1	2.26	0.94 ( $P$ ), 0.95 ( $\mathcal{E}$ )	0.06
Dense	1.36E-3	5.90E-4	1.04	1.77	7.54E-2	1.39E-1	1.01	0.17

### Reynolds stress and momentum transport

Results from ADV measurements across the canopy-water interface showed a 16% decrease in Reynolds stress within the dense seagrass meadow (one-way ANOVA,  $p = 0.05$ ). At the sparse site turbulence was significantly enhanced within the meadow (one-way ANOVA,  $p < 0.05$ ), likely due to stem-generated turbulence as flow penetrates the more open canopy. Utilizing PIV, Reynolds stress increased with height above the canopy (Fig. 4.11). Flow penetration into the canopy at the sparse site led to greater Reynolds stress during both wave-dominated and current-dominated periods as compared to the dense site. Above the meadow, the vertical structures of the stress profiles at the sparse and dense sites were similar. Overall, the presence of waves enhanced Reynolds stress at both the sparse and dense meadows (Fig. 4.11).

To determine the mechanisms driving mixing across the canopy, a quadrant analysis was performed on the fluctuations in horizontal,  $u'$ , and vertical velocities,  $w'$ , that contribute to the Reynolds stress. ADV data was first filtered to select for time periods both within and above the meadow where there was turbulence with very little motion due to wave activity (wave energy < 1% of the total energy). The  $u'$  and  $w'$  values during these periods were then normalized by their standard deviations over a 10 min averaging window before the full subset of samples was sorted into each of four quadrants.

Quadrants 2 and 4 are responsible for the momentum transport through turbulent ejections (Q2), where low momentum fluid is fluxed upward into faster overlying flows, and sweeps (Q4), where high momentum fluid is fluxed downward toward the seafloor.

Momentum transport was evenly distributed between each of the quadrants at the bare site: Q1 (20%), Q2 (29%) Q3 (22%), and Q4 (29%) at  $z = 0.35$  m and Q1 (15%), Q2 (34%), Q3 (23%), and Q4 (28%) at  $z = 0.15$  m above the seafloor. Above the canopy at the dense site, ejection and sweeping events account for 52% of the Reynolds stress, similar to values over the unvegetated seafloor. Within the canopy, this increases to 72%

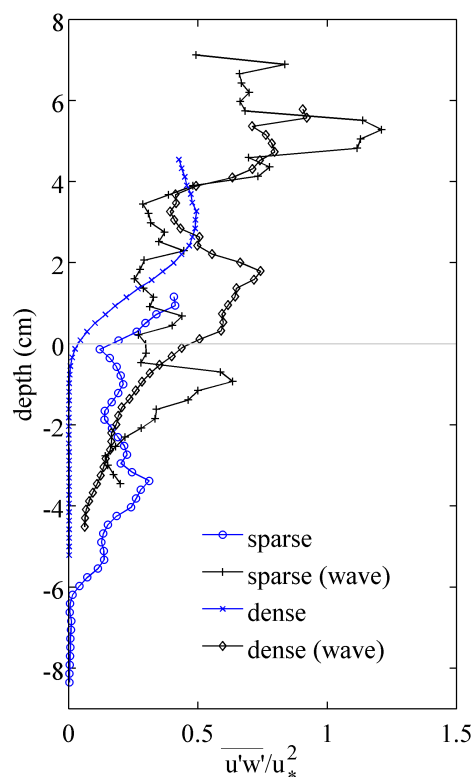


Fig. 4.11. Vertical profiles of average Reynolds stress normalized by shear velocity,  $u_*$ , across the sparse and dense seagrass canopies in the presence and absence of wave orbital motion. Spatial flow characteristics were obtained via particle image velocimetry (PIV), which were post-processed with a wave-turbulence decomposition to obtain Reynolds stress when waves were present. Grey horizontal line represents the seagrass canopy height

suggesting that mixing across the seagrass canopy is enhanced by turbulent momentum transport near the canopy-water interface. At the sparse site, transport above the canopy was distributed evenly into the Q2 and Q4 (Q1 = 19%, Q2 = 30%, Q3 = 20%, Q4 = 31%), and within the canopy was slightly dominated by turbulent ejections; Q1 (23%), Q2 (29%), Q3 (25%), Q4 (23%).

Data collected by both the ADVs and PIV at the bare site exhibited even distributions of momentum within all 4 quadrants, typical of isotropic turbulence (Fig. 4.12A). Using the spatial velocity data from the PIV, the distribution of the magnitude of Reynolds stress in each quadrant was also examined. Vertical profiles of Reynolds stress distributions were created by averaging horizontally across the PIV viewing window (Fig. 4.12B). At the bare site, Reynolds stress was evenly distributed and of similar magnitude in each quadrant (Fig. 4.12A,B). Further, Reynolds stress magnitudes did not change with vertical distance above the unvegetated seafloor (Fig. 4.12B).

Sweeps of momentum from the overlying water column down into the canopy dominated the distribution of Reynolds stress magnitudes at the dense seagrass meadow (Fig. 4.12F). Above the canopy-water interface, 40% of momentum transport was contained in Q4. Momentum transport through turbulent ejection caused by turbulence generated at the top of the canopy was confined to a narrow region, about 4 cm, across the canopy-water interface. About 2 cm into the dense canopy ( $z/h = 0.95$ ), distribution between Q2 and Q4 became equal, and Reynolds stress magnitudes approached zero, due to significant attenuation of Reynolds stress inside the dense meadow (Fig. 4.12E,F).

The more open nature of the sparsely vegetated meadow led to a divergence from the expected shift toward momentum transport dominated by turbulent sweeps. Above

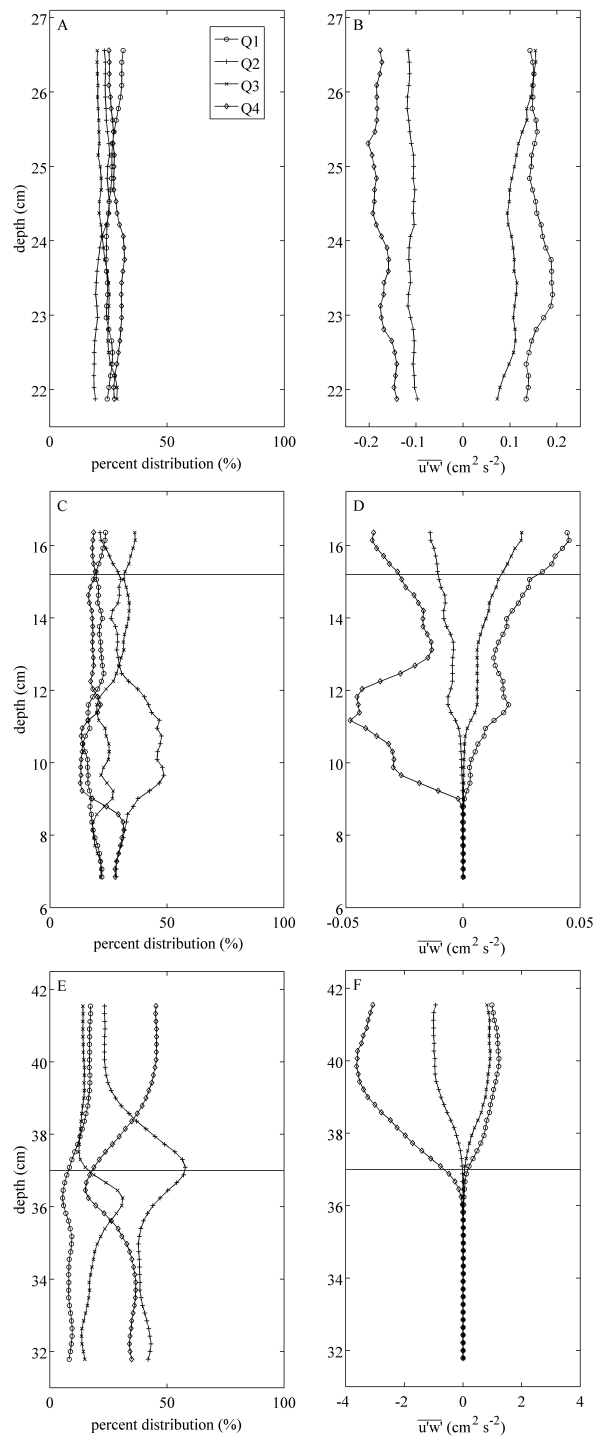


Fig. 4.12. Vertical profiles of percent distribution of Reynolds stress through quadrant analysis of the distributions of  $u'$  and  $w'$  (A,C,E), and average Reynolds stress,  $\overline{u'w'}$ , magnitudes in each quadrant (B,D,F) at the (A,B) bare, (C,D) sparse, and (E,F) dense sites. Reynolds stress distribution between quadrants, ( $Q1, Q2, Q3, Q4$ ) represents the momentum transport in the system, where motion in quadrants 2 and 4 ( $Q2, Q4$ ) represent turbulent ejections and sweeps, respectively. Y axis represents depth, for the sparse site  $z/h = 0.4 - 1.1$  and the dense site  $z/h = 0.89 - 1.16$ . Horizontal lines in C-F represent the seagrass canopy height

the meadow at  $z = 0.3$  m ( $z/h = 1.97$ ), ADV data showed distributions in Q2 and Q4 that were equivalent, each with about 30% of the total transport. Utilizing PIV to obtain finer spatial resolution near the canopy-water interface, distributions between all quadrants became more balanced, and within the canopy, momentum transport was dominated by turbulent ejections (Fig. 4.12C). However, the distribution of Reynolds stress magnitudes collected with the PIV technique show the greatest magnitude in Q4, peaking about 4 cm below the canopy-water interface ( $z/h = 0.74$ , Fig. 4.12D).

### Fluid exchange and mass transport

Interactions of the seagrass structure with turbulence generating exchange across the canopy-water interface were also observed by investigating fluid retention times within the meadow. Rhodamine WT dye was released at depths equivalent to the sampling volumes of the two ADVs. Concentration curves were obtained an average of  $6 \pm 2$  m downstream at these two vertical locations for each of the three study sites. By monitoring the concentration at a point downstream over time, the

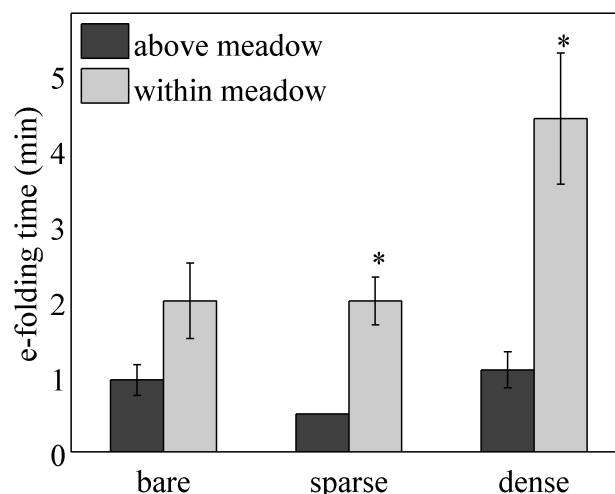


Fig. 4.13. Fluid flushing represented with the e-folding time ( $\pm 1$  standard error), which is the length of time for dye concentrations at a location to diminish to  $1/e$  of the peak concentration. Concentration curves for Rhodamine WT dye were obtained at two vertical positions in the water column, equivalent to velocimeters' sampling volumes, at each of the three study sites (bare seafloor, sparse seagrass canopy, and dense seagrass canopy). \* Denotes statistically significant difference between bars (one-way ANOVA with Bonferroni multicomparison,  $p < 0.05$ ). Note all sites had statistically different e-folding times between the two vertical sampling locations

e-folding time can be determined from this relationship (Abdelrhman 2002). The e-folding time reflects the exchange of fluids from within the meadow, and is measured as the time elapsed for the peak in dye concentration,  $C$ , to reduce to  $\frac{1}{e}C$ . During time periods surrounding dye tracer studies, average ambient velocities were  $2.8 \pm 1.0$ ,  $1.5 \pm 0.9$ , and  $3.2 \pm 1.4 \text{ cm s}^{-1}$  at the bare, sparse, and dense sites, respectively. Though ambient flow velocities were generally greater at the dense site, within the meadow, fluid flushing times were significantly larger within the dense seagrass meadow than the sparse meadow (one-way ANOVA with Bonferroni multicomparison,  $p < 0.05$ , Fig. 4.13), indicative of lower exchange rates. However, flushing rates were not statistically different between the three sites above the seagrass meadow (one-way ANOVA with Bonferroni multicomparison,  $p = 0.1596$ ). Near the unvegetated seafloor at  $z = 0.15 \text{ m}$ , dye dispersion was 2 times slower than at  $z = 0.35 \text{ m}$ . In comparison, the addition of seagrass structure enhanced the retention of fluids 4-fold within the canopy compared to above, twice as great of a reduction as at the unvegetated site (Fig. 4.13).

## DISCUSSION

Damping of tidal amplitudes in the central and northeastern portions of Florida Bay leads to currents primarily driven by winds (Wang et al. 1994). Holmquist et al. (1989) found tidal ranges of approximately 5 cm to 17 cm depending on location, which agrees well with our findings of tidal amplitudes of 3 to 4 cm in the northeast and 10 cm in the southwest, which is more heavily influenced by the Atlantic Ocean. At the sparse site, flows were predominately generated by winds, where wind and velocity magnitudes

above the meadow were well correlated (Pearson correlation factor 0.3,  $p < 0.05$ ). This is in agreement with Smith (2000) that demonstrated high correlation between wind stress and surface flows at a northern site in Florida Bay.

Reductions in velocity across the seagrass canopy were due to the development of shear, which peaks at the top of the seagrass canopy (Lacy and Wyllie-Echeverria 2011), and creates vortices that control the exchange of mass and momentum across the canopy-water interface (Nepf 2012). The thickness and magnitude of the shear layer controls the degree of exchange across the canopy (Ghisalberti and Nepf 2004). Flow within the canopy is driven by the turbulence at the top of the canopy (Finnigan 2000), and the scale of penetration of turbulence into the canopy can be determined by:

$$\delta_e = \frac{0.23 \pm 0.6}{C_D a} \quad (11)$$

where  $C_D$  is the canopy drag, estimated at  $\sim 1$  for submerged canopies (Nepf 2012), and  $a$  is the canopy frontal area per volume (Ghisalberti and Nepf 2004; Nepf 2012). For the seagrass canopies in this study, this relationship predicts a penetration depth of  $\sim 2.6$  cm and 0.99 cm at the sparse and dense sites, respectively, suggesting greater exchange within the sparsely vegetated canopy. Using the vertical profiles of velocity and Reynolds stress the turbulence penetration can be directly measured, and was defined as the location at which velocity or turbulence decayed to 10% of the maximum magnitude for a set location and flow type. Using the TKE budget, the turbulence penetration depth was also measured as the point at which dissipation and production converged, minimizing turbulent transport through vortex creation. Average measured penetration depths at the sparse meadow were  $5.2 \pm 0.9$  and  $2.4 \pm 0.4$  cm and at the dense meadow were 0 – 0.12

and  $3.0 \pm 1.1$  cm for unidirectional and wave-dominant flows, respectively. Turbulence penetration was observed at a depth up to 2 to 3 times the predicted penetration length-scale. Turbulence below the penetration depth may also represent turbulence generated in the wakes of individual stems, while turbulence within the range predicted by the penetration depth reflects the excursion of turbulence by vortices formed in the shear layer at the top of the canopy (Nepf 2012). The turbulence penetration depth was greater overall within the sparse canopy and was enhanced by wave action within the dense meadow. The limited turbulence penetration under wave conditions at the sparse site was likely due to the relatively shallow data collection.

Within the sparse canopy, dissipation rates of TKE were greater than production throughout the canopy due to greater flow penetration into the more open meadow. This greater flow penetration also led to increased Reynolds stress within the sparse canopy below the canopy-water interface. Turbulent momentum transport occurred most frequently through turbulent ejections. However, the magnitude of turbulent ejections was small, while infrequent, but high magnitude turbulent sweeps occurred, altering the overall dynamics of momentum transport. As turbulent vortices are generated at the canopy-water interface strong sweeping events occur that penetrate the canopy (Ghisalberti and Nepf 2002).

With an increase in shoot densities, TKE dissipation and production within the dense seagrass canopy were near zero. Production of TKE outweighed dissipation above the meadow, and peaked about 1.5 cm above the canopy ( $z/h = 1.04$ ). Momentum transport through turbulent ejections ( $Q_2$ ) was limited to a narrow area at the canopy-water interface, but overall was characterized by weak Reynolds stresses generated by the

canopy when averaged over all four quadrants. However, above the meadow, momentum transport most frequently occurred through turbulent sweeps (Q4), and was characterized by high magnitude for the overall Reynolds stress. Both above and within the canopy, Reynolds stress was dominated by turbulent sweeping events (one-way ANOVA with Bonferroni multicomparison,  $p < 0.05$ ), suggesting a much greater reliance on momentum transport from the overlying water column into the dense canopy.

Normalized dissipation rates of TKE were much greater across the sparse seagrass meadow than the dense meadow. The development of a shear layer causes dissipation of TKE to be high in the canopy (Finnigan 2000), dominating the TKE budget (Nimmo and Smith 2002). Separating the canopy into two regions, a source of turbulence through stem-wakes occurs in the lower canopy and a sink for shear layer turbulence occurs near the canopy-water interface (Ghisalberti and Nepf 2004), while a significant increase in seagrass density limits the development and penetration of turbulence within the canopy. A net gain in the turbulent transport rate of TKE indicates vigorous redistribution of turbulence, enhancing vertical exchange that serves to transport both momentum and scalars (Finnigan 2000; Reidenbach et al. 2010). Increased turbulent transport rates occurred at the top of the canopy for both the sparse and dense seagrass meadows, and increased flow and turbulence penetration at the sparse site led to an additional region of turbulent transport within the canopy.

Under unidirectional currents, momentum transport in vegetated canopies is typically dominated by sweeping events (Finnigan 2000) carrying high momentum fluid into the canopy from overlying flow. The prevalence of sweeping events over turbulent ejections increases with increasing density (Finnigan 2000). This was confirmed for the

*T. testudinum* meadows in Florida Bay, where at the sparse seagrass site, turbulent sweeps accounted for 23% of the Reynolds stresses, which increased to 40% within the dense seagrass meadow. Additionally, at the sparse canopy turbulent ejections accounted for a greater percentage of the momentum transport, which is similar to the dynamics expected over an unvegetated seafloor near the sediment surface (O'Connor and Hondzo 2008). Therefore, high density seagrass canopies act as a barrier to turbulence and mixing, while sparse canopies present less of a barrier and can enhance turbulence due to stem-wake generation of turbulence (Ghisalberti and Nepf 2004; Lacy and Wyllie-Echeverria 2011; Lawson et al. 2012).

Velocity penetrated deeper into the canopy in the presence of waves, and above both density canopies the development of a logarithmic profile was displaced upward into the water column. Previous studies have found that oscillatory motion always enhances flow within the canopy (Lowe et al. 2005a) and in wave dominated flows canopy drag does not influence oscillatory motion (Nepf 2012). The degree of reduction of oscillatory motion by the seagrass canopy can be predicted via the ratio of wave orbital excursion length ( $A$ ) to blade spacing ( $\Delta S$ ), such that  $A/\Delta S > 1$  indicates significant attenuation (Lowe et al. 2005a). The orbital excursion length was calculated as  $A = u_{os}/\omega$ , where  $u_{os}$  is the wave orbital velocity, and  $\omega$  is the radian wave frequency ( $\omega = 2\pi/T$ , with the wave period ( $T$ ) from directly above the canopy; Lowe et al. 2005a). For both density seagrass meadows  $A/\Delta S < 1$ , and therefore, orbital motion was expected to penetrate the seagrass canopy. While  $A/\Delta S < 1$  for both canopies, the ratio was significantly greater at the dense than at the sparse site (one-way ANOVA,  $p < 0.05$ ). As expected, orbital velocities penetrated deeper into the canopy, increasing rms velocities.

Waves also created greater dissipation and production of TKE at both density seagrass meadows by increasing the penetration depth and enhancing turbulence at the top of the canopy (Koch and Gust 1999). Further, dissipation of TKE was increased to a greater degree than production, which has been shown to occur due to flow generated by the waving of seagrass blades (Koch and Gust 1999). This was particularly apparent over the dense meadow, where the addition of waves shifted the turbulence environment from being dominated by production to being dominated by dissipation of TKE. Though greater turbulence was produced at the top of the canopy under wave conditions, results suggests turbulence due to waves may not be efficient at transporting momentum.

The efficiency of turbulent momentum transport can be determined by calculating a correlation coefficient for Reynolds stress ( $\overline{u'w'}$ ) (Finnigan 2000; Reidenbach et al. 2010):

$$r_{uw} = \frac{\overline{u'w'}}{\sigma_u \sigma_w} \quad (12)$$

where  $\sigma_u$  and  $\sigma_w$  are the standard deviations of instantaneous horizontal and vertical flow velocities, respectively. Under wave forcing, the spectral wave-turbulence decomposition was first employed, using Eq. 7, to remove oscillations in the horizontal and vertical velocity signal due to waves, and  $\overline{u'w'}$  in eq. 12 reflects only the Reynolds stress due to turbulence. The magnitude of the correlation coefficient indicates the degree of organization of the turbulence, with increasing magnitude reflecting more efficient momentum transport (Raupach et al. 1996). In vegetated layers, turbulent transport becomes more efficient through the modification of turbulence by the canopy that generates turbulent vortices (Ghisalberti and Nepf 2002; Raupach et al. 1996).

Overall, averages of  $r_{uw} = -0.16$ , and  $-0.03$  for the sparse site, and  $r_{uw} = -0.42$ ,  $-0.10$  for the dense site under unidirectional and wave dominated flows, respectively, with peak values of  $-0.5$ ,  $-0.2$ ,  $-0.6$ , and  $-0.1$ , respectively. These values are similar to published peak efficiencies of  $-0.32$  for boundary layers and  $-0.44$  for pure mixing layers (Ghisalberti and Nepf 2002). The overall increase in correlation values under unidirectional current conditions indicates more efficient transport of turbulent momentum than under wave-dominated flows. The decrease in efficiency with oscillatory motion was also found by Ghisalberti and Nepf (2006) under monami waving of the seagrass canopy due to the smaller, weaker vortices that were generated. White and Nepf (2007) determined that within a rigid porous array the efficiency was low due to periodic oscillations of the vortices that were formed. Below the canopy-water interface in the sparse canopy, the addition of waves slightly enhanced momentum transport efficiency, likely due to the increased penetration of turbulence as compared to the current-dominated flows. Efficiency is generally greater near the top of the canopy and decreases with depth into a vegetated canopy (Raupach et al. 1996; Shaw et al. 1974), and greater density canopies tend to be slightly less efficient (Raupach et al. 1996; White and Nepf 2007). From above the meadow to about 3.3 cm into the canopy ( $z/h = 0.91$ ), turbulence was more efficient at the transport of momentum in the dense meadow. Below this depth, transport was more efficient in the sparse canopy. This suggests that more coherent turbulent vortices formed over the dense seagrass canopy and near the canopy top, while greater turbulence penetration at the sparse site displaced stronger vortices down into the canopy.

Though the efficiency of the momentum transport was low within the sparse meadow, enhanced Reynolds stress and reduced shear development support mixing across the canopy, shortening flushing times. Nepf and Vivoni (2000) found that turbulence present within vegetated canopies increases exchange in the upper canopy, leading to enhanced exchange of scalars (such as nutrients and gases) across the canopy-water interface (Finnigan 2000). As seagrass shoot density increased, turbulence was damped and shear across the canopy increased, reducing the vertical extent over which mixing occurred. However, the turbulent transport of momentum into the canopy from the overlying water column was more efficient. In the presence of waves, the efficiency of momentum transport declined while turbulence within both density canopies increased, similar to trends found within the sparse canopy under unidirectional flows. Increasing current velocities have been found to stimulate seagrass photosynthesis and respiration, directly controlling oxygen fluxes, by enhancing mixing through the reduction boundary layers (Hume et al. 2011). However, wave dominated flows did not enhance oxygen exchange within the meadow due to the increased tendency to enhance sediment suspension limiting the light available for photosynthesis (Hume et al. 2011). As the turbulence momentum efficiency also tends to decrease, waves enhance penetration of flow into the meadow, but do not directly influence seagrass production. These results suggest that as shoot density increases, mixing is limited to a narrower region of the water column, and is displaced vertically above the canopy. Further, the addition of waves enhanced mixing across the canopy boundary and increased turbulent transport of momentum into the canopy. Our study highlights how increasing seagrass

shoot density reduces turbulent mixing and exchange processes, while waves enhance exchange processes.

**ACKNOWLEDGEMENTS:** We thank Kate Walsh, Matt Long, Christine Romanowich, and Tom Frankovich for field study support, Joseph Zieman for logistical support, and Jacalyn Huband for data processing technical support. We also thank the Everglades National Park for granting permission to complete field studies within the park (permit number EVER-2009-SCI-0050) and the Key Largo Ranger Station for periodic lab space. This research was funded by an Everglades Foundation Research Fellowship to JCRH and a grant from the National Science Foundation (NSF-OCE-1151314).

## **CHAPTER 5:**

### **Conclusions**

#### **RESEARCH SUMMARY**

The accelerating decline of seagrass meadows has placed these ecosystems among the most threatened on earth (Waycott et al. 2009). It is therefore important to understand how these biological systems interact with their physical environments. As the global environment experiences climate changes, alterations to the physical environment will occur, such as larger waves formed during more frequent and intense storm events (Chen et al. 2005; Easterling et al. 2000). In places like Florida Bay, where there is high natural variability, understanding the relationship between the meadow structure and physical forcings will aid restoration planning. In a highly variable environment, separating anthropogenic influences from natural cycles is difficult (Fourqurean and Robblee 1999). Understanding the physical mechanisms driving in-canopy processes, and how seagrass structure alters these processes is important for establishing the natural ecosystem patterns of the Bay. Once the natural variability can be established, trends based on the meadow structure can be used to determine where restoration efforts should focus and what anthropogenic factors would be important to monitor. Similar examples can be found for seagrasses worldwide. For example, in Virginia, *Z. marina* meadows were slower to recover where they were separated from a natural source of seeds (Orth et al. 2006), and the establishment of seedlings was less successful when physical forces resulted in the loss of seeds from the sediment surface (Marion and Orth 2012). Therefore, in these senescent meadows, seasonal patterns of morphological changes can

alter the physical environment and the proliferation of the meadow. Seagrass meadows in both of these locations have suffered extreme die-off events. Seagrass die-off occurs in response to increased temperature leading to decreased oxygen availability (Greve et al. 2003), sulfide toxicity (Borum et al. 2005), and decreased light availability (Carr et al. 2010; Lawson et al. 2007), all of which respond to alterations in the fluid environment. Stresses within the meadows, such as increased nutrient loading and wave activity, can also lead to shorter leaves that are more prone to breakage (La Nafie et al. 2012). Therefore, understanding how seagrass structure and the fluid environment interact is important in light of current seagrass decline and restoration efforts where the meadow structure is rapidly changing. In addressing specific questions pertaining to the biophysical interactions present in seagrass meadow the following was found:

- (1) How does seagrass shoot density and meadow morphology influence turbulence and wave development?

Both turbulence and wave development generally decreased within the seagrass meadows compared to neighboring unvegetated sites, which correlated well with shoot density and frontal area. With low meadow coverage, turbulence within the canopy was enhanced through flow penetration into the vegetation. Waves over the meadow were smaller and had shorter periods than those that formed over the unvegetated seafloor. Though waves were generally higher frequency, as orbital motion passed vertically into the canopy, the frequency of the wave motion was preferentially attenuated in the higher frequency bands.

Therefore, the meadows served as low-pass filters of wave energy near the seafloor.

- (2) What are the combined effects of waves and currents, in concert with meadow morphology, on sediment suspension?

The influence of waves and currents on sediment suspension within the meadow was quantified through a combined bed shear stress. Suspended sediment concentrations were generally lower within the meadow than were present at the unvegetated site. However, enhanced suspension compared to the bare site was found in the winter when the canopy frontal area was at a minimum. Sediment suspension within the meadows was also better correlated to local bed stresses during this time. Poor correlation during other seasons suggests that measured bulk suspended sediment concentrations arose in part through transport into the meadow from the neighboring unvegetated seafloor. This was further supported by decreased correlation coefficients across the spatial density gradient, where the meadow had lower shoot density but was further from a sediment source. Even with high shoot densities, suspended sediment concentration were positively correlated to wave orbital velocities, but not mean currents, suggesting that waves play an important role in the local suspension of sediments.

- (3) How are the driving mechanisms for mixing across a seagrass canopy influenced by shoot density and flow conditions?

The degree of mixing across vegetated canopies is limited by the development of shear layers. These form coherent vortex structures at the canopy-water interface, which have a constant penetration depth set by the canopy frontal

area per volume (Nepf et al. 2007). However, enhanced flow penetration in the sparse meadows led to enhanced turbulence deeper in the canopy than predicted by the penetration of shear-layer vortices alone. With increasing seagrass density, momentum transport across the canopy became more reliant on turbulent sweeps of high momentum fluid into the canopy from the overlying water column, and mixing was restricted to a narrower region characterized by more coherent vortex structures. This led to an increase in the overall efficiency of momentum transport. Further, in the presence of waves, though flow penetration into the meadow was enhanced, the efficiency of momentum transport decreased for both densities. Overall, the flushing-time for the canopies scaled with meadow development, suggesting the density of the canopy restricts mixing across the canopy-water interface.

## **SITE COMPARISON**

### **Physical characteristics and study species**

Using Florida and Virginia together as case studies, a larger-scale question of how benthic biological structures interact with and alter their physical environment can be addressed. While wind speeds in Florida were significantly greater than in Virginia during sampling periods (one-way ANOVA,  $p < 0.05$ ), the two sites experienced a similar range of wind speeds overall (Fig. 5.1). Further, all sites at both locations had the same range of fetch lengths (one-way ANOVA with Bonferroni multicomparison on fetch lengths at 30° intervals,  $p = 0.31$ ). The average water column depth was approximately 1 m deeper in Florida, while tidal amplitudes were significantly greater in

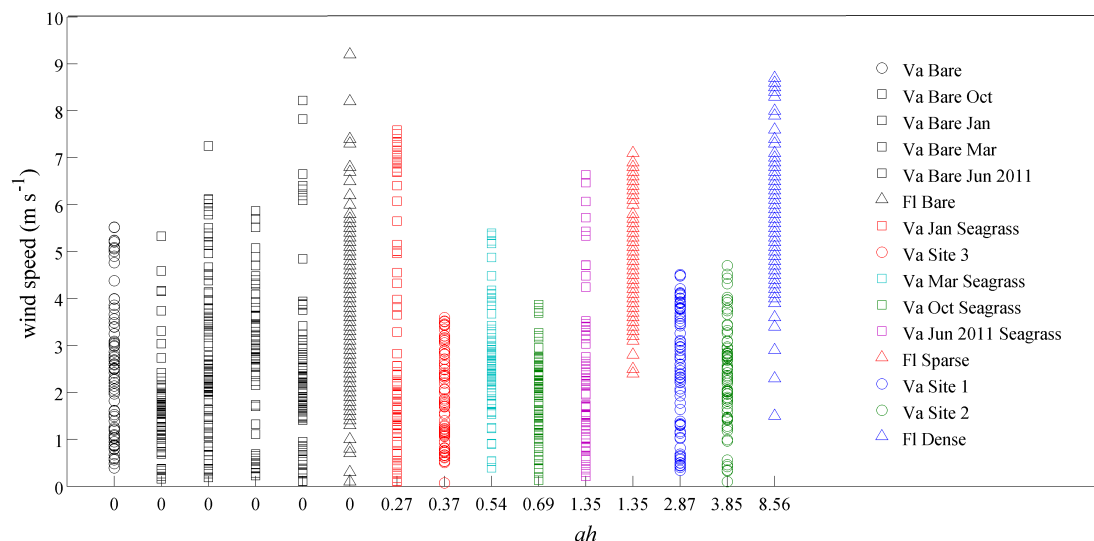


Fig. 5.1. Wind speed at each research site. X-axis represents the canopy frontal area to denote site location.

Virginia (one-way ANOVA,  $p < 0.05$ ). Therefore, we expect that in Virginia the meadow would experience larger tidally-driven currents. Though there is potential for larger waves to form in Florida, we expect the wave stress at the meadow to be similar to that in Virginia due the attenuation of wave motion with depth.

The study species at the two locations are also comparable; both are strap-bladed species (Kuo and den Hartog 2006) and the range of blade lengths, canopy heights, and shoot densities monitored for the two different species' meadows were not significantly different (one-way ANOVA,  $p > 0.09$ , Table 5.1). *Thalassia testudinum* tended to have a thicker leaf width than *Zostera marina*, leading to a larger frontal area for a comparable shoot density (Table 5.1). Frontal areas,  $ah$ , for the two meadow types ranged from 0.27 in the *Z. marina* meadow during the winter to 8.6 in the dense *T. testudinum* meadow in Florida. These values correspond to  $0.02 < a < 0.2 \text{ cm}^{-1}$ , which is within literature values for seagrasses, typically  $0.01 < a < 1 \text{ cm}^{-1}$  (Luhar et al. 2008). We expect frontal area, in addition to shoot density, to be important in predicting changes to physical processes as it

incorporates many of the important morphological attributes of the meadow. Frontal area reflects the meadow structure through the projection of the meadow's obstruction to flow as the ratio of the space occupied by the meadow per unit volume of seafloor and water column. However, shoot density neglects any role of canopy height or meadow morphology. This main hypothesis was tested in this thesis by relating the attenuation of velocity, turbulence, and wave development, normalized by ambient conditions, and subsequent trends in mixing and sediment suspension to both shoot density and frontal area, regardless of seagrass species.

Table 5.1. Seagrass morphometrics for South Bay, Virginia, and Florida Bay, Florida. Values represent the mean and standard deviations. Canopy height represents the average of the longest 2/3 of the blades sampled,  $\Delta S$  is the spacing between canopy elements, and  $ah$  is the canopy frontal area. Number of blades/shoot in Florida was obtained from literature values (Irlandi et al. 2002)

Site Location	Site Name	Blade Length (cm)	Canopy Height (cm)	Blade Width (cm)	Density (shoots m <sup>-2</sup> )	Blades/Shoot	$\Delta S$ (cm)	$ah$
VA	Site1	21 ± 8	25 ± 5	0.3 ± 0.1	560 ± 70	4.8 ± 1.3	1.6	2.87
VA	Site2	28 ± 13	36 ± 10	0.4 ± 0.1	390 ± 80	4.3 ± 0.9	2.1	3.85
VA	Site3	16 ± 9	20 ± 7	0.3 ± 0.1	150 ± 80	3.7 ± 1.0	8.8	0.37
VA	Oct-10	19 ± 7	23 ± 5	0.2 ± 0.1	350 ± 50	3.0 ± 0.9	2.8	0.69
VA	Jan-11	13 ± 7	16 ± 5	0.2 ± 0.1	310 ± 60	2.6 ± 1.0	3.2	0.27
VA	Mar-11	12 ± 5	15 ± 3	0.2 ± 0.1	350 ± 90	4.0 ± 1.4	2.4	0.54
VA	Jun-11	23 ± 11	29 ± 3	0.2 ± 0.1	440 ± 140	4.2 ± 1.2	2.1	1.35
FL	Sparse	14 ± 2	15 ± 2	0.7 ± 0.3	260 ± 30	2.7	2.9	1.35
FL	Dense	33 ± 7	37 ± 5	0.8 ± 0.2	480 ± 80	2.7	1.9	8.56

### Seagrass influence on velocity structure

As expected, larger tidal fluctuations in Virginia led to higher average ambient velocities above the meadow and at the unvegetated control site than were found in Florida. However, the meadows behaved similarly in reducing near-bed flows within the canopies. Percent reductions in velocity across the canopy-water interface were between

44% and 83% for the full range of meadow types and shoot densities. Comparatively, over a respective change in height above an unvegetated seafloor, average reduction in fluid velocity was 44% in Virginia and 22% in Florida. This agrees well with findings from a study by Lacy and Wyllie-Echeverria (2011), where flow reductions were between 40% and > 70% for a *Z. marina* meadow in the Puget Sound, WA, of frontal area per volume ( $a$ ) approximately  $0.02 \text{ cm}^{-1}$ . They found that flow reductions were greater in more dense portions of the seagrass meadow, and concluded that even sparse canopies formed a mixed shear-layer and rough-wall boundary layer that significantly attenuated currents (Lacy and Wyllie-Echeverria 2011).

To establish a relationship between canopy structure and near-bed flows, normalized velocity within the canopy,  $u/\Delta U$  where  $\Delta U$  is the difference in velocity above the canopy to within, was plotted against both shoot density and frontal area (Fig. 5.2A,B). Normalized velocity varied linearly with seagrass density regardless of the species type ( $R^2 = 0.63$ ), and frontal area was a poor indicator of near-bed flows (linear best-fit  $R^2 = 0.1$ ). The degree of flow reduction within the canopy was also plotted against seagrass density and frontal area. Variations in ambient conditions were accounted for by quantifying the percent reduction in velocity across the canopy-water interface. Further, to isolate the influence of the meadow, the percent reduction at each seagrass site was divided by the percent reduction present over neighboring unvegetated seafloor, i.e.  $\frac{\%reduction_{va}}{\%reduction_{va \text{ bare}}}$  (Fig. 5.2C,D). The degree of flow reduction varied logarithmically with increasing meadow structure, and was more responsive to the overall canopy structure, represented by the frontal area ( $R^2 = 0.81$ ), than density ( $R^2 = 0.31$ ). These findings, consistent for very different tidal environments and two seagrass species,

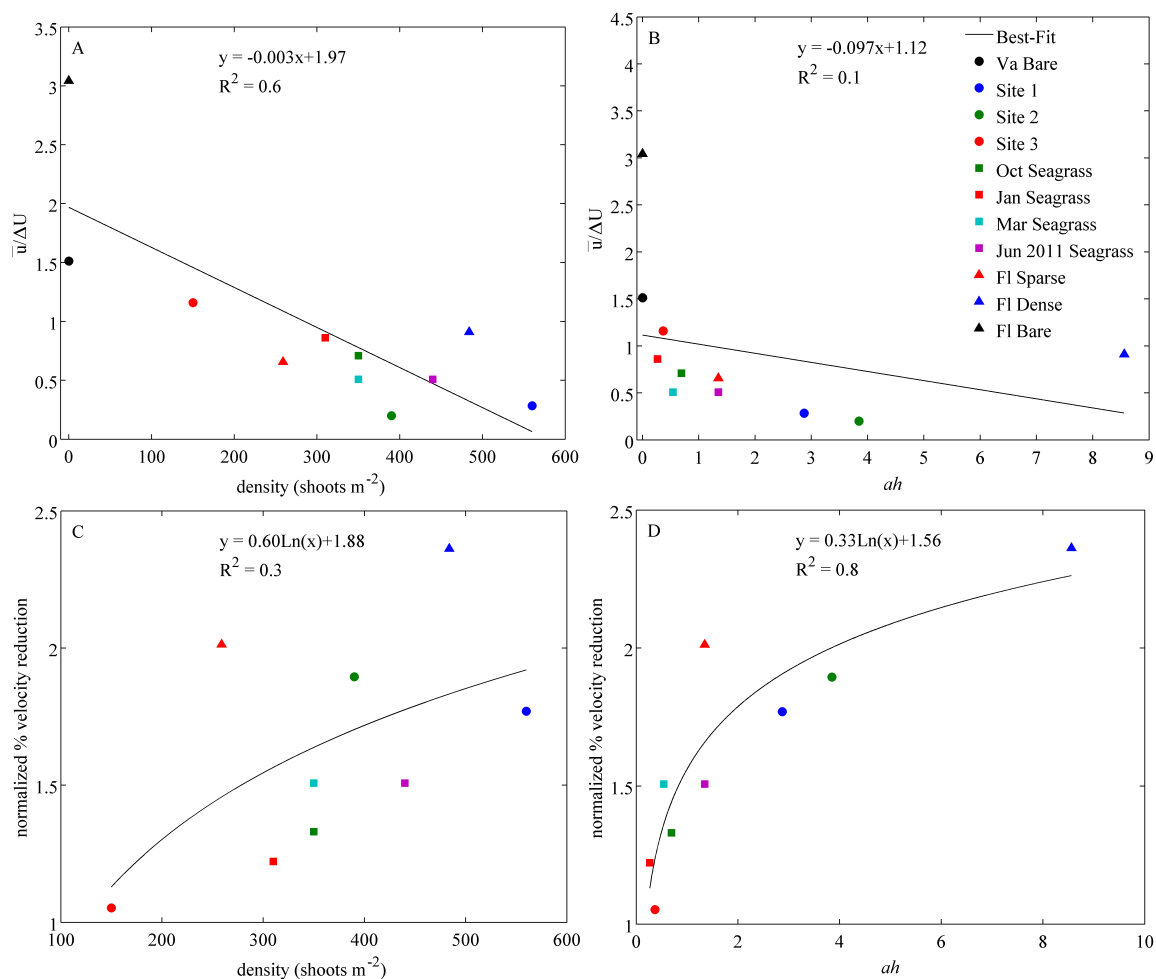


Fig. 5.2. (A,B) Normalized velocity near the seafloor ( $z_2 = 0.1$  m in Virginia, and 0.1 m, 0.15 m and 0.3 m at the bare, sparse and dense sites in Florida, respectively), where  $\Delta U = U_{z_1} - U_{z_2}$  (where  $z_1 = 0.5$  m in Virginia, and 0.3 m, 0.35 m and 0.5 m at the bare, sparse, and dense sites in Florida, respectively) as a function of (A) shoot density and (B) canopy frontal area,  $ah$ . (C,D) Normalized percent reduction in velocity vertically across the canopy-water interface as a function of (C) shoot density and (D) canopy frontal area, where normalization was performed by dividing the percent reduction at the meadow by the percent reduction present at the bare site over the same vertical distance in the water column

suggest that in-canopy velocities depend on the amount of open space on the seafloor for fluid to move within, while the degree of penetration of currents into the canopy depends on the full meadow structure presenting an obstruction to the flow. Ghisalberti (2009) determined that the drag length scale, which incorporates the canopy frontal area per volume, provided a more accurate measure of flow resistance for a wide range of canopy types than porosity. The reduction of velocity compared to the bare site may be a result of

increasing canopy friction with the meadow height (Fonseca and Fisher 1986), which is incorporated into the frontal area calculation. The meadow's ability to reduce current velocities near the seafloor has been shown to stabilize the habitat by limiting sediment suspension, enhancing organic detrital retention, and providing refuge for other organisms (Fonseca and Fisher 1986).

The structure of velocity present within the two meadows was further enumerated with vertical profiles for low- and high-density sites in both species' meadows. The sparse and dense sites in Florida (with densities of 259 and 484 shoots  $m^{-2}$ , respectively) and Site 3 and Site 1 during June 2011 in Virginia (with densities 150 and 440 shoots  $m^{-2}$ ,

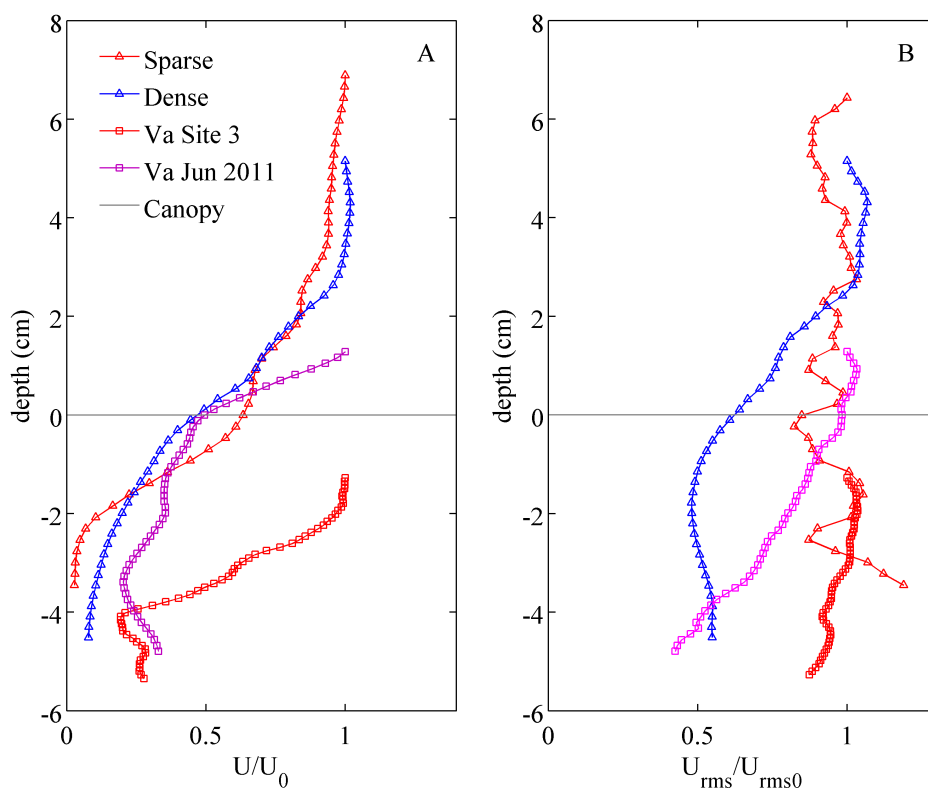


Fig. 5.3. (A) Velocity profiles within the sparse and dense sites in Florida and Virginia (Site 3 and June 2011 seagrass meadow) normalized by the velocity at the top of each profile. (B) RMS velocity profiles within the sparse and dense sites in Florida and Virginia normalized by rms velocity at the top of each profile. Horizontal grey line represents the seagrass canopy. Mean estimates were formed by averaging horizontally across the PIV velocity vectors

respectively) were compared (Fig. 5.3A). In all instances, the presence of the seagrass caused the development of a shear layer, as expected for meadows with  $ah > 0.1$  (Nepf 2012). In both locations where profiles overlapped, enhanced flows were found in the lower density canopies, consistent with the prediction from the relationship of in-canopy flows to shoot density (Fig. 5.2 A). However, it is also clear that profiles in Virginia had overall higher velocities than present in the meadows in Florida. Within the canopy, enhanced flows in Virginia at the dense site compared to the Florida dense site could arise from the lower canopy frontal area of the *Z. marina* meadow. Profiles represent velocity normalized by the maximum value at the top of the canopy. Since the profiles do not all cover the same distance across the canopy-water interface, this leads to normalized velocities that only scale the shear development, not correcting for ambient conditions. In Florida, the profiles all cross the canopy by  $\geq 2$  cm, allowing for the velocity at the top of the profile to account for ambient conditions. Therefore, in Florida, normalizations served to correct for both ambient conditions and scaling the shear development, which was not possible in Virginia. As we found in Florida, it is also possible that wave motion present within the meadow caused enhanced flow penetration in Virginia as waves were generally larger in Virginia than Florida during our sampling periods.

### **Seagrass influence on wave development**

Wave development was damped by the *Z. marina* meadow in Virginia. Overall, waves were larger with longer periods at the bare site over the full range of wind speeds and water depths. Further, attenuation of wave development scaled with the canopy frontal area; under the same depths and wind forcing, significant wave heights and

periods were smallest in the summer and most similar to the bare site in the winter. While overall wave periods were shortened as waves traveled across the meadow, linear wave theory predicts that closer to the seafloor wave frequencies will appear to be lengthened as higher frequency motions are attenuated through the water column. This predicted vertical attenuation of wave frequencies with depth was clearly visible in decreases of  $S_{uu}$  within the wave band of the velocity spectra ( $0.3 < f < 1$ ) at the unvegetated site as well as the seagrass sites. Additionally, vertical attenuation of  $S_{uu}$  across the canopy-water interface within the meadow shows a relatively larger attenuation in the higher frequencies of the wave band beyond that found at the bare site and greater than expected from linear wave theory, suggesting the meadow acts a low-pass filter (Lowe et al. 2007). Further, the shift to lower frequencies within the meadow was present within both the *Z. marina* and *T. testudinum* meadows, and scaled with canopy frontal area. In the winter and spring,  $S_{uu}$  above and below the canopy-water interface were similar, with no attenuation in the peak wave frequency. In Florida, profiles of  $S_{uu}$  were obtained with PIV data, which show attenuation occurred at the canopy-water interface (Fig. 4.8).

The translation of  $S_{uu}$  in the wave band suggests that orbital motion resulting from the long period frequencies of the wave band will penetrate the canopy. The degree of penetration of orbital motion can be predicted by the ratio of the wave excursion length,  $A$ , to the blade spacing,  $\Delta S$ , such that  $A/\Delta S > 1$  indicates significant attenuation (Lowe et al. 2005a). For the full density range of both *Z. marina* and *T. testudinum* meadows monitored in this study,  $A/\Delta S$  was  $< 1$ . Though orbital velocity was lower within the canopy than above, this was due to the natural attenuation of wave motion with depth, as measured bed orbital velocities,  $u_{os}$ , were not significantly different than those predicted

by linear wave theory,  $u_{om}$ . This excursion of wave orbital motion into the canopy will serve to enhance in-canopy flows (Lowe et al. 2005a). Though wave development was limited within the meadow as compared to an unvegetated seafloor, oscillatory motion is not altered by canopy drag, and therefore was expected to translate into the canopy (Luhar et al. 2010; Nepf 2012).

Vertical profiles of rms velocities, equivalent to the wave orbital velocity ( $u_{os}$ ), were obtained for sparse and dense canopy frontal areas in the *Z. marina* and *T. testudinum* meadows (fig. 5.3B). Normalized rms profiles showed enhanced flows for both canopy types as compared to mean flow velocity. The sparse canopies of both species had similar in-canopy rms velocities, which were greater than those present within the dense canopies, and showed deeper penetration of larger velocities. This enhancement of in-canopy flow by waves resulted in increased Reynolds stresses, decreased shear development, and greater TKE penetration into the meadow in Florida. Similar trends have been found within *T. testudinum* and *Posidonia oceanica* meadows (Granata et al. 2001; Koch and Gust 1999), and enhancement of turbulence by the interaction of current and wave activity has been noted by Grant and Madsen (1979). However, in Virginia temporally averaged Reynolds stress and TKE were not statistically different under wave- versus current-dominated flows, though reductions in Reynolds stress across the canopy-water interface were smaller with wave-dominance. Averages in Virginia represent a much longer time series than is available from the PIV data. Therefore, increases in turbulence with waves may occur on short time scales, periodically enhancing mixing and fluid exchange across the canopy (Ghisalberti and Nepf 2006; Lowe et al. 2005b). This indicates that for both species meadows, the full

range of canopy areas studied benefit from the presence of waves as mixing across the canopy-water interface facilitates the exchange of dissolved nutrients, waste-products, and gasses within the canopy where the meadow can make use of resources for growth (Lowe et al. 2005b; Thomas and Cornelisen 2003).

### **Seagrass influence on turbulence and mass transport**

In systems where both currents and waves are present, it is necessary to separate the influence of waves from that of turbulence; therefore, a spectral wave decomposition was performed on all field data collected. To determine turbulence levels present within the canopy, which serve to exchange water masses across the barrier formed by the top of the canopy, both a single-point (ADV) and a fine-scale spatial grid (PIV) of velocity were measured. The Phase method for separating wave signals for turbulence was employed on the ADV data and modified for use with the PIV data, allowing for the examination of the spatial structure of turbulence across the canopy-water interface. Study sites in Florida had a relatively clear water column and overall low energy, ideal for collecting PIV data over more traditional acoustic methods. The clear water column allowed for better control of the light quality and clearer images. Relatively low suspended particulates led to much lower correlation values for ADV data, which created larger error in the Reynolds stress calculation. In Virginia, ADV data was more robust and instantaneous values with low correlations due to blade interference and exposure at low tide were able to be removed. In Florida, after applying the wave turbulence decomposition, 10 min averages with poor correlation values were filtered, shortening the available temporal data set. However, spectral decomposition with PIV data resulted in

less error and greater spatial resolution. This allowed for a detailed description of the turbulence structure in both current and wave-dominated flows. PIV data in Virginia was more difficult to obtain due to greater turbidity scattering light and blurring the image quality. Short data sets were obtained when flow velocity was low during low tide. While velocity data was obtained through both point measurements above and within the canopy, as well as fine-scale spatial measurements at both locations, we found that high-energy, high-turbidity environments were more suited to acoustic measurements from the ADV while low-energy, high-clarity environments were ideal for the optical measurements of the PIV.

After removing the wave signal, Reynolds stress was normalized as  $\frac{\overline{uw}}{\Delta U^2}$ , where  $\Delta U^2$  is the change in velocity vertically across the canopy. Temporal averages were obtained after time periods with  $\Delta U^2 \rightarrow 0$  were removed. For all study sites in both Virginia and Florida, average normalized Reynolds stress within the canopy decreased

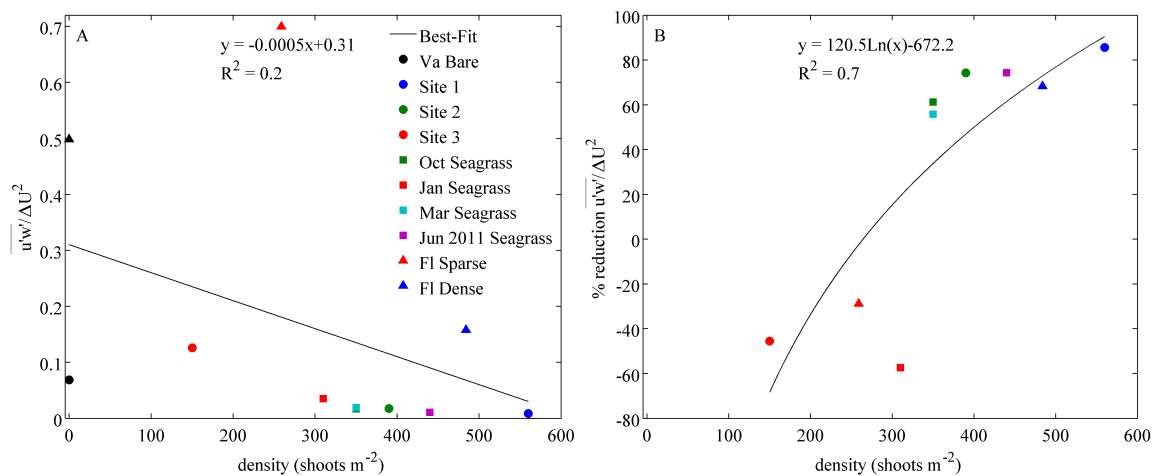


Fig. 5.4. (A) Normalized Reynolds stress,  $\frac{\overline{uw}}{\Delta U^2}$ , near the seafloor ( $z_2 = 0.1$  m in Virginia, and 0.1 m, 0.15 m and 0.3 m at the bare, sparse and dense sites in Florida, respectively), where  $\Delta U = U_{z_1} - U_{z_2}$  ( $z_1 = 0.5$  m in Virginia, and 0.3 m, 0.35 m and 0.5 m at the bare, sparse, and dense sites in Florida, respectively) as a function of shoot density. (B) Percent reduction in normalized Reynolds stress within the seagrass canopy compared to neighboring unvegetated sites. Negative percent reduction represents an increase in  $\frac{\overline{uw}}{\Delta U^2}$  within the seagrass canopy

linearly with increasing shoot density (fig. 5.4A,  $R^2 = 0.18$ ), suggesting the meadow structure generally served to decrease near-bed turbulence. Further, the percent reduction within the canopy to comparable near-bed values over a neighboring unvegetated seafloor increased logarithmically with increasing seagrass density and frontal area ( $R^2 = 0.65$  and  $0.45$ , respectively, fig. 5.4B). Low shoot density, with negative percent reduction ( $\frac{\overline{u'w'_b} - \overline{u'w'_g}}{\overline{u'w'_g}}$ , where subscripts  $b$  and  $g$  represent the bare and seagrass sites, respectively), showed an increase in turbulence compared to the bare site during similar time periods (i.e. within the same season). While both frontal area and shoot density can indicate in-canopy turbulence reduction compared to the bare site, enhancement of turbulence within the meadow was better correlated to shoot density. The 3 lowest densities, *Z. marina* Site 3, *Z. marina* meadow in January, and the sparse *T. testudinum* meadow, all showed enhanced turbulence within the canopy. Turbulence can be produced within the canopy through flow interaction with individual shoots and the excursion of turbulent vortices formed by instabilities in the shear layer at the canopy-water interface (Ghisalberti and Nepf 2004). For vegetated shear layers, vortex structures have a fixed penetration into the meadow determined by the canopy frontal area per volume,  $a$  (Nepf et al. 2007), such that increasing  $a$  leads to more limited vortex incursion. The canopies with the 3 lowest densities also were within the 4 shortest canopy heights. Therefore, stem-generated turbulence, as well as the combined influence of increased penetration lengths and shorter canopy heights, caused enhanced turbulence near the seafloor.

The turbulence structure suggested by the ADV point measurements was confirmed with vertical profiles of Reynolds stress obtained with the PIV (Fig. 5.5). During wave-dominated flows,  $\overline{u'w'}$  from the turbulence portion of the velocity spectra

were compared for the dense and sparse *T. testudinum* and *Z. marina* meadows (*Z. marina* Site 3 and June 2011). The low density *Z. marina* meadow had the greatest in-

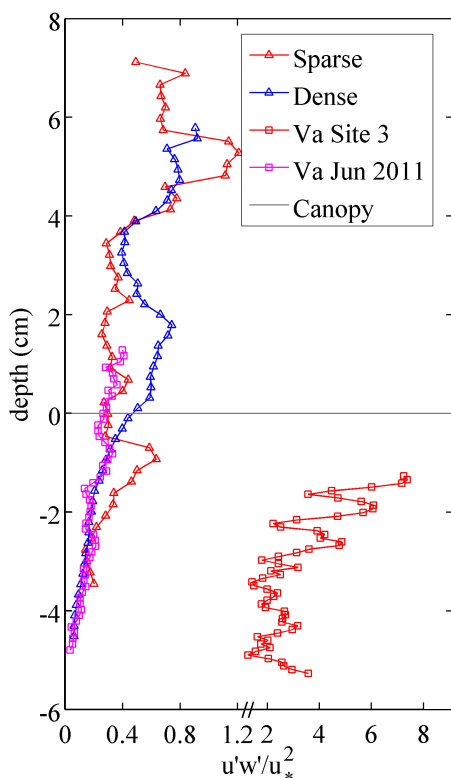


Fig. 5.5. Vertical profiles of average Reynolds stress normalized by shear velocity,  $u^*$ , for sparse and dense sites in Florida and Virginia (Site 3 and June 2011 seagrass meadow). Spatial flow characteristics were obtained via particle image velocimetry (PIV), which were post-processed with a wave-turbulence decomposition to obtain Reynolds stress in oscillatory flow conditions. Grey horizontal line represents the seagrass canopy height. Note discontinuity in x-axis between 1.2 and 2

canopy turbulence, by an order of magnitude, followed by the sparse *T. testudinum* meadow (note-discontinuity in x-scale), while profiles from the dense meadows had the least turbulence. Further, both dense meadows had similar vertical normalized turbulence magnitudes and profile forms.

Vortices formed at the canopy-water interface through the development of shear layers enhance vertical mixing (Abdelrhman 2003; Ghisalberti and Nepf 2004). Shear layers were predicted to form for the full range of canopy frontal areas in our study. In January, the *Z. marina* meadow represented a frontal area near the transition point for a sparse canopy, and therefore had less shear development. Mixing across the canopy-water interface is related to the momentum transport, quantified through a quadrant analysis of

the probability density function (pdf) of  $u'$  and  $w'$ . Near the sediment surface, ejections (Q2) of low momentum fluid upward into the water column will contribute more to the Reynolds stress (O'Connor and Hondzo 2008). Conversely, within vegetated shear

layers, sweeps (Q4) of high momentum fluid into the canopy from the overlying water column will dominate the momentum flux (Raupach et al. 1996). In general, over the unvegetated seafloor in both Florida and Virginia, contributions to ejection and sweeping events averaged 62% in the water column and 67% closer to the seafloor. Over the seagrass meadows, ejection/sweep events accounted for an average of 66% of the Reynolds stress, while in the canopy this increased to 71%. This shift represents an increased dominance in sweeping events, in general agreement with previous studies (Raupach 1981). The degree of increased prevalence of ejections controlling momentum transport within the canopy was related to the canopy development. The change in the percentage of the pdf distribution in Q4 across the canopy-water interface showed a

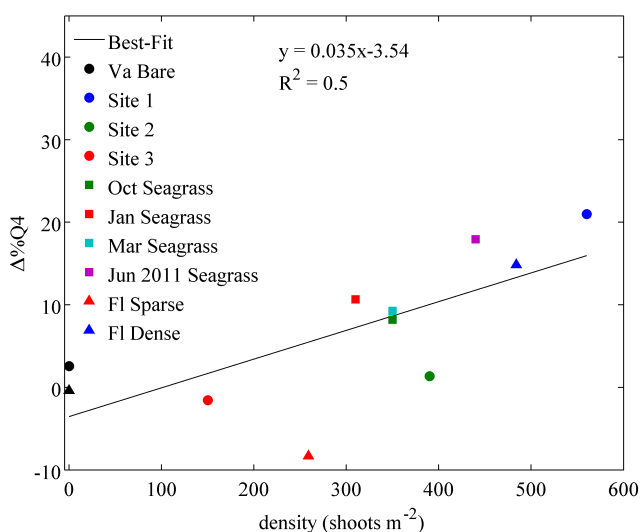


Fig. 5.6. Shift in probability density function in quadrant 4 ( $\Delta\%Q4$ ) across the canopy-water interface or over a comparable change in depth at a neighboring unvegetated site ( $\%Q4_{z_1} - \%Q4_{z_2}$ , where  $z_1$  and  $z_2$  are the measurement heights above the seafloor) representing the frequency of turbulent ejections in the Reynolds stress. Negative values represent a decrease in the frequency of turbulent ejections within the canopy

greater shift to momentum transport dominated by turbulent sweeps with increasing shoot density (Fig. 5.6). This suggests that with increasing shoot density, the seagrass becomes more reliant on the transport of fluids into the meadow from the overlying water column ( $R^2 = 0.50$ ). However, at the lowest densities for both species of seagrass there was a decrease in the momentum transport through sweeps, and rather, an increased tendency for

turbulent ejections within the canopy (Q2 dominance of 36% in the *Z. marina* meadow

and 29% in the *T. testudinum* meadow). This shift to momentum transport predominantly through turbulent ejections is likely due to enhanced Reynolds stresses from increased flow penetration and larger vortices formed by the shear layer of the sparse canopies. PIV analysis in Florida reflected the structure of Reynolds stress distributions under current-dominated flow conditions. Results suggested mixing was enhanced within the sparse canopy, but limited to a narrow region near the canopy-water interface by more coherent vortex structures at the dense site.

The efficiency of momentum transport was found to increase with increasing canopy-frontal area for both meadow densities (Fig. 5.7). Enhanced efficiency near the

top of the canopy suggests that turbulence formed here transported a greater amount of momentum than present in the surface layer above (Finnigan 2000). While the efficiency of momentum transport was greater, mixing was reduced with increasing density. Turbulence values were low, flow was limited, and the penetration depth of the shear layer vortices was limited to a narrow

region. Increased efficiency in momentum transport thins the boundary layer, enhancing the organism's ability to exchange fluids and dissolved constituents (Hearn et al. 2001; Thomas and Cornelisen 2003), which is particularly important within dense canopies

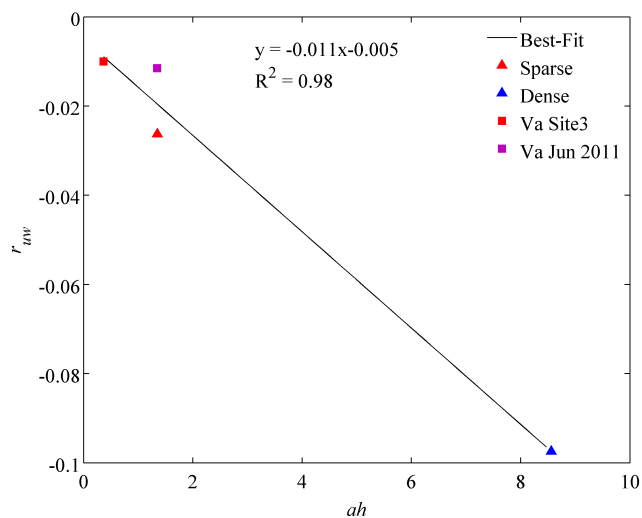


Fig. 5.7. Average efficiency of momentum transport ( $r_{uw}$ ) obtained from PIV measurements under wave-dominated flows within the sparse and dense sites in Florida and Virginia (Site 3 and June 2011 seagrass meadow) as a function of canopy frontal area. Increasingly negative values indicate increased efficiency

where fluid exchange is restricted to a narrow region near the canopy-water interface. For a wide range of canopy types, Ghisalberti (2009) found that the shear penetration into the canopy was related to the canopy drag length scale, and controlled the residence of water within the canopy. To investigate the residence time of water within the meadows in Virginia and Florida, mixing across the canopy-water interface was quantified through the e-folding time for dye dispersion. The e-folding time represents the flushing time of fluids from within the meadow, and was calculated across the spatial density gradient in the *Z. marina* (Sites 1, 2, and 3) and the *T. testudinum* meadows. To determine the effect of canopy structure on fluid exchange, flushing times within the canopy were normalized by the e-folding time for dye dispersion above the canopy, then divided by the ratio of velocity within the canopy to above. Normalized flushing times increased with increasing canopy frontal area ( $R^2 = 0.13$ ) and density ( $R^2 = 0.37$ ), suggesting that increasing the meadow structure serves to drastically reduce mixing and fluid exchange.

### **Sediment suspension and light limitation**

Sediment grain size in Florida,  $D_{84} = 90 \pm 31 \mu\text{m}$ , was similar within the sparse meadow to that present within the *Z. marina* meadow in Virginia,  $D_{84} = 130 \pm 17 \mu\text{m}$ ; however, within the dense meadow, the grain size increased to  $646 \pm 380 \mu\text{m}$ . This increase in sediment grain size at the dense site leads to a reduced sensitivity of the OBS, complicating the collection of suspended sediment data in Florida. Suspended sediment and water column chlorophyll levels are typically low in the subtropical Florida Bay; Philips et al. (1995) found tripton levels near our research sites of 7 to 15  $\text{mg l}^{-1}$ . During our study period, suspended sediment concentrations were frequently near the minimum

concentration limit of the OBS, indicating that suspended sediment was not an important factor within the meadows studied in Florida Bay. However, previous studies of sediment suspension in the lagoonal systems in Virginia suggest that sediment suspension drives light limitation for these seagrass (Lawson et al. 2007). Therefore, understanding the influence of waves and currents on near-bed processes, and the effects of meadow structure are important aspects of determining the growth parameters of the meadow in Virginia.

Physical forcing by currents and waves on the seafloor was quantified through a combined bed shear stress (as per Lawson et al. 2007). Both waves and currents are essential for the transport of sediment. Wave activity will tend to initiate sediment suspension; however, orbital motions induced by the waves will not necessarily transport sediment, rather once sediment is suspended, it can be carried by unidirectional currents that may not be sufficient for the initial suspension (Heller 1987). Over unvegetated seafloor total bed shear stress ( $\tau_b$ ) was greater than necessary to initiate the suspension of sediment > 90% of the sampling periods with an overall average  $\tau_b > \tau_{cr}$ . In the absence of significant benthic structure ( $ah < 0.6$ ),  $\tau_b > \tau_{cr}$  within the meadow 80 to 85% of the sampling time except at Site 3. Though the shoot density and frontal area were both low, the location within the meadow led to smaller waves and lower bed shear stresses. Therefore, the meadow structure, location, and physical environment are all important parameters in understanding the influence of the meadow on sediment suspension. With increased seagrass development ( $ah > 0.6$ ) for both Sites 1 and 2, bed shear magnitudes were greater than the critical threshold only 20 to 57% of the time. This reduction in bed shear with increased meadow development led to a 60% reduction in SSC for meadows

with  $ah > 1.3$ , whereas minimum development in the winter enhanced SSC compared to the unvegetated site. Further, periods of increased SSC were significantly positively correlated to  $\tau_b$  at the unvegetated site during all deployments and within the meadow for minimal canopy development. Correlation values decreased with increasing canopy frontal area as well as with the location in the meadow. A drop in correlation values suggests that the suspended sediment is in part transported into the meadow rather than locally suspended. Therefore, the relatively close location of Site 1 to the edge of the meadow and the unvegetated site where sediment is suspended resulted in slightly higher correlations than present at Sites 2 or 3.

Seasonal changes in sediment size monitored in a *Posidonia sinuosa* meadow showed a shift to finer sediments in the summer due to reduced water motion promoting the settlement of sediment, and coarser values in the winter when motion was greater (van Keulen and Borowitzka 2003), suggesting suspension of fine sediment in the winter that had previously settled in the summer. Our results are consistent with these findings on sediment suspension within seagrass meadows. Over time, the restored meadows in Virginia show a shift toward finer sediment as the meadow ages (McGlathery et al. 2012), suggesting the seasonal patterns observed in the *Z. marina* meadow tend toward a net deposition of fine sediment throughout the year. Additional studies have shown sediment scouring around individual canopy elements (Bouma et al. 2009); therefore, for the *Z. marina* meadow in the winter, the decrease in shoot density would enhance scouring and the finer grain sediment would more easily be suspended than the coarser sediment present at the bare site. Koch (1999) suggested that alternation between erosion of sediment within a *T. testudinum* meadow on flood tides, and deposition during other

parts of the tidal cycle when flows were weaker, may serve to maintain the depth of seagrass meadows in the water column. In contrast, the more traditional view of meadows as depositional environments would suggest that meadow depth would decrease over time. Therefore the patterns of erosion in the winter and spring, versus SSC translating into the meadow in the summer at higher canopy frontal areas, may aid the meadow in maintaining a depth that balances their light and submergence requirements.

The percent reduction in SSC within the seagrass from the bare site varied logarithmically with the canopy frontal area (Fig. 5.8,  $R^2 = 0.47$ ). Light intensity at the seagrass canopy and over the

unvegetated seafloor was measured with HOBO light loggers during all deployments. Correcting for ambient light availability above the water column, the correlation between light levels and SSC was determined. At the bare site, SSC and light intensity were significantly negatively correlated, suggesting that as SSC

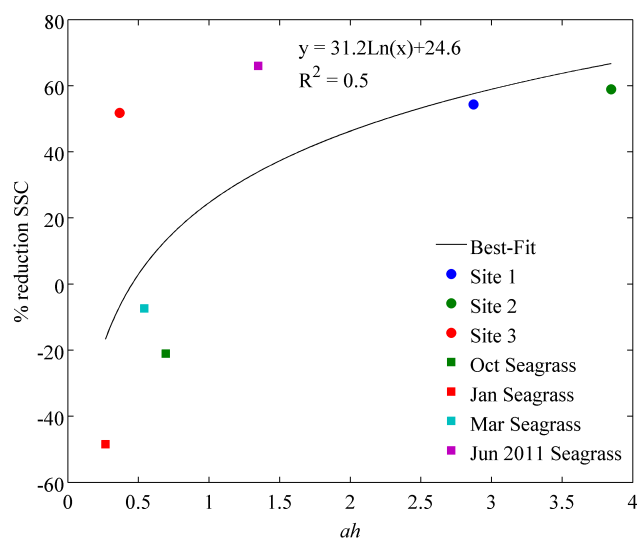


Fig. 5.8. Percent reduction in suspended sediment concentrations (SSC) near the seafloor within seagrass meadows from values at comparable depths over neighboring unvegetated sites. Negative values represent an increase in SSC within the seagrass canopy

increased, the available light decreased. This was also true for SSC above the seagrass canopies in the winter and spring. Correlations tended to decrease as canopy frontal area increased and as correlations between SSC and shear stress decreased. At the seagrass meadow in June 2011, and at Sites 2 and 3, SSC and light were positively correlated, with Pearson correlation values of 0.29, 0.3, and 0.07 ( $p < 0.05$ ), respectively. This

suggests that when SSC are from local suspension, the available light will decrease. However, sediment that is likely transported into the meadow from neighboring bare seafloor is not significantly decreasing light availability. Overall decreases in SSC compared to the bare site, as well as within the canopy, suggest that with increased canopy frontal area and protection from the surrounding meadow, the canopy shifts to net deposition of sediment to maintain light quality for growth.

## **SUMMARY AND FUTURE DIRECTIONS**

This research provides evidence that both shoot density and overall structure, represented by the canopy frontal area, are important factors in predicting how flexible biological structures interact with their physical environment. Physical forces within the canopy were generally predicted by the shoot density. However, the reductions in processes occurring within the canopy compared to a control (unvegetated) location were often better predicted by the frontal area. It is likely that this difference is due to the role of the canopy height in the development of the shear layer; however, additional research is needed to perform a sensitivity analysis on the morphological properties controlling the frontal area calculation for seagrass canopies. Canopy height scaled positively with shoot density ( $R^2 = 0.3$ ), and was included in calculations of frontal area. Relationships between flow properties and canopy height were similar to both density and frontal area, though only normalized flushing times and reductions in suspended sediment concentrations were more responsive to canopy height. Our research also showed an increase in the efficiency of momentum transport with increasing meadow coverage, though the mechanisms for this increase are not well understood. Finally, while sediment suspension

was clearly a function of the meadow morphology, the influence of suspended sediment on local light availability was inconclusive. Further investigation in how sediment transported into the meadow influences light through alternating periods of settling and wave induced resuspension is necessary.

Seagrass meadows in Virginia and Florida both exhibited the ability to alter their physical environments to promote growth. In Virginia, the expansion of the meadow has served to reduce current velocity and turbulence within the canopy, shifting the environment from net erosional to one promoting sediment deposition during the majority of the year; thereby promoting photosynthesis by enhancing light availability. Lower canopy coverage in the spring promoted increased orbital motion, turbulence, and flow within the canopy, which can serve to distribute seeds (Granata et al. 2001; Orth et al. 2012) and promote further expansion of the meadow. As these meadows have also been found to have shorter canopy heights and lower densities in the first four years of their development (McGlathery et al. 2012), sediment scouring found in the low frontal area meadows of our study indicates that early in meadow establishment, wave action and sediment suspension will be particularly important. This may be further exacerbated by the susceptibility of seedlings growing from seeds that have simply settled on the sediment surface to disturbance (Marion and Orth 2012). Seasonal enhancement of sediment suspension, and increased suspension in relation to low frontal area will create a barrier to meadow establishment. However, seeds settling within or near larger established meadows are likely to benefit from their proximity as was found in the spatial density study in Virginia, where protection is offered from the wave and suspended sediment damping occurring in the larger meadow. Finally, for both *Z. marina* and *T.*

*testudinum* meadows, increased density reduced mixing to a narrow region near the canopy-water interface that is driven by highly efficient momentum transport, while wave penetration into a wide range of shoot densities enhanced exchange processes, thereby increasing mass transport necessary to sustain an established meadow.

**REFERENCES**

- Abdelrhman, MA. 2002. Modeling how a hurricane barrier in New Bedford Harbor, Massachusetts, affects the hydrodynamics and residence times. *Estuaries* 25(2): 177-196.
- Abdelrhman, MA. 2003. Effect of eelgrass *Zostera marina* canopies on flow and transport. *Marine Ecology Progress Series* 248: 67-83.
- Ackerman, JD, and A Okubo. 1993. Reduced mixing in a marine macrophyte canopy. *Functional Ecology* 7: 305-309.
- Ackerman, JD. 1997. Submarine pollination in the marine angiosperm *Zostera marina* (Zosteraceae). II. Pollen transport in flow fields and capture by stigmas. *American Journal of Botany* 84(8): 1110-1119.
- Ackerman, JD. 2002. Diffusivity in a marine macrophyte canopy: Implications for submarine pollination and dispersal. *American Journal of Botany* 89(7): 1119-1127.
- Agawin, NSR, and CM Duarte. 2002. Evidence of direct particle trapping by a tropical seagrass meadow. *Estuaries* 25: 1205-1209
- Anderson, SM, and AC Charters. 1982. A fluid dynamics study of seawater flow through *Gilidium nudifrons*. *Limnology and Oceanography* 27(3): 399-412.

Barko, JW, MS Adams, and NL Clesceri. 1986. Environmental factors and their consideration in the management of submerged aquatic vegetation: A review. *Journal of Aquatic Plant Management* 24: 1-10.

Benilov, AY, and BN Filyushkin. 1970. Application of methods of linear filtration to an analysis of fluctuations in the surface layer of the sea. *Izvestiya, Atmospheric and Oceanic Physics* 6: 810-819.

Bennet, SJ, and JL Best. 1996. Mean flow and turbulence structure over fixed ripples and the ripple-dune transition. In: Ashworth PJ, Bennet SJ, Best JL, McLelland SJ (eds) *Coherent Flow Structures in Open Channels*. John Wiley, New York.

Bertuccioli, L, GI Roth, J Katz, and TR Osborn. 1999. A submersible particle image velocimetry system for turbulence measurements in the bottom boundary layer. *Journal of Atmospheric and Oceanic Technology* 16: 1635-1646.

Borum, J, O Pedersen, TM Greve, TA Frankovich, JC Zieman, JW Fourqurean, and CJ Madden. 2005. The potential role of plant oxygen and sulphide dynamics in die-off events of the tropical seagrass, *Thalassia testudinum*. *Journal of Ecology* 93: 148-158.

Bouma, TJ, M Friedrichs, P Klaassen, BK van Wesenbeek, FG Brun, S Temmerman, MM van Katwijk, G Graf, and PMJ Herman. 2009. Effects of shoot stiffness, shoot size

and current velocity on scouring sediment from around seedlings and propagules. *Marine Ecology Progress Series* 388: 293-297.

Boynton, WR, and WM Kemp. 1985. Nutrient regeneration and oxygen consumption by sediments along an estuarine salinity gradient. *Marine Ecology Progress Series* 23: 45-55.

Bradley, K, and C Houser. 2009. Relative velocity of seagrass blades: Implications for wave attenuation in low-energy environments. *Journal of Geophysical Research* 114: F01004. doi: 10.1029/2007JF000951.

Bricker, JD, S Inagaki, and SG Monismith. 2005. Bed drag coefficient variability under wind waves in a tidal estuary. *Journal of Hydraulic Engineering* 131(6): 497-508.

Bricker, JD, and SG Monismith. 2007. Spectral wave-turbulence decomposition. *Journal of Atmospheric and Oceanic Technology* 24: 1479-1487.

Bryan, KR, HW Tay, CA Pilditch, CJ Lundquist, and HL Hunt. 2007. The effects of seagrass (*Zostera muelleri*) on boundary-layer hydrodynamics in Whangapoua Estuary, New Zealand. *Journal of Coastal Research* SI50: 668-672.

Carlson Jr., PR, LA Yarbrow, and TR Barber. 1994. Relationship of sediment sulfide to mortality of *Thalassia testudinum* in Florida bay. *Bulletin of Marine Science* 54(3):733-746.

Carr, J, P D'Odorico, K McGlathery, and P Wiberg. 2010. Stability and bistability of seagrass ecosystems in shallow coastal lagoons: Role of feedbacks with sediment resuspension and light attenuation. *Journal of Geophysical Research* 115: G03011. doi: 10.1029/2009JG001103.

Carr, JA, P D'Odorico, KJ McGlathery, and PL Wiberg. 2012. Modeling the effects of climate change on eelgrass stability and resilience: Future scenarios and leading indicators of collapse. *Marine Ecology Progress Series* 448: 289-301.

Chapelle, A. 1995. A preliminary model of nutrient cycling in sediments of a Mediterranean lagoon. *Ecological Modelling* 80: 131-147.

Chen, Q, H Zhao, K Ju, and SL Douglass. 2005. Prediction of wind waves in a shallow estuary. *Journal of Waterway, Port, Coastal, and Ocean Engineering* 131: 137-148.

Chen, S, LP Sanford, EW Koch, F Shi, and EW North. 2007. A nearshore model to investigate the effects of seagrass bed geometry on wave attenuation and suspended sediment transport. *Estuaries and Coasts* 30(2): 296-310.

Christiansen, T, PL Wiberg, and TG Milligan. 2000. Flow and sediment transport on a tidal marsh surface. *Estuarine, Coastal and Shelf Science* 50: 315-331.

Cornelisen, CD, and FIM Thomas. 2004. Ammonium and nitrate uptake by leaves of the seagrass *Thalassia testudinum*: Impact of hydrodynamic regime and epiphyte cover on uptake rates. *Journal of Marine Systems* 49: 177-194.

Cornelisen, CD, and FIM Thomas. 2009. Prediction and validation of flow-dependent uptake of ammonium over a seagrass-hardbottom community in Florida bay. *Marine Ecology Progress Series* 386: 71-81.

Costanza, R, R d'Arge, R de Groot, S Farber, M Grasso, B Hannon, K Limburg, S Naeem, RB O'Neill, J Paruelo, RG Raskin, P Sutton, and M van den Belt. 1997. The value of the world's ecosystem services and natural capital. *Nature* 387: 253-260.

Cowen, EA, KA Change, and Q Liao. 2001. A single-camera coupled PTV-LIF technique. *Experiments in Fluids* 31: 63-73.

de Boer, WF. 2007. Seagrass-sediment interactions, positive feedbacks and critical thresholds for occurrence: A review. *Hydrobiologia* 591: 5-24.

Dean, RG, and RA Dalrymple. 1991. *Water wave mechanics for engineers and scientists*. Singapore: World Scientific.

Dennison, WC, and RS Alberte. 1985. Role of daily light period in the depth distribution of *Zostera marina* (eelgrass). *Marine Ecology Progress Series* 25: 51-61.

Denny, MW. 1988. Biology and the mechanics of the wave-swept environment.

Princeton, NJ: Princeton University Press.

Dolbeth, M, PG Cardoso, SM Ferreira, T Verdelhos, D Raffaelli, and MA Pardal. 2007.

Anthropogenic and natural disturbance effects on a macrobenthic estuarine community over a 10-year period. *Marine Pollution Bulletin* 54: 576-585.

Duarte, CM. 1991. Seagrass depth limits. *Aquatic Botany* 40: 363-377.

Duarte, CM, and J Cebrian. 1996. The fate of marine autotrophic production. *Limnology and Oceanography* 41(8): 1758-1766.

Easterling, DR, GA Meehl, C Parmesan, SA Changnon, TR Karl, and LO Mearns. 2000.

Climate extremes: Observations, modeling and impacts. *Science* 289: 2068-2074.

Eckman, JE. 1983. Hydrodynamic processes affecting benthic recruitment. *Limnology and Oceanography* 28(2): 241-257.

Ehrhardt, NM, and CM Legault. 1999. Pink shrimp, *Farfantepenaeus duorarum*,

recruitment variability as an indicator of Florida Bay dynamics. *Estuaries* 22(2B): 471-483.

Fagherazzi, S, and PL Wiberg. 2009. Importance of wind conditions, fetch and water levels on wave-generated shear stresses in shallow intertidal basins. *Journal of Geophysical Research* 114: F03022. doi: 10.1029/2008JF001139.

Finnigan, J. 2000. Turbulence in plant canopies. *Annual review of fluid mechanics* 32: 519-571.

Fonseca, MS, JS Fisher, JC Zieman, and GW Thayer. 1982. Influence of the seagrass, *Zostera marina L.*, on current flow. *Estuarine and Coastal Shelf Science* 15:351-364.

Fonseca, MS, and JS Fisher. 1986. A comparison of canopy friction and sediment movement between four species of seagrass with reference to their ecology and restoration. *Marine Ecology Progress Series* 29: 15-22.

Fonseca, MS, and JA Cahalan. 1992. A preliminary evaluation of wave attenuation by four species of seagrass. *Estuarine Coastal and Shelf Science* 35:565-576.

Fonseca, MS, and MAR Koehl. 2006. Flow in seagrass canopies: the influence of patch width. *Estuarine, Coastal and Shelf Science* 67: 1-9.

Fourqurean, JW, and MB Robblee. 1999. Florida Bay: A history of recent ecological changes. *Estuaries* 22(2B): 345-357.

Gacia, E, TC Granata, and CM Duarte. 1999. An approach to measurement of particle flux and sediment retention within seagrass (*Posidonia oceanica*) meadows. *Aquatic Botany* 65: 255-268.

Gacia, E, and CM Duarte. 2001. Sediment retention by a Mediterranean *Posidonia oceanica* meadow: The balance between deposition and resuspension. *Estuarine, Coastal and Shelf Science* 52: 505-514.

Gambi, MC, ARM Nowell, and PA Jumars. 1990. Flume observations on flow dynamics in *Zostera marina* (eelgrass) beds. *Marine Ecology Progress Series* 61: 159-169.

Gaylord, B, DC Reed, L Washburn, and PT Raimondi. 2004. Physical-biological coupling in spore dispersal of kelp forest macroalgae. *Journal of Marine Systems* 49: 19-39.

Ghisalberti, M, and HM Nepf. 2002. Mixing layers and coherent structures in vegetated aquatic flows. *Journal of Geophysical Research* 107 (2) 3011 doi: 10.1029/2001JC000871.

Ghisalberti, M, and HM Nepf. 2004. The limited growth of vegetated shear layers. *Water Resources Research* 40: W07502 doi: 10.1029/2003WR002776

Ghisalberti, M, and H Nepf. 2005. Mass transport in vegetated shear flows.

Environmental Fluid Mechanics 5: 527-551.

Ghisalberti, M, and H Nepf. 2006. The structure of the shear layer in flows over rigid and flexible canopies. Environmental Fluid Mechanics 6: 277-301.

Ghisalberti, M. 2009. Obstructed shear flows: Similarities across systems and scales.

Journal of Fluid Mechanics 641: 51-61.

Granata, TC, T Serra, J Colomer, X Casamitjana, CM Duarte, and E Gacia. 2001. Flow and particle distributions in a nearshore seagrass meadow before and after a storm.

Marine Ecology Progress Series 218: 95-106.

Grant, WD, and OS Madsen. 1979. Combined wave and current interaction with a rough bottom. Journal of Geophysical Research 84: 1797–1808.

Grass, A. 1971. Structural features of turbulent flow over smooth and rough boundaries.

Journal of Fluid Mechanics 50:233-255.

Greve, TM, J Borum, and O Pedersen. 2003. Meristematic oxygen variability in eelgrass (*Zostera marina*). Limnology and Oceanography 48(1): 210-216.

Grizzle, RE, FT Short, CR Newell, H Hoven, and L Kindblom. 1996. Hydrodynamically induced synchronous waving of seagrass: 'monami' and its possible effects on larval mussel settlement. *Journal of Experimental Marine Biology and Ecology* 206: 165-177.

Gross, TF, and AR Nowell. 1983. Mean flow and turbulence scaling in a tidal boundary layer. *Continental Shelf Research* 2:109-126.

Gruber, RK, and WM Kemp. 2010. Feedback effects in a coastal canopy-forming submersed plant bed. *Limnology and Oceanography* 55(6): 2285-2298.

Hall, MO, MJ Durako, JW Fourqurean, and JC Zieman. 1999. Decadal changes in seagrass distribution and abundance in Florida Bay. *Estuaries* 22(2B): 445-459.

Hansen, JCR, and MA Reidenbach. 2012. Wave and tidally driven flows in eelgrass beds and their effect on sediment suspension. *Marine Ecology Progress Series* 448: 271-287.

Hansen, JCR, and MA Reidenbach. 2013. Seasonal growth and senescence of a *Zostera marina* seagrass meadow alters wave-dominated flow and sediment suspension within a coastal bay. *Estuaries and Coasts* doi: 10.1007/s12237-013-9620-5.

Hasegawa, N, M Hori, and H Mukai. 2008. Seasonal changes in eelgrass functions: current velocity reduction, prevention of sediment resuspension, and control of sediment-water column nutrient flux in relation to eelgrass dynamics. *Hydrobiologia* 596:387-399.

Hearn, CJ, MJ Atkinson, and JL Falter. 2001. A physical derivation of nutrient-uptake rates in coral reefs: Effects of roughness and waves. *Coral Reefs* 20:347-356.

Heller, DY. 1987. Sediment transport in seagrass beds. MS thesis, University of Virginia, Charlottesville, VA.

Hines, ME, and Wm. B Lyons. 1982. Biogeochemistry of nearshore Bermuda sediments. I. Sulfate reduction rates and nutrient generation. *Marine Ecology Progress Series* 8: 87-94.

Holmquist, JG, VN Powell, and S Sogard. 1989. Sediment, water level and water temperature characteristics of Florida Bay's grass-covered mud banks. *Bulletin of Marine Science* 44:348-364.

Hume, AC, P Berg, and KJ McGlathery. 2011. Dissolved oxygen fluxes and ecosystem metabolism in an eelgrass (*Zostera marina*) meadow measured with the eddy correlation technique. *Limnology and Oceanography* 56(1): 86-96.

Irlandi, E, B Orlando, S Maciá, P Biber, T Jones, L Kaufman, D Lirman, and ET Patterson. 2002. The influence of freshwater runoff on biomass, morphometrics, and production of *Thalassia testudinum*. *Aquatic Botany* 72: 67-78.

Jing, L, and PV Ridd. 1996. Wave-current bottom shear stresses and sediment resuspension in Cleveland Bay, Australia. *Coastal Engineering* 29: 169-186.

Kaimal, J, and J Finnigan. 1994. Atmospheric boundary layer flows: their structure and measurement. New York: Oxford University Press.

Keane, RD, and RJ Adrian. 1990. Optimization of particle image velocimeters. Part 1: Double pulsed systems. *Measurement Science and Technology* 1: 1202-1215.

Koch, EW. 1994. Hydrodynamics, diffusion-boundary layers and photosynthesis of the seagrass *Thalassia testudinum* and *Cymodocea nodosa*. *Marine Biology* 118: 767-776.

Koch, EW. 1999. Sediment resuspension in a shallow *Thalassia testudinum* banks ex König bed. *Aquatic Botany* 65: 269-280.

Koch, EW, and G Gust. 1999. Water flow in tide- and wave-dominated beds of the seagrass *Thalassia testudinum*. *Marine Ecology Progress Series* 184: 63-72.

Koch, EW, JD Ackerman, J Verduin, and M van Keulen. 2006. Fluid dynamics in seagrass ecology – from molecules to ecosystems. In: *Seagrasses: Biology, Ecology and Conservation*, ed. AWD Larkum, RJ Orth, and C Duarte, 193-225. Amsterdam: Springer.

Kundu, P. 1990. *Fluid Mechanics*. New York: Academic.

Kuo, J, and C den Hartog. 2006. Seagrass morphology, anatomy, and ultrastructure. In: Seagrasses: Biology, Ecology and Conservation, ed. AWD Larkum, RJ Orth, and C Duarte, 51-87. Amsterdam: Springer.

La Nafie, YA, CB de los Santos, FG Brun, MM van Katwijk, and TJ Bouma. 2012. Waves and high nutrient loads jointly decrease survival and separately affect morphological and biomechanical properties in the seagrass *Zostera noltii*. *Limnology and Oceanography* 57(6): 1664-1672.

Lacey, RWJ, and AG Roy. 2008. Fine-scale characterization of the turbulent shear layer of an in-stream pebble cluster. *Journal of Hydraulic Engineering* 134  
doi:10.1061/(ASCE)0733-9429(2008)134:7(1925).

Lacy, JR, and S Wyllie-Echeverria. 2011. The influence of current speed and vegetation density on flow structure in two macrotidal eelgrass canopies. *Limnology and Oceanography: Fluids and Environments* 1:38-55.

Laima, MJC, H Matthiesen, and LC Lund-Hansen. 1998. Resuspension studies in cylindrical microcosms: Effects of stirring velocity on the dynamics of redox sensitive elements in a coastal sediment. *Biogeochemistry* 43(3): 293-309.

Lawson, SE, PL Wiberg, KJ McGlathery, and DC Fugate. 2007. Wind-driven sediment suspension controls light availability in a shallow coastal lagoon. *Estuaries and Coasts* 30(1): 102-112.

Lawson, SE, KJ McGlathery, and PL Wiberg. 2012. Enhancement of sediment suspension and nutrient flux by benthic macrophytes at low biomass. *Marine Ecology Progress Series* 448: 259-270.

Liao, Q, HA Bootsma, J Xiao, J Val Klump, A Hume, MH Long, and P Berg. 2009. Development of an in situ underwater particle image velocimetry (UWPIV) system. *Limnology and Oceanography: Methods* 7:169-184.

Lowe, RJ, JR Koseff, and SG Monismith. 2005a. Oscillatory flow through submerged canopies: 1. Velocity structure. *Journal of Geophysical Research* 110: C10016. doi: 10.1029/2004JC002788.

Lowe, RJ, JR Koseff, and SG Monismith. 2005b. Oscillatory flow through submerged canopies: 2. Canopy mass transfer. *Journal of Geophysical Research* 110: C10017, doi: 10.1029/2004JC002789.

Lowe, RJ, JL Falter, JR Koseff, and SG Monismith. 2007. Spectral wave flow attenuation within submerged canopies: Implications for wave energy dissipation. *Journal of Geophysical Research* 112: C05018, doi: 10.1029/2006JC003605.

Lu, SS, and WW Willmarth. 1973. Measurements of the structure of the Reynolds stress in a turbulent boundary layer. *Journal of Fluid Mechanics* 60: 481-571.

Luhar, M, J Rominger, and H Nepf. 2008. Interaction between flow, transport and vegetation spatial structure. *Environmental Fluid Mechanics* 8: 423-439.

Luhar, M, S Coutu, E Infantes, S Fox, and H Nepf. 2010. Wave-induced velocities inside a model seagrass bed. *Journal of Geophysical Research* 115: C12005. doi: 10.1029/2010JC006345.

Madsen, JD, PA Chambers, WF James, EW Koch, and DF Westlake. 2001. The interaction between water movement, sediment dynamics and submersed macrophytes. *Hydrobiologia* 444:71-84.

Marion, SR, and RJ Orth. 2012. Seedling establishment in eelgrass: Seed burial effects on winter losses of developing seedlings. *Marine Ecology Progress Series* 448: 197-207.

Mass, T, A Genin, U Shavit, M Grinstein, and D Tchernov. 2010. Flow enhances photosynthesis in marine benthic autotrophs by increasing the efflux of oxygen from the organism to the water. *Proceedings of the National Academy of Sciences* 107(6): 2527-2531.

McGlathery, K, IC Anderson, and AC Tyler. 2001. Magnitude and variability of benthic and pelagic metabolism in a temperate coastal lagoon. *Marine Ecology Progress Series* 216: 1-15.

McGlathery, K, LK Reynolds, LW Cole, RJ Orth, SR Marion, and A Schwarzschild. 2012. Recovery trajectories during state change from bare sediment to eelgrass dominance. *Marine Ecology Progress Series* 448: 209-221.

Moore, KA, RJ Orth, and JF Nowak. 1993. Environmental regulation of seed germination in *Zostera marina* L. (eelgrass) in Chesapeake Bay: Effects of light, oxygen and sediment burial. *Aquatic Botany* 45: 79-91.

Nagelkerken, I, G van der Velde, MW Gorissen, GJ Meijer, T van't Hof, and C den Hartog. 2000. Importance of mangroves, seagrass beds and the shallow coral reef as a nursery for important coral reef fishes, using a visual census technique. *Estuarine, Coastal and Shelf Science* 51: 31-44.

Nagelkerken, I, S Kleijnen, T Klop, RACJ van den Brand, E Cocheret de la Morinière, and G van der Velde. 2001. Dependence of Caribbean reef fishes on mangroves and seagrass beds as nursery habitats: A comparison of fish faunas between bays with and without mangroves/seagrass beds. *Marine Ecology Progress Series* 214: 225-235.

Nagelkerken, I, CM Roberts, G van der Velde, M Dorenbosch, MC van Riel, E Cocheret de la Morinière, and PH Nienhuis. 2002. How important are mangroves and seagrass beds for coral-reef fish? The nursery hypothesis tested on an island scale. *Marine Ecology Progress Series* 244: 299-305.

Nepf, HM, JA Sullivan, and RA Zavistoski. 1997. A model for diffusion within emergent vegetation. *Limnology and Oceanography* 42(8): 1735-1745.

Nepf, HM. 1999. Drag, turbulence, and diffusion in flow through emergent vegetation. *Water Resources Research* 35(2): 479-489.

Nepf, HM, and EW Koch. 1999. Vertical secondary flows in submersed plant-like arrays. *Limnology and Oceanography* 44(4): 1072-1080.

Nepf, HM, and ER Vivoni. 2000. Flow structure in depth-limited, vegetated flow. *Journal of Geophysical Research* 105:28547-28557.

Nepf, H, M Ghisalberti, B White, and E Murphy. 2007. Retention time and dispersion associated with submerged aquatic canopies. *Water Resources Research* 43: W04422. doi: 10.1029/2006WR005362.

Nepf, HM. 2012. Flow and transport in regions with aquatic vegetation. *Annual Review of Fluid Mechanics* 44: 123-142.

Nimmo Smith, WAM, P Atsavapranee, J Katz, and TR Osborn. 2002. PIV measurements in the bottom boundary layer of the coastal ocean. *Experiments in Fluids* 33: 962-971.

Nishihara, GN, and JD Ackerman. 2006. The effect of hydrodynamics on the mass transfer of dissolved inorganic carbon to the freshwater macrophyte *Vallisneria americana*. *Limnology and Oceanography* 51(6): 2734-2745.

O'Connor, BL, and M Hondzo. 2008. Dissolved oxygen transfer to sediments by sweep and eject motions in aquatic environments. *Limnology and Oceanography* 53(2): 566-578.

Orth, RJ, ML Luckenbach, SR Marion, KA Moore, and DJ Wilcox. 2006. Seagrass recovery in the Delmarva Coastal Bays, USA. *Aquatic Botany* 84: 26-36.

Orth, RJ, and KJ McGlathery. 2012. Eelgrass recovery in the coastal bays of the Virginia Coast Reserve, USA. *Marine Ecology Progress Series* 448: 173-176.

Orth, RJ, KA Moore, SR Marion, D Wilcox, and D Parrish. 2012. Seed addition facilitates *Zostera marina* L. (eelgrass) recovery in a coastal bay system (USA). *Marine Ecology Progress Series* 448: 177-195.

Peralta, G, FG Brun, JL Perez-Llorens, and TJ Bouma. 2006. Direct effects of current velocity on the growth, morphometry and architecture of seagrasses: A case study on *Zostera noltii*. Marine Ecology Progress Series 327: 135-142.

Peterson, CH, RA Luettich Jr., M Fiorenza, and GA Skilleter. 2004. Attenuation of water flow inside seagrass canopies of differing structure. Marine Ecology Progress Series 268: 81-92.

Phlips, EJ, TC Lynch, and S Badylak. 1995. Chlorophyll *a*, tripton, color, and light availability in a shallow tropical inner-shelf lagoon, Florida Bay, USA.

Precht, E, and M Huettel. 2003. Advective pore-water exchange driven by surface gravity waves and its ecological implication. Limnology and Oceanography 48(4): 1674-1684.

Raupach, MR. 1981. Conditional statistics of Reynolds stress in rough-wall and smooth-wall turbulent boundary layers. Journal of Fluid Mechanics 108: 363-382.

Raupach, MR, RA Antonia, and S Rajagopalan. 1991. Rough-wall turbulent boundary layers. Applied Mechanics Review 44(1): 1-25.

Raupach, MR, JJ Finnigan, and Y Brunet. 1996. Coherent eddies and turbulence in vegetation canopies: The mixing-layer analogy. Boundary-Layer Meteorology 78: 351-382.

Reidenbach, MA, JR Koseff, and SG Monismith. 2007. Laboratory experiments of fine-scale mixing and mass transport within a coral canopy. *Physics of Fluids* 19: 075107.

Reidenbach, MA, NT George, and MAR Koehl. 2008. Antennule morphology and flicking kinematics facilitate odor sampling by the spiny lobster, *Panulirus argus*. *Journal of Experimental Biology* 211: 2849-2858.

Reidenbach, MA, M Limm, M Hondzo, and MT Stacey. 2010. Effects of bed roughness on boundary layer mixing and mass flux across the sediment-water interface. *Water Resources Research* 46: W07530, doi: 10.1029/2009WR008248.

Risgaard-Petersen, N, T Dalsgaard, S Rysgaard, PB Christensen, J Borum, K McGlathery, and LP Nielsen. 1998. Nitrogen balance of a temperate eelgrass *Zostera marina* bed. *Marine Ecology Progress Series* 174: 281-291.

Robblee, MB, TR Barber, PR Carlson Jr., MJ Durako, JW Fourqurean, LK Muehlstein, D Porter, LA Yarbrow, RT Zieman, and JC Zieman. 1991. Mass mortality of the tropical seagrass *Thalassia testudinum* in Florida Bay (USA). *Marine Ecology Progress Series* 71: 297-299.

Sand-Jensen, K, and J Borum. 1991. Interactions among phytoplankton, periphyton, and macrophytes in temperate fresh-waters and estuaries. *Aquatic Botany* 41:137-175.

- Sand-Jensen, K. 2008. Drag forces on common plant species in temperate streams: Consequences of morphology, velocity and biomass. *Hydrobiologia* 610(1): 307–319.
- Schanz, A, and H Asmus. 2003. Impact of hydrodynamics on development and morphology of intertidal seagrasses in the Wadden Sea. *Marine Ecology Progress Series* 261: 123-134.
- Shaw, RH, RH Silversides, and GW Thurtell. 1974. Some observations of turbulence and turbulent transport within and above plant canopies. *Boundary-Layer Meteorology* 5:429-449.
- Sheridan, PF. 1992. Comparative habitat utilization by estuarine macrofauna within the mangrove ecosystem of Rookery Bay, Florida. *Bulletin of Marine Science* 50(1): 21-39.
- Shi, JZ, ME Luther, and S Meyers. 2006. Modelling of wind wave-induced bottom processes during the slack water periods in Tampa Bay, Florida. *International Journal for Numerical Methods in Fluids* 52: 1277-1292.
- Short, FT, LK Muehlstein, and D Porter. 1987. Eelgrass wasting disease: cause and recurrence of a marine epidemic. *Biological Bulletin* 173:557-562.

Smith, NP. 2000. Observations of shallow-water transport and shear in western Florida Bay. *Journal of Physical Oceanography* 30: 1802-1808.

Stapel, J, TL Aarts, BHM van Duynhoven, JD de Groot, PHW van den Hoogen, and MA Hemminga. 1996. Nutrient uptake by leaves and roots of the seagrass *Thalassia hemprichii* in the Spermonde Archipelago, Indonesia. *Marine Ecology Progress Series* 134: 195-206.

Stapleton, KR, and DA Huntley. 1995. Seabed stress determinations using the inertial dissipation method and the turbulent kinetic energy method. *Earth Surface Processes and Landforms* 20: 807-815.

Stevens, AW, and JR Lacy. 2012. The influence of wave energy and sediment transport on seagrass distribution. *Estuaries and Coasts* 35: 92-108.

Sveen, JK. 2004. An Introduction to MatPIV v.1.6.1. University of Cambridge, UK.

Sveen, JK, and EA Cowen. 2004. Quantitative imaging techniques and their applications to wavy flows. World Scientific Publishing, Singapore.

Taylor, D, S Nixon, S Granger, and B Buckley. 1995. Nutrient limitation and the eutrophication of coastal lagoons. *Marine Ecology Progress Series* 127: 235-244.

Thomas, FIM, CD Cornelisen, and JM Zande. 2000. Effects of water velocity and canopy morphology on ammonium uptake by seagrass communities. *Ecology* 81(10): 2704-2713.

Thomas, FIM, and CD Cornelisen. 2003. Ammonium uptake by seagrass communities: Effects of oscillatory versus unidirectional flow. *Marine Ecology Progress Series* 247: 51-57.

Thompson, CEL, CL Amos, and G Umgiesser. 2004. A comparison between fluid shear stress reduction by halophytic plants in Venice Lagoon, Italy and Rustico Bay, Canada – analyses of in situ measurements. *Journal of Marine Systems* 51: 293–308.

Townsend, AA. 1976. *The structure of turbulent shear flow*, 2<sup>nd</sup> ed. Cambridge University Press, Cambridge.

Trowbridge, JH. 1998. On a technique for measurement of turbulent shear stress in the presence of surface waves. *Journal of Atmospheric and Oceanic Technology* 15: 290-298.

van derHeide, T, EH van Nes, GW Geerline, AJP Amolders, TJ Bouma, and MM van Katwijk. 2007. Positive feedbacks in seagrass ecosystems: Implications for success in conservation and restoration. *Ecosystems* 10: 1311-1322.

van Keulen, M, and MA Borowitzka. 2003. Seasonal variability in sediment distribution along an exposure gradient in a seagrass meadow in Shoalwater Bay, Western Australia. *Estuarine, Coastal and Shelf Science* 57:587-592.

Verduin, JJ, and JO Backhaus. 2000. Dynamics of plant-flow interactions for the seagrass *Amphibolis antarctica*: Field observations and model simulations. *Estuarine, Coastal and Shelf Science* 50: 185-204.

Vogel, S. 1981. *Life in Moving Fluids*. Boston: Willard Grant.

Wainright, SC. 1990. Sediment-to-water fluxes of particulate material and microbes by resuspension and their contribution to the planktonic food web. *Marine Ecology Progress Series* 62: 271-281.

Wang, JD, J van de Kreeke, N Krishnan, and D Smith. 1994. Wind and tide response in Florida Bay. *Bulletin of Marine Science* 54(3): 579-601.

Ward, LG, WM Kemp, and WR Boynton. 1984. The influence of waves and seagrass communities on suspended particulates in an estuarine embayment. *Marine Geology* 59: 85-103.

Waycott, M, CM Duarte, TJB Carruthers, RJ Orth, WC Dennison, S Olyarnik, A Calladine, JW Fourqurean, KL Heck JR., AR Hughes, GA Kendrick, WJ Kenworthy, FT

Short, and SL Williams. 2009. Accelerating loss of seagrasses across the globe threatens coastal ecosystems. *Proceedings of the National Academy of Sciences* doi: 10.1073/pnas.0905620106.

White, BL, and HM Nepf. 2007. Shear instability and coherent structures in shallow flow adjacent to a porous layer. *Journal of Fluid Mechanics* 593: 1-32.

Wiberg, PL, and JD Smith. 1983. A comparison of field data and theoretical models for wave current interactions at the bed on the continental shelf. *Continental Shelf Research* 2: 147-162.

Wiberg, PL, and CR Sherwood. 2008. Calculating wave-generated bottom orbital velocities from surface-wave parameters. *Computer and Geosciences* 34: 1243-1262.

Widdows, J, ND Pope, MD Brinsley, H Asmus, and RM Asmus. 2008. Effects of seagrass beds (*Zostera noltii* and *Z. marina*) on near-bed hydrodynamics and sediment resuspension. *Marine Ecology Progress Series* 358: 125-136.

Worcester, SE. 1995. Effects of eelgrass beds on advection and turbulent mixing in low current and low shoot density environments. *Marine Ecology Progress Series* 126:223-232.

Zhu, W, R van Hout, L Luznik, HS Kang, J Katz, and C Meneveau. 2006. A comparison of PIV measurements of canopy turbulence performed in the field and in a wind tunnel model. *Experiments in Fluids* 41: 309-318.

Zieman, JC, JW Fourqurean, and RL Iverson. 1989. Distribution, abundance and productivity of seagrasses and macroalgae in Florida Bay. *Bulletin of Marine Science* 44: 292-311.

Zieman, JC, JW Fourqurean, and TA Frankovich. 1999. Seagrass die-off in Florida Bay: Long-term trends in abundance and growth of turtle grass, *Thalassia testudinum*. *Estuaries* 22(28): 460-470.

Zimmerman, RC, JL Reguzzoni, and RS Alberte. 1995. Eelgrass (*Zostera marina* L.) transplants in San Francisco Bay: Role of light availability on metabolism, growth and survival. *Aquatic Botany* 51:67-86.